Adressage de Nanomédicaments à base de squalène

Duc Trung Bui

UNIVERSITÉ PARIS-SUD 11

ECOLE DOCTORALE :

INNOVATION THÉRAPEUTIQUE : DU FONDAMENTAL A L'APPLIQUÉ

PÔLE : PHARMACOTECHNIE ET PHYSICO-CHIMIE PHARMACEUTIQUE

DISCIPLINE : Pharmacotechnie et Biopharmacie

ANNÉE 2013 - 2014 SÉRIE DOCTORAT N° 1264

THÈSE DE DOCTORAT

soutenue le 23/12/2013

par

Duc Trung BUI

Adressage de nanomédicaments à base de squalène

Directeur de thèse :	Patrick COUVREUR	Professeur (Université Paris-Sud)
Co-directeur de thèse :	Julien NICOLAS	CR CNRS (Université Paris-Sud)
Composition du jury :		
Rapporteurs :	Juergen SIEPMANN	Professeur (Université Lille)
	Didier GIGMES	DR CNRS (Université Aix-Marseille)
Examinateurs :	Didier DESMAELE	DR CNRS (Université Paris-Sud)
	L. Harrivardhan REDDY	Chercheur (Sanofi R&D)

Remerciements

Ce travail a été réalisé à l'Institut Galien Paris-Sud (Faculté de Pharmacie, Université Paris-Sud) dirigé par le Professeur Elias Fattal que je remercie très sincèrement pour son chaleureux accueil.

Je tiens à exprimer ma profonde reconnaissance envers le Professeur Juergen Siepmann et le Docteur Didier Gigmes, qui, malgré leurs lourdes responsabilités, m'ont fait l'honneur de juger ce travail en qualité de rapporteur.

Je suis également très honoré que le Docteur L. Harivardhan Reddy ait accepté de participer à ce jury en tant qu'examinateur.

Je tiens à remercier le Professeur Patrick Couvreur et le Docteur Julien Nicolas, mes deux encadrants de thèse, pour leur aide précieuse et leurs conseils toujours pertinents tout au long de cette thèse.

Un grand merci également au Docteur Didier Desmaële qui m'a beaucoup appris tout au long de ma thèse, et ce particulièrement en chimie organique.

J'exprime ma sincère gratitude au Docteur Andrey Maksimenko qui m'a enseigné la culture cellulaire et au Docteur Simon Harrisson pour ses nombreux conseils en polymérisation radicalaire contrôlée.

Je tiens également à remercier le Docteur Christine Vauthier (équipe 6, UMR 8612) pour sa collaboration fructueuse concernant l'activation du complément, Valérie Nicolas (IFR 141) pour son aide précieuse en microscopie confocale, Sandrine Zanna (ENSCP, UMR 7045) pour les expériences d'XPS, Estelle Morvan (BioCIS) pour son aide en RMN et Claire Gueutin (UMR 8612) pour son aide en HPLC.

Je tiens à remercier le Professeur Christian Cavé et toute son équipe, dont Frédéric Hendra et Pierre Daligaux, pour leurs encouragements.

Un grand merci enfin à tous mes collègues du laboratoire : le Dr Fatima Zouhiri, le Dr Simona Mura, le Dr Sinda Lepêtre-Mouelhi, Julie Mougin, Sabrina Valetti, Alice Gaudin, Eric Buchi, Nadia Abed, Vianney Delplace et aux anciens membres, Joachim Caron, Davide Brambilla, Eric Sliwinsky, Bettina Ralay-Ranaivo, Valentina Agostoni et Hubert Chapuis, avec qui j'ai passé de très bons moments.

Merci également à tous ceux que j'ai côtoyés au laboratoire de l'UMR CNRS 8612 et au sein de la faculté (statuaires, étudiants, stagiaires, personnels techniques et administratifs) et à mes amis qui me soutiennent et m'encouragent.

Mes remerciements s'adresseront enfin à l'Université des Sciences et des Technologies de Hanoi (USTH) pour le soutien financier.

En dernier lieu, je remercie ma famille qui a toujours su me soutenir.

Sommaire

Liste des abréviations

ζ	zeta potential
5-FU	5-fluorouracile
Ara-C	1-β-D-arabinofuranosylcytosine
ATRP	Atom transfer radical polymerization
CLRP	Controlled/living radical polymerization
Cryo-TEM	Cryogenic transmission electron microscopy
DCM	Dichloromethane
DLS	Dynamic light scattering
DMAP	4-Dimethylaminopyridine
DMF	Dimethylformamide
DMEM	Eagle's minimal essential medium
Dox	Doxorubicin
Dtx	Doxetaxel
D_z	Mean diameter of the nanoparticles in intensity
Đ	Dispersity
FBS	Fetal bovine serum
FUdR	5-fluoro-2'-deoxyuridine
Gem	Gemcitabine
LRP	Living radical polymerization
M_n	Number-average molar mass
MTT	3-(4,5-dimethylthiazol-2-yl)-2,5-diphenyltetrazolium bromide)
MTX	Methotrexate
NMP	Nitroxide-mediated polymerization
NMR	Nuclear magnetic resonance spectroscopy

PBS	Phosphate buffered saline
PEG	Poly(ethylene glycol)
PI	Polyisoprene
PMMA	Poly(methyl methacrylate)
PSD	Particle size distribution
Ptx	Paclitaxel
RAFT	Reversible addition-fragmentation chain transfer
Rho	Rhodamine
RPMI	Roswell park memorial institute medium
SLN	Solid lipid nanoparticles
Sq	Squalene
SqMA	Squalenyl methacrylate
SEC	Size Exclusion Chromatography
TBS	Tert-butyldimethylsilyl
THF	Tetrahydrofuran
USPIO	Ultrasmall particles of iron oxide
XPS	X-ray photoelectron spectroscopy

Introduction générale

L'adressage (ou délivrance spécifique) de molécules thérapeutiques vers un organe, un tissu ou une cellule malade constitue aujourd'hui un défi majeur pour le traitement des maladies humaines, notamment infectieuses, cancéreuses ou d'origine génétique. En effet, les principes actifs sont confrontés, de par leurs caractéristiques physico-chimiques, à de nombreux obstacles (passage des barrières biologiques, dégradation et métabolisation) dès lors que le site d'administration est différent du site d'action. L'obtention de concentrations thérapeutiques efficaces sur le site d'action ne peut donc se faire qu'au prix d'une déperdition importante en principe actif au niveau d'autres tissus ou cellules. Ceci occasionne généralement des effets toxiques importants voire rédhibitoires, conduisant à l'arrêt du traitement parfois en dépit d'une efficacité intrinsèque.

Les nanotechnologies offrent de formidables outils pour résoudre ce problème via l'élaboration de vecteurs de médicaments de structures et de caractéristiques bien définies. S'appuyant sur de nouveaux concepts physico-chimiques et sur le développement de nouveaux matériaux polymère, la recherche galénique a permis de concevoir des nanosystèmes d'administration innovants (*e.g.*, nanoparticules, micelles, liposomes, etc), capables de protéger la molécule biologiquement active de la dégradation et d'en contrôler la libération en terme de localisation et de durée (contrôle à la fois spatial et temporel).

L'une des applications principales des systèmes nanoparticulaires dans le domaine biomédical concerne le traitement du cancer.[1-2] L'approche classique pour concevoir de tels édifices colloïdaux consiste à encapsuler de manière physique un principe actif anticancéreux au sein du nanovecteur (*e.g.*, dans la matrice polymère pour les nanoparticules polymère ou dans le contenu aqueux des liposomes). En revanche, même si de nombreux résultats prometteurs ont été obtenus (essai *in vivo* et parfois essais cliniques), certaines limitations importantes demeurent : (i) le '*burst release*' qui consiste en un libération rapide d'une grande fraction de principes actifs adsorbés à la surface des nanoparticules, ce qui peut induire des effets toxiques ; (ii) des éventuels phénomènes de cristallisation lors de l'encapsulation de principes actifs faiblement solubles dans la matrice polymère et surtout (iii) des taux de chargement en principes actifs très médiocres (au maximum de quelques pourcents). Afin de résoudre au moins partiellement ces problèmes, la stratégie dite « prodrogue »,[3] qui consiste en une liaison covalente entre le principe actif et le matériau qui constitue le nanovecteur, a été utilisée.[4-5] Parmi les différentes manières de concevoir des prodrogues nanoparticulaires, la technique dite de « squalénisation », qui utilise le squalène comme composant du nanovecteur, a connu un fort développement ces dernières années.[6] Le squalène est un

triterpène composé de 30 atomes de carbone est sa structure est organisée en six unités isoprèniques qui sont toutes en configuration *trans*. Ce lipide est présent en grande quantité dans l'huile du foie de requins et en moindre quantité dans les huiles céréalières. Par ailleurs, il est également présent dans le sébum humain. Le squalène est un précurseur de la biosynthèse des stérols.[7] Le concept de « squalénisation » a été développé par Patrick Couvreur et son équipe en 2006[8] et consiste à coupler le squalène à des principes actifs, notamment des anticancéreux (*e.g.*, gemcitabine, cisplatin, paclitaxel, doxorubicine…), pour former des composés conjugués qui, par auto-assemblage en solution aqueuse, forment des nanoparticules stables de diamètres compris entre 100 et 200 nm. Du fait des masses molaires relativement proches des principes actifs utilisés et du squalène, les taux de chargement de ces nanoparticules en principes actifs avoisinent les 40-50%, ce qui est remarquablement élevé. L'exemple de référence dans ce domaine est la nanoparticule de gemcitabine-squalène (Gem-Sq). La gemcitabine est un analogue de la déoxycytidine qui est utilisé en clinique pour traiter différents types de tumeurs (*e.g.*, pancréas, poumon, sein, etc).[9-12] Les nanoparticules de Gem-Sq ont démontré des activités anticancéreuses considérables *in vitro* et *in vivo* sur des modèles expérimentaux de leucémies et de cancers pancréatiques, bien supérieures à celles obtenues avec la Gem libre.[13] Par ailleurs, cette amélioration d'efficacité thérapeutique s'est accompagnée par une baisse de toxicité.[14-15]

Néanmoins, il a été montré que lorsque les nanoparticules de Gem-Sq sont injectées par voie intraveineuse, elles sont rapidement éliminées de la circulation sanguine par le système réticulo-endothélial. En ce sens, une stratégie visant à augmenter le temps de demi-vie plasmatique des nanoparticules en utilisant du squalène couplé au poly(éthylène glycol) lors de l'auto-assemblage de la Gem-Sq a été développée mais s'est avérée infructueuse, du fait d'une déstructuration colloïdale intervenant au cours de la PEGylation.[16]

C'est dans ce contexte scientifique que s'est situé mon sujet de thèse. Mes deux objectifs principaux étaient les suivants :

- Résoudre le problème de PEGylation observé lors du co-auto-assemblage Sq-PEG/Sq-Gem et concevoir ainsi des nanoparticules « furtives » à base de squalène.
- Proposer une stratégie pour élaborer des nanoparticules fonctionnalisées à base de squalène afin de permettre un adressage spécifique des principes actifs vers les cellules/tissus cible.

Ce manuscrit est divisé en cinq chapitres. La première partie consiste en une revue de la littérature concernant la synthèse et la préparation de prodrogues lipidiques nanoparticulaires pour le traitement du cancer. Les trois chapitres suivants, rédigés sous forme de publications, présentent les avancées accomplies au cours de la thèse en réponse à notre problématique. Chacun de ces chapitres comporte une sous-section intitulée « supplementary information » pour étoffer et compléter les données présentées dans le corps de texte. Enfin, la dernière partie du manuscrit est une discussion générale de l'ensemble des résultats et une proposition de perspectives qui décrivent brièvement ce qu'il resterait à étudier à l'issue de cette thèse.

Cette thèse a été réalisée dans le cadre le l'ERC Advanced Grant TERNANOMED.

References

1. Nie, S.; Xing, Y.; Kim, G. J.; Simons, J. W. *Annu. Rev. Biomed. Eng.* **2007,** *9*, 257.
2. Wang, M.; Thanou, M. *Pharmacol. Res.* **2010,** *62*, 90.
3. Albert, A. *Nature* **1958,** *182*, 421.
4. Kratz, F.; Müller, I. A.; Ryppa, C.; Warnecke, A. *ChemMedChem* **2008,** *3*, 20.
5. Bildstein, L.; Dubernet, C.; Couvreur, P. *Adv. Drug Delivery Rev.* **2011,** *63*, 3.
6. Desmaële, D.; Gref, R.; Couvreur, P. *J. Control. Rel.* **2012,** *161*, 609.
7. Cattel, L.; Ceruti, M.; Balliano, G.; Viola, F., 2,3-Oxidosqualene Cyclase and Squalene Epoxidase as Target Enzymes for the Development of New Sterol Biosynthesis Inhibitors. In *Regulation of Isopentenoid Metabolism*, American Chemical Society: 1992; Vol. 497, pp 174.
8. Couvreur, P.; Stella, B.; Reddy, L. H.; Hillaireau, H.; Dubernet, C.; Desmaële, D.; Lepêtre-Mouelhi, S.; Rocco, F.; Dereuddre-Bosquet, N.; Clayette, P.; Rosilio, V.; Marsaud, V.; Renoir, J.-M.; Cattel, L. *Nano Lett.* **2006,** *6*, 2544.
9. Hertel, L. W.; Boder, G. B.; Kroin, J. S.; Rinzel, S. M.; Poore, G. A.; Todd, G. C.; Grindey, G. B. *Cancer Res.* **1990,** *50*, 4417.
10. Burris, H. A.; Moore, M. J.; Andersen, J.; Green, M. R.; Rothenberg, M. L.; Modiano, M. R.; Cripps, M. C.; Portenoy, R. K.; Storniolo, A. M.; Tarassoff, P.; Nelson, R.; Dorr, F. A.; Stephens, C. D.; Von Hoff, D. D. *J. Clin. Oncol.* **1997,** *15*, 2403.
11. Murad, A. M. *Oncology (Williston Park)* **2003,** *17*, 26.
12. Toschi, L.; Cappuzzo, F. *Onco Targets Ther* **2009,** *2*, 209.

13. Reddy, L. H.; Dubernet, C.; Mouelhi, S. L.; Marque, P. E.; Desmaele, D.; Couvreur, P. *J. Control. Rel.* **2007,** *124*, 20.
14. Reddy, L. H.; Khoury, H.; Paci, A.; Deroussent, A.; Ferreira, H.; Dubernet, C.; Decleves, X.; Besnard, M.; Chacun, H.; Lepetre-Mouelhi, S.; Desmaele, D.; Rousseau, B.; Laugier, C.; Cintrat, J.-C.; Vassal, G.; Couvreur, P. *Drug Metab. Dispos.* **2008,** *36*, 1570.
15. Reddy, L. H.; Marque, P.-E.; Dubernet, C.; Mouelhi, S.-L.; Desmaele, D.; Couvreur, P. *J. Pharmacol. Exp. Ther.* **2008,** *325*, 484.
16. Bekkara-Aounallah, F.; Gref, R.; Othman, M.; Reddy, L. H.; Pili, B.; Allain, V.; Bourgaux, C.; Hillaireau, H.; Lepetre-Mouelhi, S.; Desmaele, D.; Nicolas, J.; Chafi, N.; Couvreur, P. *Adv. Funct. Mater.* **2008,** *18*, 3715.

Chapitre I

Synthesis of Nanoparticulate Systems Based on Lipid Anticancer Prodrug

*Duc Trung Bui, Patrick Couvreur and Julien Nicolas**

Manuscript in preparation

Résumé

Dans ce premier chapitre, nous nous proposons de faire une étude bibliographique portant sur la conception de nanoparticules de prodrogues lipidiques, soit encapsulées à l'intérieure de nanoparticules (nanoparticules polymère, micelles, liposomes, nanoparticules solide lipide, etc.) ou soit étant capables de former de par leur structure des édifices colloïdaux sans apport d'autres composés. Nous focaliserons notre recherche dans le domaine du cancer.

Cette étude permettra d'avoir une vision récente de l'état de l'art dans ce domaine et ainsi mettre en lumière les éventuels manque et/ou limitations des systèmes existants.

1. Introduction

In the field of anticancer drug delivery, there has been a growing interest in the use of drug nanocarriers in order to improve therapeutic efficacy and reduce the risks of adverse reactions due to the inherent toxicity of drugs.[1-4] A great deal of effort is currently been paid to the design of nanocarriers able to safely transport various kinds of drugs and to efficiently release their load at their site of action.[5-7] Among the different classes of nanoparticulate systems, polymer nanoparticles,[8-10] micelles,[11] liposomes,[12] solid lipid nanoparticles,[13] magnetic nanoparticles,[14] or dendrimers[15-16] are the most extensively investigated.

Usually, drugs are encapsulated/physically entrapped inside nanocarriers during the formulation process (*e.g.*, self-assembly for polymer nanoparticles and micelles, extrusion for liposomes, etc.). Although the use of drug-loaded nanocarriers has conducted to very promising results in the recent literature,[17-22] many systems still present severe limitations that may hamper their further translation to clinical trials and therefore to the market. Among them, the 'burst' release, which consists in the quick and uncontrolled release of a significant fraction of the adsorbed drug which is only adsorbed at the surface of the nanocarriers, can be harmful to patients, conversely to the sustained drug release at the diseased area. Additionally, the difficulty to encapsulate poorly-soluble drugs that tend to crystallize may lead to colloidal destabilization and may necessitate the use of organic co-solvents during the formulation process. Finally, poor drug-loadings are generally observed (typically a few percent) which requires the administration of high quantities carrier materials to obtain a therapeutic effect, which can itself provide toxicity. For all these reasons, alternative strategies have been developed in order to alleviate or even suppress the aforementioned drawbacks. One of these strategies takes advantage of the prodrug concept[23] and has received considerable attention in the field of nanoparticulate systems. A prodrug is formed by the covalent linkage between a drug and a (macro)molecule, and is further metabolized *in vivo* into an active metabolite.[24] The use of prodrugs in drug delivery provides important benefits such as: (i) a sustained drug release (mediated by chemical or enzymatic hydrolysis of the drug-moiety/promoiety); (ii) an increase of the drug chemical stability and solubility and (iii) a reduced toxicity before the metabolization occurs.[25] Overall, the prodrug strategy provides a rationale for achieving tailor-made physico-chemical, pharmacokinetic and pharmacological features.

By combining the prodrug strategy with the use of nanoparticulate systems as drug carriers, optimized formulations have been recently reported.[26-27] They helped to resolve the

poor solubility of some prodrugs, to reduce adverse effects, and therefore to improve cancer therapy. Among the different classes of moieties/promoieties attached to the drugs, lipids such as fatty acids, cholesterol derivatives, phospholipids or triglycerides, have been used. They perhaps represent the materials of choice due to their biocompatibility, which probably explains why lipids have also been intensively used as nanocarrier materials (*e.g.*, liposomes, solid-lipid nanoparticles, nanoemulsion, etc.). Indeed, prerequisites regarding the design of nanocarriers for drug delivery are that the materials must be nontoxic, biocompatible and cleared from the body, for instance by biodegradation or bioerosion. It has also to be noted that nanomedicines currently available or in late clinical stages are made of lipids: Doxil® (liposomal doxorubicin), Caelix® (PEGylated liposomal doxorubicin) and Ambisome® (liposomal formulation of amphotericin B).[22] Additionally, structural similarities between lipid-based nanocarriers and lipid prodrugs may facilitate prodrug loading/insertion, for instance due to facile nanocarriers membrane anchoring. In this regards, the present review will discuss recent achievements in the field of lipid-based prodrug nanocarriers and will focus on cancer therapy. The reader who want more details about non-lipid polymer prodrug nanoparticles is referred to the following review.[27]

2. Lipid prodrug nanoparticulate systems

For the sake of simplicity, all anticancer drug structures that are discussed herein and their coupling sites are reported in Figure 1.

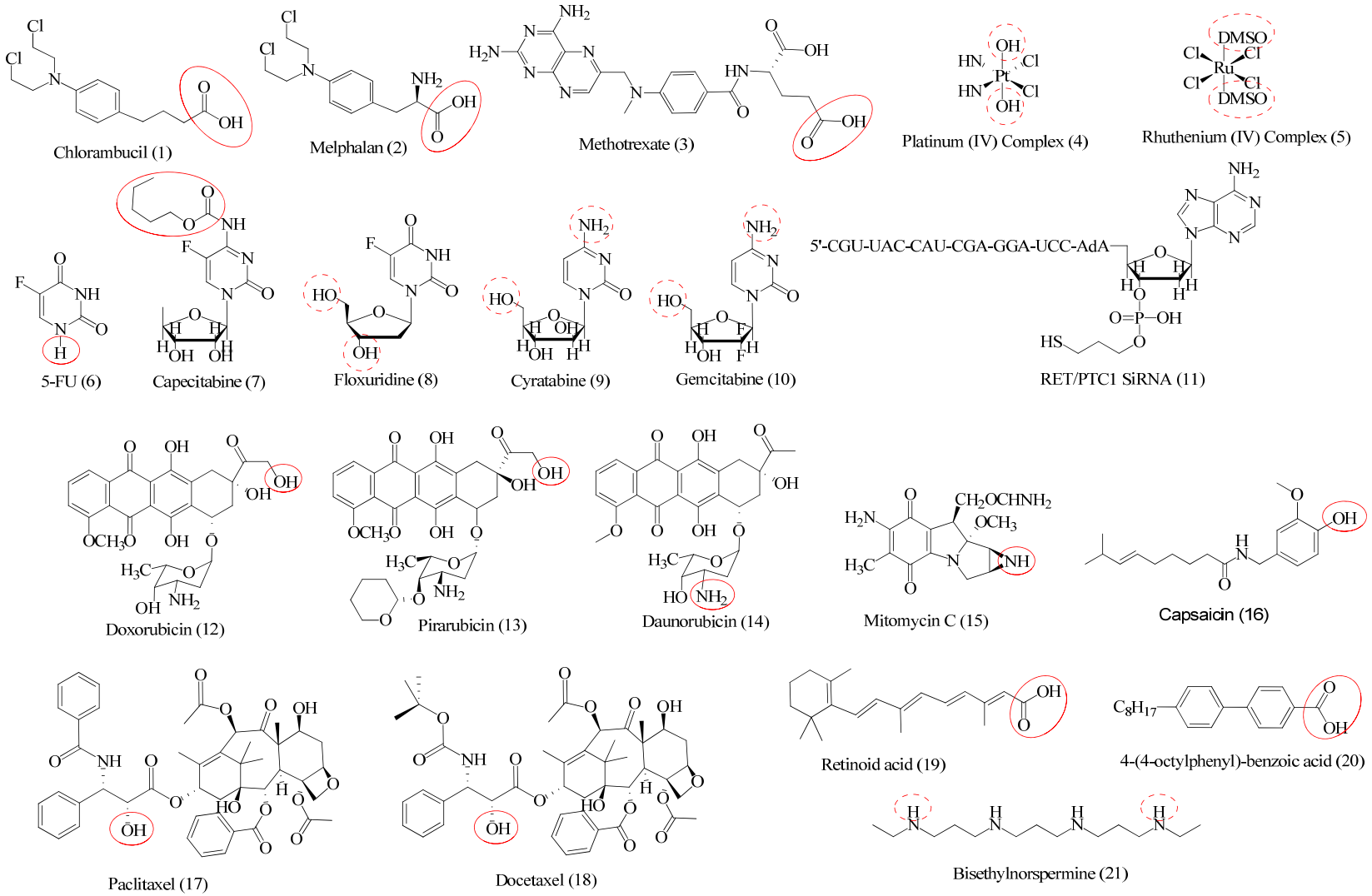

Figure 1. Name and chemical structures of all anticancer drugs described in this review. The circled parts correspond to the coupling sites with the lipid moieties.

2.1 Alkylating agents

The alkylating agents represent one of the most important classes of antitumor drugs. They possess chemical groups that can form covalent bonds with nucleophilic moieties in the DNA, thus preventing its replication and therefore cancer cell proliferation.

A typical example is the design of prodrug ether phospholipid conjugates from the anticancer drug **chlorambucil** that exhibited C_{16} and C_{18} ether chains with phosphatidylcholine or phosphatidylglycerol headgroups (Figure 2).[28] All four prodrugs led to unilamellar liposomes (86–125 nm) and were hydrolyzed by phospholipase A2, resulting in chlorambucil release. The liposomal formulations displayed cytotoxicity against HT-29, MT-3, and ES-2 cancer cell lines in the presence of phospholipase A2, with IC_{50} values in the 8–36 μM range.

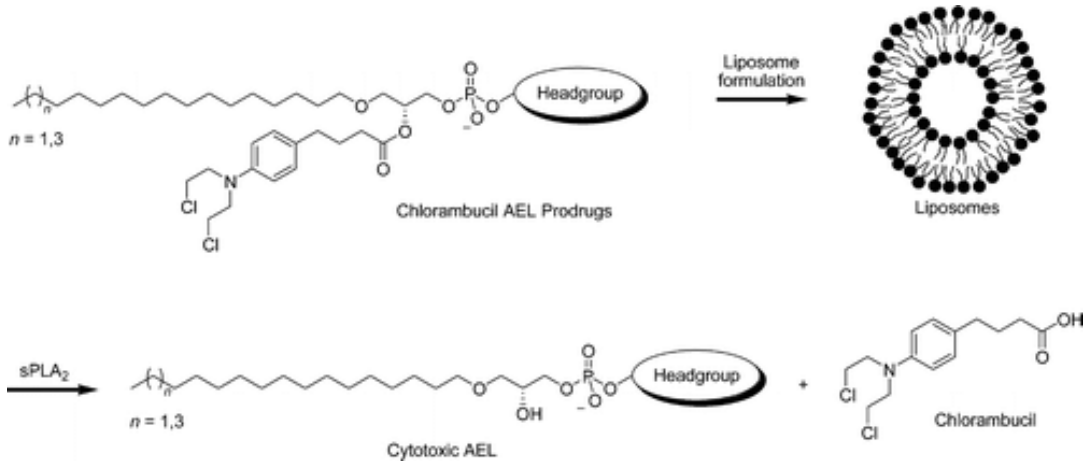

Figure 2. Synthesis of liposomes based on chlorambucil anticancer ether lipid prodrugs. Reproduced with permissions from ref. [28].

In a similar fashion, liposomes of **melphalan** (also called **sarcolysin)** prodrugs (obtained from the conjugation of the drug to *rac*-1,2-dioleoylglycerol through a ester linkage) have been obtained by blending natural phospholipids (phosphatidylcholine and phosphtidylinositol) with the prodrugs (9:1; mol:mol) during the extrusion process (Figure 3).[29] It was shown that the prodrugs were completely inserted into very stable, unilamellar liposomes of 50–150 nm in diameter. Also, lipid derivative of melphalan, obtained by its condensation with dioleoylglycerol, was shown to be well-retained in the liposome membrane, which exhibited a higher cytotoxic activity than free sarcolysinin *in vitro* (CaOv cells) and a much higher antitumor activity *in vivo* (P388 leukemia).[30] It was also shown that

further increase in the efficacy of these lipid derivatives can be attained by incorporating a carbohydrate vector, to target cancer cells, in the liposomal membrane.[30-31]

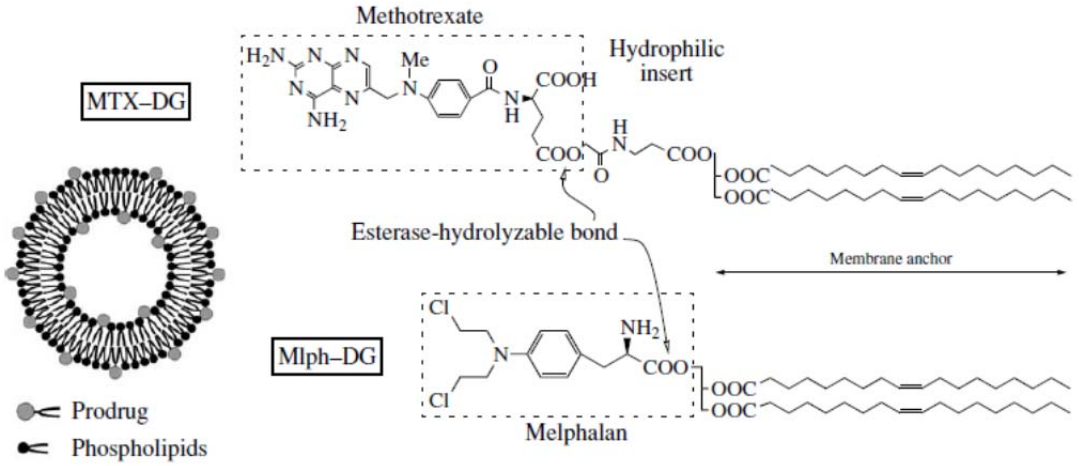

Figure 3. Molecular structures of lipid–drug conjugates and a drug-carrying liposome. Reproduced with permissions from ref. [29].

Cisplatin, which is known to be one of most widely used agent in the treatment of solid tumor, was conjugated to squalene (Sq), a natural lipid widely distributed in nature and a precursor of the cholesterol biosynthesis.[32] The conjugate was self-assembled in the presence of ultrasmall particles of iron oxide (USPIO) as a MRI agent. The resulting composite nanoparticles enabled the transport of an unusually high amount of anticancer compounds, without any 'burst release' of the drug and with simultaneous visualization of the tumor tissue. An interesting feature of this system also relied on the potential magnetic guidance to the tumor site *in vivo*, in order to enhance even further the therapeutic efficacy of the treatment.

2.2 Antimetabolite agents

Antimetabolites have an importance role in cancer treatment as most of them interfere with nucleic acid synthesis or nucleotide synthesis. Therefore, these compounds block DNA production and inhibit cell division and the growth of tumors.[33]

Using a similar synthetic pathway as for melphalan (see part 2.1), the antifolate drug **methotrexate** (MTX) has been linked to *rac*-1,2-dioleoylglycerol and the resulting prodrug was formulated with natural phospholipids in order to give mixed liposomes with diameters in the 100–150 nm range (Figure 3).[29,34] Not only they overcame tumor cell resistance to the drug (the drug resistance of human leukemia cells has been decreased 114 times compared to

free MTX),[29] but they also demonstrated hemocompatibility through a reduced complement activation and coagulation cascades in human blood.[31]

Pyrimidine analogues, such as **gemcitabine (Gem)** or **5-fluorouracile (5-FU)**, are other active molecules that have been extensively used in cancer therapy as they can cause profound inhibition of DNA chain elongation through substituting cytidine and thymidine bases.[35-36]

5-FU has been directly acylated by stearyl chloride to obtain N_1-stearyl-5-FU (5-FUS) and incorporated into solid lipid nanoparticles (SLN) up to ~20% drug payload.[37] Compared to free 5-FU injections, a study on the distribution of 5-FU-loaded SLN in mice showed that the latter could double 5-FU concentrations in mice livers. Different prodrug analogues of 5-FU have also been derivatized with lipid moieties in order to be formulated into nanocarriers. For instance, a series of **capecitabine**-based prodrugs was prepared from a broad range of different lipids (Figure 4) such as: palmityl,[38-39] phytanyl,[38] oleyl,[38,40] phytanyl,[38] stearyl,[40] linoleyl,[40] and linolenyl.[40] The different prodrugs were then employed in the formation nanostuctured nanoparticles containing 10% of Pluronic F127 as surfactant and exhibiting average diameters ranging between 160 and 700 nm, depending on the nature of the prodrugs. Interestingly, different morphologies were obtained such as solid-lipid nanoparticles, cubosomes of gyroids and double diamonds. These prodrug formulations were found to significantly enhance the anticancer activity against various cancer cell lines *in vitro* compared to free capecitabine, to slow down tumour progression of mouse 4T1 breast tumour and nearly halt the growth of a human MDA-MB-231 breast tumour in mouse xenografts.[38-40]

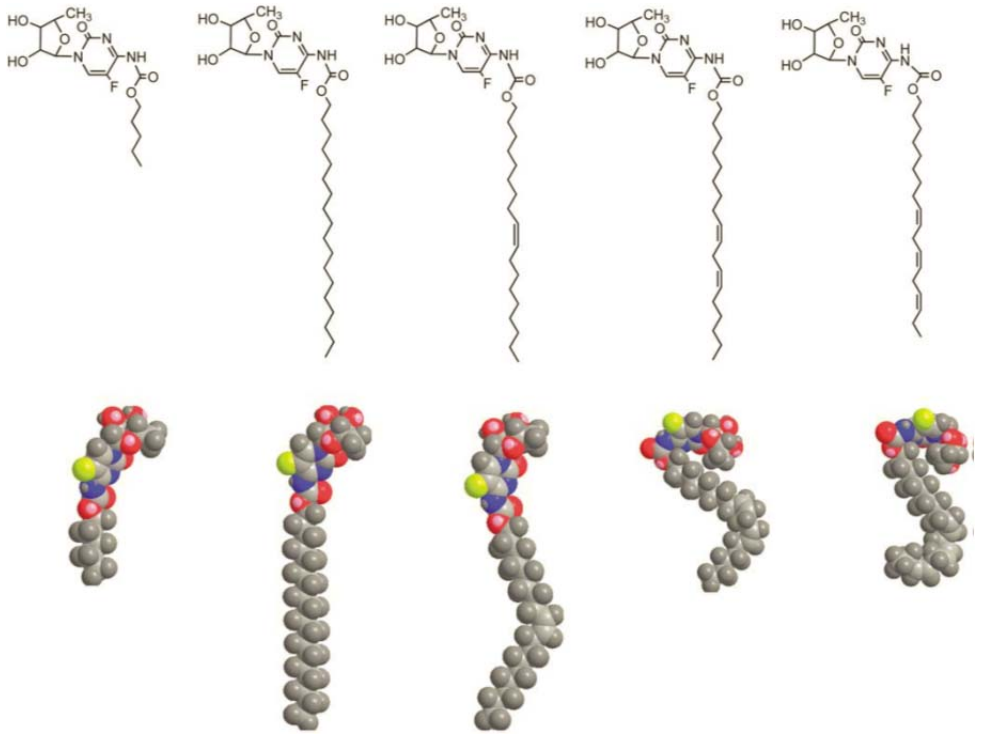

Figure 4. Chemical structure and energy minimized (space filling model) of (from left to right) capecitabine, 5-FCSte, 5-FCOle, 5-FCLle and 5-FCLln. Reproduced with permission from ref. [40].

To achieve improved liposomal retention of **floxuridine** (5-fluoro-2'-deoxyuridine, FUdR), a 5-FU analogue, the drug was converted to a lipophilic prodrug by esterifying the free hydroxyl groups in the deoxyribose moiety with fatty acids of different chain lengths (dipalmitate (C_{16}) and dioctanoate (C_8)) and further incorporated in liposomes.[41] The dipalmitoyl derivative could be incorporated up to 13 mol.% in solid-type liposomes but to only 2 mol.% in fluid-type counterparts. Whereas liposomal FUdR-dioctanoate inhibited cell growth in the same concentration range as unesterified FUdR, FUdR-dipalmitate was more than two orders of magnitude less potent in inhibiting cell proliferation. Interestingly, in fluid-type liposomes, antiproliferative activity of FUdR-dipalmitate was several-fold higher than in solid-type liposomes. FUdR-dioctanoate was also incorporated into solid lipid nanoparticles up to 29% drug payload, resulting in improved delivery (~11 fold higher) to the brain compared to the single molecular prodrug.[42] The dipalmitoylated derivative of FUdR was also incorporated in the bilayer of immunoliposomes surface-fonctionalized by a monoclonal antibody against the rat colon carcinoma (CC531).[43-44] It was shown that immunoliposomes containing FUdR-dipalmitate caused a much stronger inhibition of CC531 cell growth *in vitro* than FUdR-dipalmitate in non-targeted liposomes.[44]

Micelles of **cytarabine** (1-β-D-arabinofuranosylcytosine or *ara*-C) and **cytidine** conjugates of thioether lipid (1-*S*-alkylthioglycerol) linked by a pyrophosphate diester bond have also been prepared and evaluated for their antitumor activity against an *ara*-C[2] sensitive (L1210/0) and two *ara*-C resistant L1210 lymphoid leukemia sublines in mice.[45] Whereas all cytidine conjugates were ineffective on these cell lines, micelles of cytarabine prodrugs (especially *ara*-CDP-rac-l-*S*-hexadecyl-2-0-palmitoyl-l-thioglycerol and *ara*-CDP-rac-l-*S*-octadecyl-2-*O*-palmitoylthioglycerol) produced significant increase in life span (~250-370%) in mice bearing L1210/0 leukemia. In another study, cytarabine was linked to a cholesteryl moiety (N^4-[*N*-(cholesteryloxycarbonyl)glycyl]-1-*β*-D-arabinofuranosyl-cytosine) and efficiently entrapped into liposomes, leading to superior anticancer activity *in vivo* on mice bearing L1210 leukemia than the free drug and the prodrug alone.[46] Prodrug-bearing liposomes were also found to inhibit the growth of a human lung adenocarcinoma A549 xenograft implanted under the renal capsule more efficiently than the free drug. In another study, N^4-Hexadecyl-1-β-D-arabinofuranosylcytosine (hxd^{4}ara-C), a new cytostatic derivative of ara-C, was linked to phospholipids containing differently substituted glycerol residues (*e.g.*, 1-*O*-octadecyl-rac-glycero-3-phosphoryl-(3→5'), 1,2-*O*-dipalmitoyl-rac-glycero-3-phosphoryl-(3→5')-N^4-palmitoyl, 1,2-O-dioctadecyl-rac-glycero-3-phosphoryl-(3→5')-N^4-palmitoyl and 1-*O*-octadecyl-rac-glycero-3-phosphoryl-(3→5')) *via* a phosphodiester-linkage.[47] These conjugates formed stable liposomes with matrix lipids and exerted antileukemic effects *in vivo* on L1210 tumor-bearing mice, whereas conjugates from combined palmitoyl, octadecyl and hexadecyl moieties were poorly active or even inactive. Cytarabine was also conjugated to squalenic acid (Figure 5). Although no biological evaluation of the resulting prodrug was shown, its enhanced affinity compared to the free drug for multi-lamellar vesicles of dimyristoylphosphatidylcholine (DMPC) was demonstrated, thus opening the way to the use of liposome-containing Sq-cytarabine for drug delivery purposes.[48]

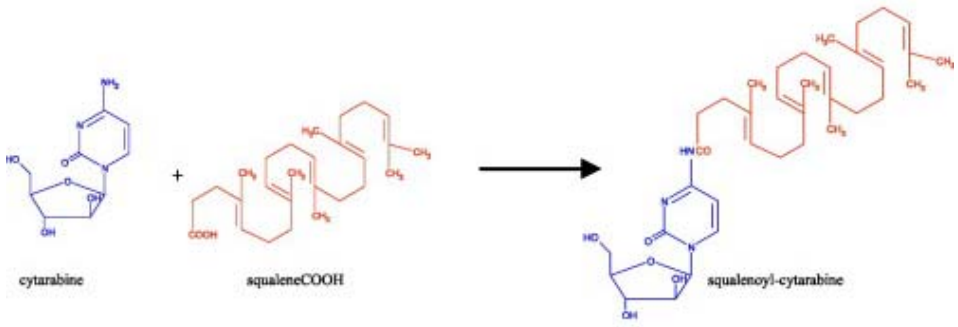

Figure 5. Synthesis of *n*-squalenoyl cytarabine conjugate. Reproduced with permission from ref. [48].

Gem is by far the most employed antimetabolite in the lipid prodrug area, likely due to its demonstrated activity against a wide range of solid tumors (*e.g.*, colon, lung, pancreatic, breast, bladder and ovarian cancers).[49] Gem has been linked to various lipids (*e.g.*, C_{12}, C_{15}, C_{18} or C_{20} in chain length) and the resulting conjugates were incorporated into liposome, nanoparticles, solid lipid nanoparticles or self-assembled nanoparticles.[50-55] Composite liposomes containing phospholipids and lipid-based Gem prodrugs were shown to protect the drug from degradation in blood plasma, thus ensuring enhanced plasma haft-time and intracellular release of the drug.[50] Compared to free Gem, the prodrugs exhibited improved affinity with lipid vesicles employed as both model biomembranes and carriers in the transport of antitumor drugs.[51] This study suggested that the prodrug lipophilic tail should modulate the transport and the release of Gem inside the cellular compartments.

Regarding biological evaluations, it was shown that the pharmacokinetic behavior of stearoyl-Gemcitabine (C_{18}-Gem) prodrug-containing liposomes increased the plasma half-life of Gem, resulting in increased accumulation in tumor cells and a higher level of antitumoral efficacy *in vivo* (Figure 6).[54] Importantly, SLN containing C_{18}-Gem exhibited improved cytotoxicity comparatively to free Gem when tested *in vitro* and *in vivo* against Gem-resistant cancer cell lines.[55]

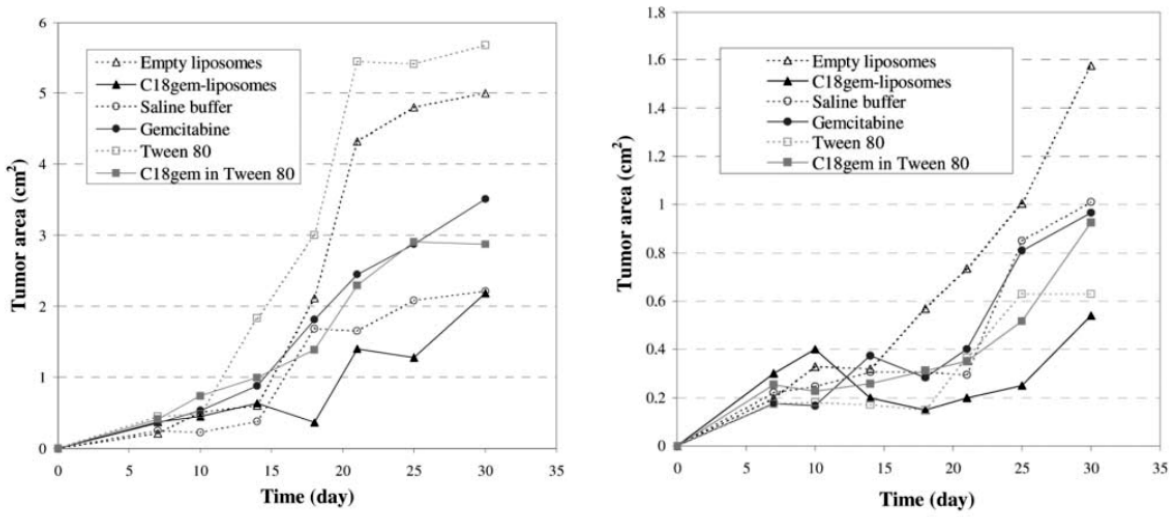

Figure 6. Left panel: Tumor area in mice grafted with HT-29 cells after i.p. injection of samples or controls at day 7. Right panel: Tumor area in mice grafted with KB 396p cells after i.p. injection of samples or controls at day 7. Values are the mean of three replications et standard deviation not reported, below 10%. Reproduced with permission from ref. [54].

These liposomes were further PEGylated by means of DSPE-PEG_{2000}, which improved their accumulation in tumor tissues (>6-fold) but without affecting their *in vivo* anticancer activity in mice with pre-established human BxPC-3 tumors, compared to non-PEGylated liposomes (Figure 7).[56] Conversely, similar PEGylated liposomes showed higher cytotoxicity than free Gem on HpG2 cell model *in vivo*.[57] The liposomes were then surface functionalized with a recombinant murine EGF in order to targeted tumor cells that over-express epidermal growth factor receptor (EGFR).[58] This was successfully demonstrated *in vivo* in EGFR over-expressing MDA-MB-468 tumor-bearing mice that grew significantly slower when treated with the targeted liposomes, compared to the untargeted treatment. Moreover, C_{18}-Gem prodrugs were also incorporated into poly(lactic-*co*-glycolic acid) (PLGA) nanoparticles, which showed improved anticancer activity in TC-1 tumor-bearing mice compared to the treatment with empty nanoparticles or free Gem.[59] Several lipophilic monophosphorylated Gem prodrugs were also synthesized and incorporated into SLN. All these nanoparticles showed a significantly higher cytotoxicity than free Gem and Gem prodrugs in cells that are deficient in deoxycytidine kinase.[60]

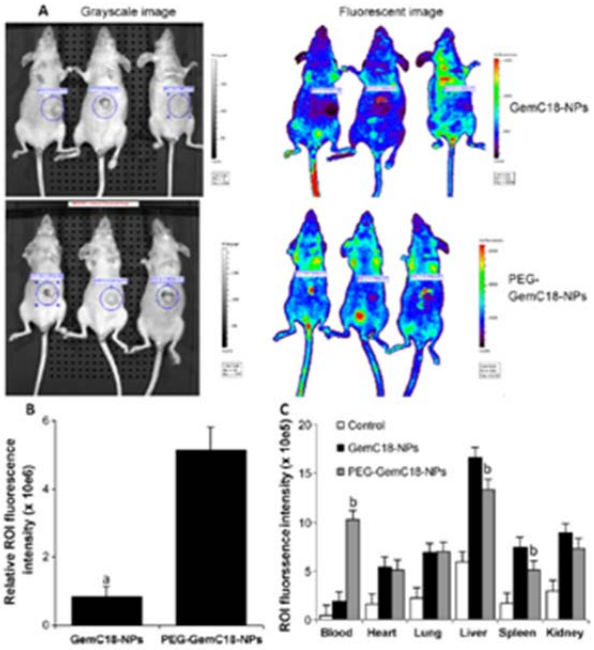

Figure 7. *In vivo* and *ex vivo* imaging of C_{18}-Gem and PEGylated C_{18}-Gem nanoparticles. (A) IVIS images of athymic mice 24 h after injection of fluorescein-labeled PEGylated or not C_{18}-Gem nanoparticles. (B) Relative fluorescence intensity values in BxPC-3 tumor (circular ROI in A). (C) Tissue distribution of fluorescein-labeled PEGylated or not C_{18}-Gem nanoparticles 24 h after injection. Reproduced with permission from ref. [56]

Remarkably, it has been shown that squalene (Sq), a natural and biocompatible lipid, can act as an efficient prodrug building block through its linkage to various drugs leading to self-stabilized prodrug nanoassemblies of diameters ranging from 100 to 300 nm.[61] This was first shown in 2006 with the design of Sq-Gem nanoassemblies.[62] These nanoconstructs displayed a specific supramolecular organization made of hexagonal molecular packing of Sq-Gem, resulting from the stacking of direct or inverse cylinders and demonstrated a promising *in vivo* activity on P388 tumor-bearing mice (Figure 8).[63]

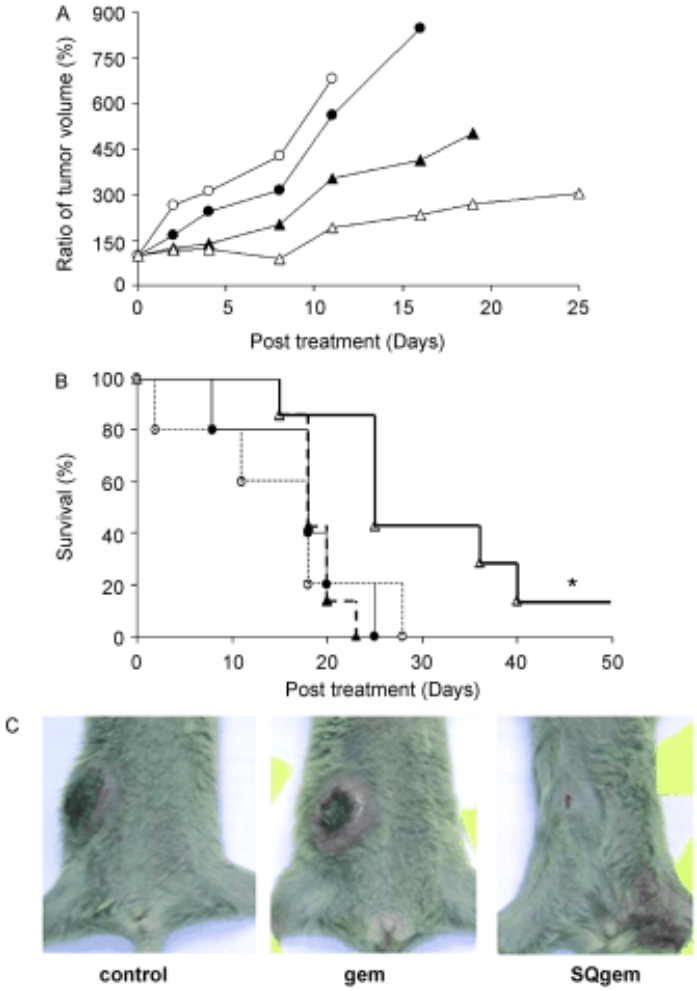

Figure 8. Anticancer activity of Sq-Gem nanoassemblies and free Gem (5 $mg.kg^{-1}$ equivalent doses) following intravenous treatment (on days 0, 4, 8, and 13) of mice bearing P388 subcutaneous tumours. (A) Tumour progression: Control (black spheres), saline (white spheres), Gem (black diamonds), Sq-Gem nanoassemblies (white diamonds). (B) Survival curve of mice: Control (solid line), saline (dotted line), gem (dashed line), Sq-Gem nanoassemblies (heavy solid line). (C) Photograph showing the difference in tumour growth in mice following the completion of indicated treatment. Reproduced with permission from ref.[63]

Compared to free Gem, Gem-Sq nanoassemblies presented also a 3-fold higher cytotoxicity *in vitro* and *in vivo* on murine resistant leukemia L1210 10K cells and in human leukemia resistant cell line CEM/ARAC8C, without altering blood parameters, even at doses higher than those typically used for anticancer evaluations.[64] Remarkably, these nanoassemblies displayed higher antiproliferative and cytotoxic effects than free Gem in chemoresistant human Panc1 tumor cells, decreased significantly the tumor growth, prevented tumor cell invasion and prolonged the survival time of tumor bearing mice.[65] From a pharmacokinetics viewpoint, the nanoassemblies triggered controlled and prolonged release of Gem and displayed considerably greater half-life (~4-fold) and mean residence time (~7.5-fold) compared to Gem administered as a free drug in mice.[66] The linkage of Gem to 1,1',2-trisnorsqualenic acid also noticeably delayed the metabolization of Gem into its inactive difluorodeoxyuridine (dFdU) metabolite, compared to Gem alone. Additionally, Sq-Gem nanoassemblies also underwent considerably higher distribution to the organs of the reticuloendothelial system, such as the spleen and the liver. These nanoassemblies were also orally administered in RNK-16 LGL leukemia-bearing rats and demonstrated higher intracellular accumulation and retention compared with free Gem.[67] It has to be noted that the toxicological profile of Sq-Gem nanoassemblies was similar to that of the parent drug, and that they did not display hepatotoxicity, which is one of the clinical encountered toxicities of Gem.[68] The potential candidature of Sq-Gem nanoassemblies for clinical trials was further supported by an *in vitro* evaluation on a 60 human tumor cell line panel performed under National Cancer Institute's Developmental Therapeutics Program, which demonstrated the high antiproliferative activity of the squalenoyl gemcitabine nanomedicine in a large panel of various cancer cells, suggesting its broad anticancer activity.[69] From a mechanistic point of view, it was shown that the cell uptake occurred through an albumin-enhanced diffusion of molecular Gem-Sq across the aqueous medium, rather than through a direct interaction between the nanoassemblies and the cells.[70] Further investigations revealed that Gem-Sq accumulated within cellular membranes, especially in those of the endoplasmic reticulum.[71] Besides, Gem was found to be directly delivered in the cell cytoplasm where it was converted to its biologically active triphosphate metabolite or exported from the cells through membrane transporters. Eventually, due to its amphiphilic nature, the cell uptake of Gem-Sq relied on its insertion into cellular membranes, which could lead to the formation of non-lamellar structures and to membrane permeation.[72]

Interestingly, PEGylation of Sq-Gem nanoassemblies was attempted through the co-self-assembly of Sq-Gem and Sq-PEG_{2000}.[73] Although the *in vitro* cytotoxic activity was preserved and even enhanced, the colloidal integrity of such nanoconstructs was significantly altered as the higher the Sq-PEG derivative amount, the lower the size of the resulting nanoassemblies. It was hypothesized that by anchoring through their Sq moiety, the PEG derivatives altered the organization of the nanoassemblies *via* the swelling of the inverted hexagonal phases. This issue was addressed by either: (i) the preparation of PEGylated liposomal formulations containing Gem-Sq[74] and (ii) the synthesis of short Gem-poly(squalene methacrylate) (Gem-PSqMA) conjugates by the RAFT technique, that led to stable nanoparticles upon PEGylation (**see Chapter III for more details**).[75] Very recently, fluorescent and targeted nanoparticles based on Gem-Sq have been prepared, using biotin as a cancer cell recognition ligand and rhodamine as a fluorescent moiety (Figure 9, **see also Chapter II for more details**).[76] The method was very simple and relied on the concomitant self-assembly of the different Sq-based building blocks to furnish stable multifunctional nanoparticles. They demonstrated improved internalization in different cancer cell lines (*e.g.*, MCF-7, M109, HeLa), as well as greater anticancer activity than non-functionalized Gem-Sq nanoparticles.

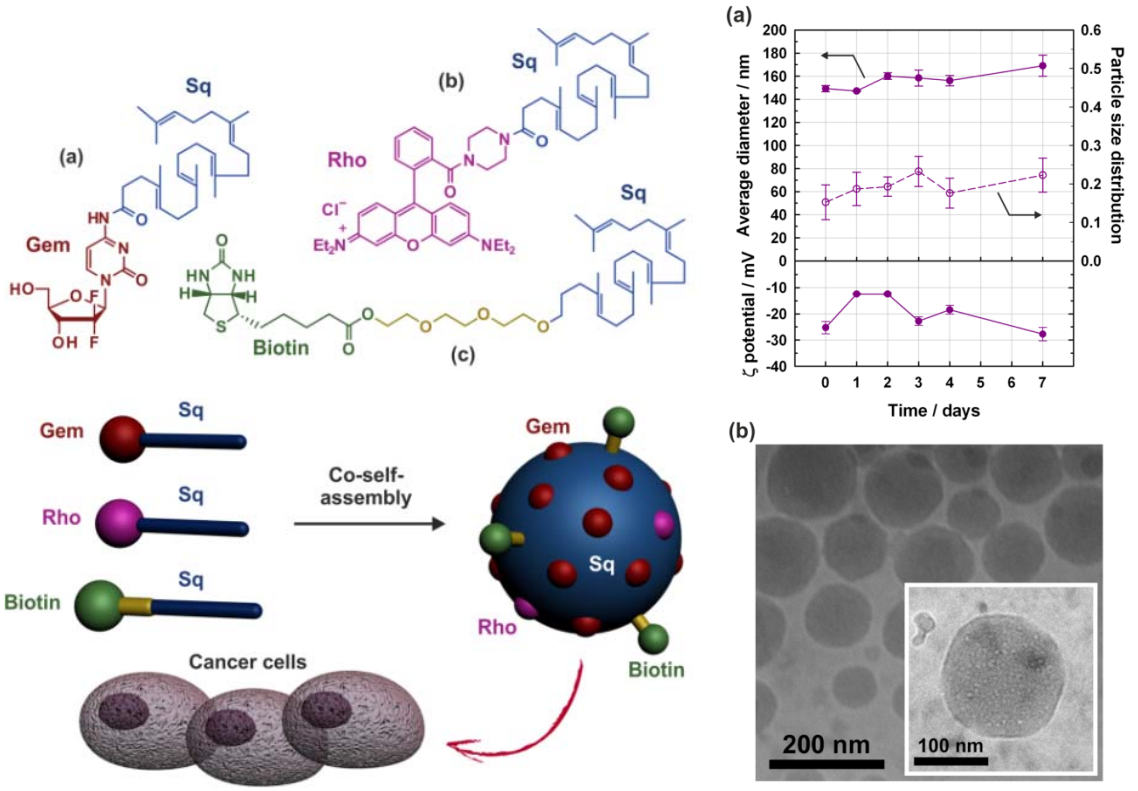

Figure 9. Left panel: structure of gemcitabine-squalene (Gem-Sq, a), rhodamine-squalene (Rho-Sq, b) and biotin-squalene (Biotin-Sq, c), and their co-self-assembly to prepare multifunctional nanoparticles for cancer cell targeting. Right panel: Evolution of the average diameter, the particle size distribution and the zeta potential with time (a), and cryogenic transmission electron microscopy images (b) of Gem-Sq/Biotin-Sq/Rho-Sq (86:9:5 wt.%) multifunctional nanoparticles. Adapted with permissions from ref. [76].

As an alternative to Gem-Sq, Sq-Gem monophosphate was synthesized using phosphoramidite chemistry and self-assembled into unilamellar nanostructures of 100 nm that displayed promising anticancer activity on non-resistant L1210 WT and resistant L1210 10K cell lines.[77-78] These results suggested that Sq conjugates of negatively charged nucleotide analogues efficiently penetrated into tumour cells. The versatility of the squalenoylation approach was also illustrated by the preparation of magnetic nanoassemblies through encapsulation of iron oxide for both magnetic guidance and imaging purposes.[32,79]

Others polyisoprenoid structures have been tested as prodrug building block for Gem, either molecular (*e.g.*, monoisoprenyl, geranylacetyl, prenylacetyl, farnesylacetyl)[80-81] or macromolecular such as short polyisoprene (PI) chains (**see Chapter IV for more details**).[82] It was shown that modulation of the polyisoprenoyl chain length has a great effect of the antitumor activity.[80] Interestingly, Gem-PI also led to significant *in vivo* anticancer activity on

MiaPaCa-2 tumor bearing mice, thus expanding this approach to polymer architectures (Figure 10).

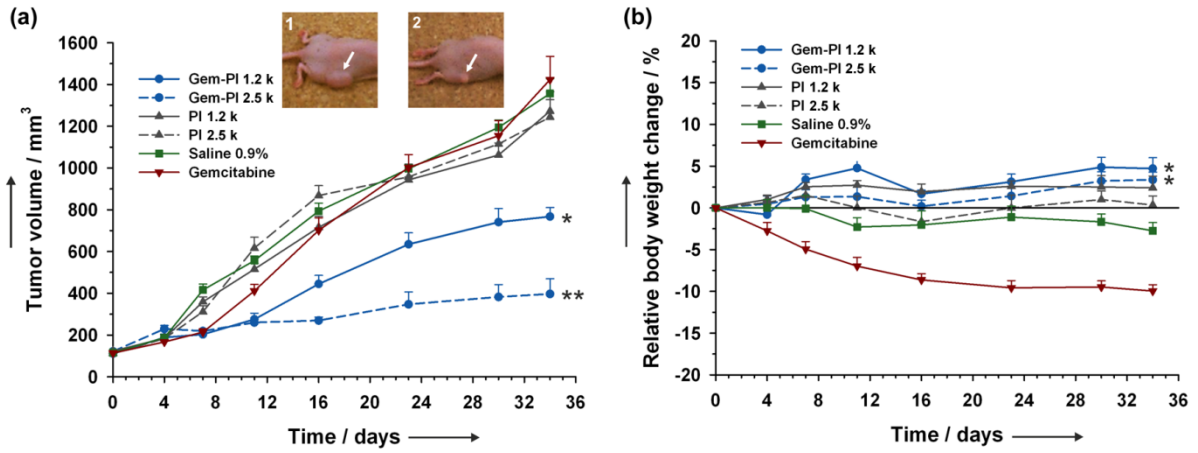

Figure 10. *In vivo* anticancer activity of gemcitabine (▼, 7 mg.kg^{-1}) and Gem-PI NPs (●, 1.2 kDa and 2.5 kDa, 7 mg.kg^{-1} Gem-equivalent dose) compared to control experiments (saline, PI), following i.v. treatment (on days 0, 4, 8 and 12) on mice bearing MiaPaCa-2 subcutaneous tumors. The values are the mean ± SD (n = 6). Reproduced with permissions from ref. [82].

2.3 DNA intercalators

DNA intercalators are used in chemotherapeutic treatments to inhibit DNA replication in rapidly growing cancer cells. Many drugs have been used as DNA intercalators, among them: Daunomycin (Cerubidine®, Daunoxome®), Doxorubicin (Adriblastine®, Caelyx®, Myocet®), Irinotecan (Camptosar®, Campto®), Topotecan (Hymcamtin®), Etoposide (Celltop®, Vepeside®) and Etoposide phosphate (Etopophos®).

Doxorubicin (Dox), an anthracycline widely used to treat solid and hematological tumors, has only been scarcely investigated as lipidic prodrug nanoparticles. The only one example reported the synthesis of Dox-Sq conjugate that formed nanostructures by self-assembly.[83] It was indeed discovered that the chemical linkage of Dox with Sq, led to the formation of Sq-Dox nanoassemblies of 130 nm mean diameter, but with an original "loop-train" structure. This new nanomedicine demonstrates: (i) high drug payload, (ii) decreased toxicity of the coupled anticancer compound, (iii) improved therapeutic response, (iv) use of biocompatible transporter material and (v) ease of preparation, all criteria which were not combined in the currently available nanodrugs. Cell culture viability tests and apoptosis assays showed that

Dox-Sq nanoassemblies displayed comparable antiproliferative and cytotoxic effects than the native doxorubicin, due to the high activity of apoptotic mediators such as caspase-3 and PARP. *In vivo* experiments have shown that the Dox-Sq nanomedicine dramatically improved the anticancer efficacy, as compared with free Dox. Particularly, the M109 lung tumors that did not respond to Dox treatment were found inhibited by 90% when treated with Dox-Sq nanoassemblies. Dox-Sq-treated MiaPaCa-2 pancreatic tumor xenografts in mice decreased by 95% compared to the tumors in the saline-treated mice, which was significantly higher than the 29% reduction achieved by native doxorubicin. Concerning toxicity, SQ-Dox nanoassemblies showed a five-fold higher maximum tolerated dose than the free drug, and moreover, the cardiotoxicity study has evidenced that Dox-Sq nanoassemblies did not cause any myocardial lesions such as those induced by the free doxorubicin treatment. Interestingly, they were also able to encapsulate iron oxide as imaging agent for theranostic purposes.[32]

In another study, **Pirarubicin** (also called THP-Doxorubicin), a Dox analogue, was derivatized with a palmitic acid moiety and further emulsified with a simple PEG-phosphatidylcholine derivative leading to nanoparticles of 30-50 nm in size.[84] The pharmacokinetic properties of the nanoparticles indicated accumulation of the drug at tumor sites.

Apolipoprotein E-enriched liposomes containing a lipophilic derivative of **daunorubicin**, another anthracycline, have been prepared by emulsification, and were intended to be recognized by low-density lipoprotein (LDL) receptors of cancer cells.[85] Compared to free daunorubicin, the targeted prodrug-containing liposomes had longer circulation half-life and led to a 5-fold higher accumulation in the liver when tested in rats with up-regulated hepatic LDL receptors.

Mitomycin C, a chemotherapeutic agent with antitumour antibiotic activity, has been turned into a *N*-(cholesteryloxycarbonyl)glycyl mitomycin C conjugate and then trapped into liposomes that showed significant antitumor activity against the L1210 leukemia cancer cells[86-87] and P 388 leukemia *in vitro*.[88] *In vivo* experiments showed that these prodrug-bearing liposomes inhibited the growth of subcutaneously-implanted Colon 26 adenocarcinoma and human mammary carcinoma MX-1 xenograft.[88] They also successfully maintained prodrug blood levels over a prolonged period of time, although their therapeutic efficacy was almost equal to that of the free prodrug in aqueous solution. A lipid prodrug

based on mitomycine C (2,3-(distearoyloxy)propane-1-dithio-4′-benzyloxycarbonyl-mitomycine C) was formulated in PEGylated liposomes exhibiting average diameters in the 43–90 nm range (Figure 11). They also gave significantly higher anticancer activity than free mitomycine C and than other drugs such as Dox and Gem in a Panc-1 model.[89] In addition, they led to enhanced antitumor effects, compared to PEGylated liposomal formulation of Dox (DOXIL) in M109R tumor model.[90]

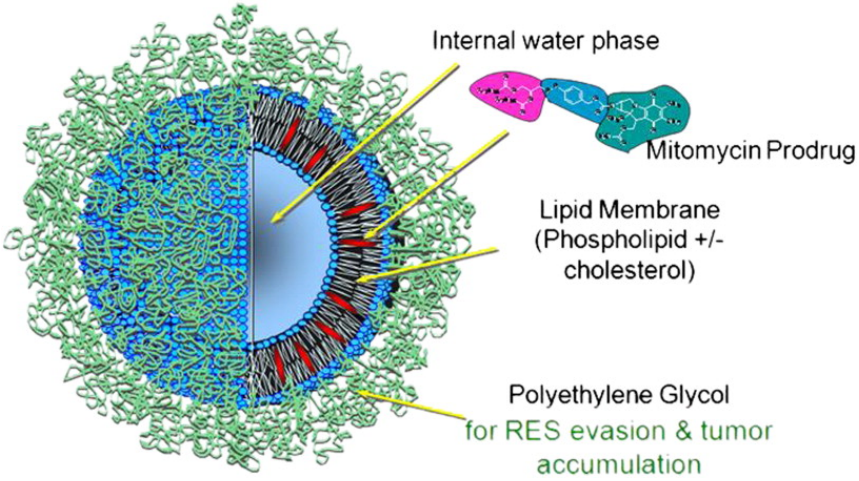

Figure 11. Lipid prodrug based on mitomycine C (2,3-(distearoyloxy)propane-1-dithio-4′-benzyloxycarbonyl- mitomycine C) formulated into PEGylated liposomes. Reproduced with permissions from ref. [89].

2.4 Antimitotic agents

Antimitotic agents (also termed mitotic inhibitors) are anticancer drugs that inhibit mitosis or cell division *via* disruption of microtubules. These drugs are used to treat different kinds of cancers including breast, lung, myelomas, lymphomas and leukemias. The most widely employed antimitotic inhibitors for prodrug design are **paclitaxel (Ptx)** and **doxetaxel (Dtx)**.

A series of lipophilic Ptx prodrugs has been synthesized by conjugating a succession of increasingly hydrophobic lipid anchors to the drug, using succinate or diglycolate cross-linkers and formulated in lipid nanoparticles stabilized by a PEG-*b*-PS stabilizer (Figure 12).[91] Although nanoparticles incorporating succinate prodrugs showed no evidence of efficacy in HT29 human colorectal tumor xenograph models, anticancer activity of diglycolate prodrug nanoparticles increased with the anchor hydrophobicity. They also provided significantly

enhanced therapeutic activity over commercially formulated paclitaxel at the maximum tolerated dose.

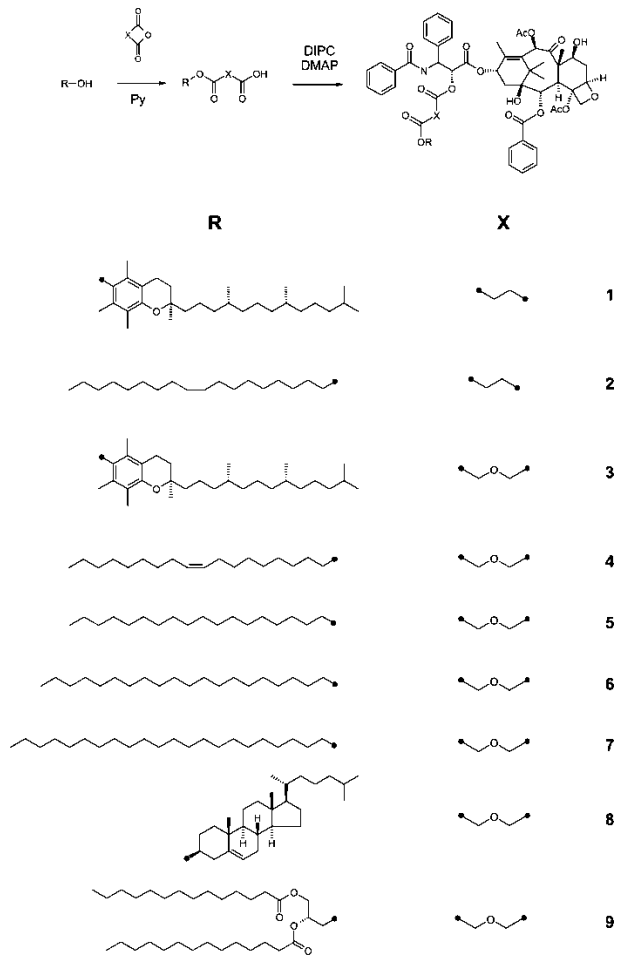

Figure. 12. Synthesis of lipophilic paclitaxel prodrugs. Reproduced with permissions from ref. [91].

Ptx oleate, another lipophilic derivative of Ptx, was encapsulated by oil/water lipid emulsion within nanoparticles of about 50 nm that gave effective cytotoxic activity against Hela cancer cells and promising pharmacokinetic data obtained in rabbits.[92] Ptx was also derivatized with behenic acid (2'-behenoyl-Ptx) and incorporated into SLN.[93] Preliminary biological assessments demonstrated that the prodrug-containing SLN were more efficient than Taxol in a subcultaneous 4T1 mouse mammary carcinoma model. A targeted system was also reported and consisted in folic-acid-decorated lipid nanoparticles containing Ptx-7-carbonyl-cholesterol (Tax-Chol) as a prodrug.[94] These nanoparticles showed greater uptake and cytotoxicity *in vitro* on FR-overexpressing KB and M109 tumor cells than the non-targeted counterparts. Further *in vivo* experiments with M109 tumor-bearing mice conducted to higher tumor growth inhibition and animal survival with the targeted system.

The above-mentioned "squalenoylation" strategy was also applied to Ptx whereby various Sq-linker-Ptx conjugates, differing from the nature of the spacer (*e.g.*, ester, succinyl, diglolyl, PEG_3, PEG_{11}), were synthesized in order to extract preliminary structure activity relationships.[95] It resulted that among all conjugates tested *in vitro*, the one with a diglycolate linker gave the best results. By tuning even further the nature of the linker between Ptx and Sq, it was shown that *cis,cis*-deca-5,8-dienoyl linker led to comparable cytotoxicity *in vivo* than the parent drug but revealed a much lower subacute toxicity.[96] Sq-Ptx also showed remarkable encapsulation into phospholipid bilayers of multilamellar vesicles compared to that of the free drug, suggesting this system to be considered as carrier for the prodrug.[97]

Dtx, another member of the Taxane family, is also usually difficult to encapsulate into liposomal formulations. To circumvent this issue, Dtx was derivatized with *N*-methyl-piperazinyl butanoic acid to form the corresponding lipid-based prodrug (2'-O-(*N*-methyl-piperazinyl butanoyl) docetaxel) that could be loaded up to 40% into liposomes.[98] When tested *in vivo* in a xenograft model of breast cancer in mice, the prodrug-loaded liposomes had a higher drug plasma level and were much more effective than Taxotere. Another lipid derivative of Dtx, 2'-(2-bromohexadecanoyl)-Dtx, was successfully entrapped up to 57% in liquid oil-filled lipid nanoparticles.[99] Interestingly, these nanoparticles showed greater cytotoxicity than free Dtx *in vitro* on 4T1 cancer cells. This was confirmed by *in vivo* experiments on 4T1 tumor-bearing mice with markedly greater anticancer efficacy and survival benefit over all control treatments.

2.5 Other anticancer drugs

Retinoids are known to exhibit anticancer activity again various types of cancers such as breast, prostate and colon. However, like other anticancer drugs, they face low bioavailability, low water solubility and fast clearance from the bloodstream. To solve these issues, various retinoids phospholipid prodrugs have been designed and formulated as liposomes that can be degraded by secretory phospholipase A2 IIA ($sPLA_2$) *via* hydrolysis of ester groups in the *sn*-2 position of glycerophospholipids (Figure 13).[100-101] For instance, when tested *in vitro* on HT-29 and Colo205 colon cancer cells, the formulated lipid prodrugs displayed, depending on the retinoid structure, IC_{50} values in the 3-19 μM range in the presence of $sPLA_2$ whereas no effect was obtained without this enzyme.[100] Interestingly, the enzymatic hydrolysis of the prodrug was accelerated upon premixing with DPPC, and the hydrolysis was further enhanced

by PEGylation.[101] However, the faster hydrolysis of the prodrug did not improve the cytotoxicity of the formulation. Note that this strategy was also applied to sPLA2 sensitive prostaglandin prodrug liposomes, even if cell death induction was also observed in the absence of the enzyme.[102] This concept was eventually applied to **capsaicin**, whereby its prodrug spontaneously formed SUVs of 66 nm in diameter in water and upon enzymatic activation released the drug by a cyclization reaction.[103]

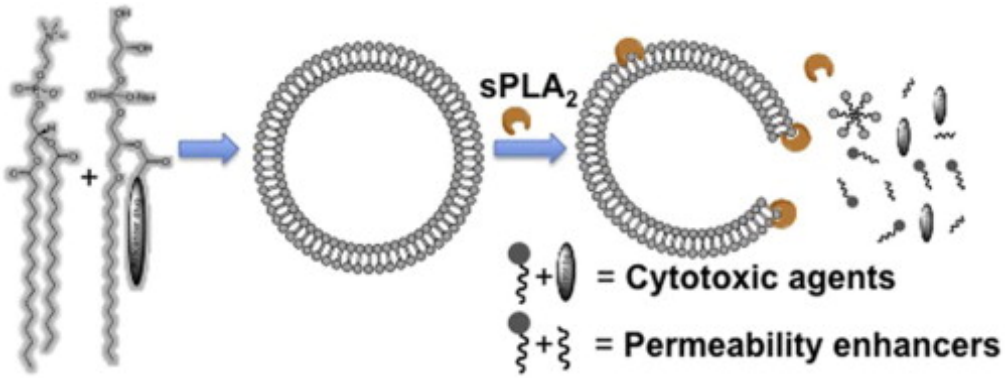

Figure 13. Liposomal formulation of retinoid prodrugs designed for enzyme triggered release. Reproduced with permission from ref. [101].

Other drug candidates have also been investigated. For instance, a lipidic prodrug of ruthenium complex that formed vesicles of 100 nm with multilamellar and unilamellar structures has been prepared *via* the synthesis of a new amphiphilic unimer able to coordinate ruthenium complexes.[104] Due to the potential applicability of ruthenium as anticancer drugs, this system may offer new perspectives in cancer therapy. A lipid prodrug of bisethylnorspermine (LS-BSP), using thiolytically sensitive dithiobenzyl carbamate linker, was also synthesized in order to function dually as gene delivery vector and, after intracellular degradation, as active pharmacologic agent that synergistically augmented the activity of a therapeutic gene in cancer.[105]

Finally, concerning nucleic acid delivery, the versatility of the "squalenoylation" approach has been recently illustrated by the synthesis of Sq-siRNA conjugates, *via* maleimide-sulfhydryl chemistry, against the junction oncogene RET/PTC1, usually found in papillary thyroid carcinoma (PTC).[106] The resulting nanoassemblies exhibited an average diameter of about 160 nm and were found to inhibit tumor growth and RET/PTC1 oncogene and oncoprotein expression.

3. Conclusion

The design of lipid anticancer prodrugs has appeared to be a promising strategy to circumvent many obstacles inherent to the administration of anticancer drugs, such as their relative fragility when they are in contact with biological fluids (drug deamination, metabolization, etc.), their poor encapsulation in colloidal nanocarriers (liposomes, polymer nanoparticles), and their high toxicity (due to the so-called 'burst release').

In the present review, we have covered the main strategies and results obtained in this field. From this literature survey, it appears that most of the well-established anticancer drugs (Gem, Dox, Ptx, cisplatin, Dtx, etc.), and/or their most used analogues, have been turned into lipid prodrugs and incorporated into different nanocarriers or even used themselves as nanocarrier materials. It is also interesting to note that there have been a plethora of different lipid structures that have been linked to anticancer drugs, thus showing the flexibility and the versatility of this general strategy. However, because it is often difficult to extract the most promising candidates from all the structures and nanoparticulate systems that have been reported so far, one can regret the lack of benchmarking investigations in order to rationalize all these results.

Remarkably, the 'squalenoylation' approach has focused a great deal of attention in the past few years. It has been extensively investigated and its efficiency has been clearly demonstrated *in vitro* and *in vivo* with different kinds of drugs (and also on different pathologies) and on various tumor models. This new nanomedicine approach may therefore be considered as a platform allowing great hope in the field of anticancer drug delivery. The starting point of my PhD thesis was the following: no functionalization strategies applied to squalene-based nanoassemblies was available and the PEGylation of such nanocarriers was not successful. These obstacles represented my two main objectives of the past three years.

4. References

1. Langer, R. *Nature* **1998,** *392*, 5.
2. Farokhzad, O. C.; Langer, R. *ACS Nano* **2009,** *3*, 16.
3. Peer, D.; Karp, J. M.; Hong, S.; Farokhzad, O. C.; Margalit, R.; Langer, R. *Nat. Nanotechnol.* **2007,** *2*, 751.
4. Couvreur, P.; Vauthier, C. *Pharm. Res.* **2006,** *23*, 1417.
5. Mura, S.; Couvreur, P. *Adv. Drug Delivery Rev.* **2012,** *64*, 1394.
6. Mura, S.; Nicolas, J.; Couvreur, P. *Nat. Mater.* **2013,** *12*, 991.

7. Sapsford, K. E.; Algar, W. R.; Berti, L.; Gemmill, K. B.; Casey, B. J.; Oh, E.; Stewart, M. H.; Medintz, I. L. *Chem. Rev.* **2013,** *113*, 1904.
8. Nicolas, J.; Mura, S.; Brambilla, D.; Mackiewicz, N.; Couvreur, P. *Chem. Soc. Rev.* **2013,** *42*, 1147.
9. Elsabahy, M.; Wooley, K. L. *Chem. Soc. Rev.* **2012,** *41*, 2545.
10. Kamaly, N.; Xiao, Z.; Valencia, P. M.; Radovic-Moreno, A. F.; Farokhzad, O. C. *Chem. Soc. Rev.* **2012,** *41*, 2971.
11. Bae, Y.; Kataoka, K. *Adv. Drug Delivery Rev.* **2009,** *61*, 768.
12. Al-Jamal, W. T.; Kostarelos, K. *Acc. Chem. Res.* **2011,** *44*, 1094.
13. Müller, R. H.; Mäder, K.; Gohla, S. *Eur. J. Pharm. Biopharm.* **2000,** *50*, 161.
14. Reddy, L. H.; Arias, J. L.; Nicolas, J.; Couvreur, P. *Chem. Rev.* **2012,** *112*, 5818.
15. Medina, S. H.; El-Sayed, M. E. H. *Chem. Rev.* **2009,** *109*, 3141.
16. Tekade, R. K.; Kumar, P. V.; Jain, N. K. *Chem. Rev.* **2008,** *109*, 49.
17. Farokhzad, O. C.; Cheng, J.; Teply, B. A.; Sherifi, I.; Jon, S.; Kantoff, P. W.; Richie, J. P.; Langer, R. *Proc. Natl. Acad. Sci. U. S. A.* **2006,** *103*, 6315.
18. Farokhzad, O. C.; Jon, S.; Khademhosseini, A.; Tran, T.-N. T.; LaVan, D. A.; Langer, R. *Cancer Res.* **2004,** *64*, 7668.
19. Hrkach, J.; Von Hoff, D.; Mukkaram Ali, M.; Andrianova, E.; Auer, J.; Campbell, T.; De Witt, D.; Figa, M.; Figueiredo, M.; Horhota, A.; Low, S.; McDonnell, K.; Peeke, E.; Retnarajan, B.; Sabnis, A.; Schnipper, E.; Song, J. J.; Song, Y. H.; Summa, J.; Tompsett, D.; Troiano, G.; Van Geen Hoven, T.; Wright, J.; LoRusso, P.; Kantoff, P. W.; Bander, N. H.; Sweeney, C.; Farokhzad, O. C.; Langer, R.; Zale, S. *Sci. Transl. Med.* **2012,** *4*, 128ra39.
20. Kolishetti, N.; Dhar, S.; Valencia, P. M.; Lin, L. Q.; Karnik, R.; Lippard, S. J.; Langer, R.; Farokhzad, O. C. *Proc. Natl. Acad. Sci. U. S. A.* **2010,** *107*, 17939.
21. Hamaguchi, T.; Kato, K.; Yasui, H.; Morizane, C.; Ikeda, M.; Ueno, H.; Muro, K.; Yamada, Y.; Okusaka, T.; Shirao, K.; Shimada, Y.; Nakahama, H.; Matsumura, Y. *Br. J. Cancer* **2007,** *97*, 170.
22. Chang, H. I.; Yeh, M. K. *Int J Nanomedicine* **2012,** *7*, 49.
23. Albert, A. *Nature* **1958,** *182*, 421.
24. Hsieh, P. W.; Hung, C. F.; Fang, J. Y. *Curr. Pharm. Des.* **2009,** *15*, 2236.
25. Rautio, J.; Kumpulainen, H.; Heimbach, T.; Oliyai, R.; Oh, D.; Jarvinen, T.; Savolainen, J. *Nat Rev Drug Discov* **2008,** *7*, 255.
26. Fang, J. Y.; Al-Suwayeh, S. A. *Expert Opin. Drug Deliv.* **2012,** *9*, 657.

27. Delplace, V.; Couvreur, P.; Nicolas, J. *Polym. Chem.* **2013**.
28. Pedersen, P. J.; Christensen, M. S.; Ruysschaert, T.; Linderoth, L.; Andresen, T. L.; Melander, F.; Mouritsen, O. G.; Madsen, R.; Clausen, M. H. *J. Med. Chem.* **2009,** *52*, 3408.
29. Vodovozova, E. L.; Kuznetsova, N. R.; Kadykov, V. A.; Khutsyan, S. S.; Gaenko, G. P.; Molotkovsky, Y. G. *Nanotechnol Russia* **2008,** *3*, 228.
30. Kozlov, A. M.; Korchagina, E. Y.; Vodovozova, E. L.; Bovin, N. V.; Molotkovskii, Y.; Syrkin, A. B. *Bull Exp Biol Med* **1997,** *123*, 381.
31. Kuznetsova, N. R.; Sevrin, C.; Lespineux, D.; Bovin, N. V.; Vodovozova, E. L.; Meszaros, T.; Szebeni, J.; Grandfils, C. *J. Control. Rel.* **2012,** *160*, 394.
32. Arias, J. L.; Reddy, L. H.; Othman, M.; Gillet, B.; Desmaële, D.; Zouhiri, F.; Dosio, F.; Gref, R.; Couvreur, P. *ACS Nano* **2011,** *5*, 1513.
33. Peters, G. J.; van der Wilt, C. L.; van Moorsel, C. J.; Kroep, J. R.; Bergman, A. M.; Ackland, S. P. *Pharmacol. Ther.* **2000,** *87*, 227.
34. Vodovozova, E. L.; Evdokimov, D. V.; Molotkovsky, J. G. *Russian Journal of Bioorganic Chemistry* **2004,** *30*, 599.
35. Gesto, D. S.; Cerqueira, N. M.; Fernandes, P. A.; Ramos, M. J. *Curr. Med. Chem.* **2012,** *19*, 1076.
36. Longley, D. B.; Harkin, D. P.; Johnston, P. G. *Nat. Rev. Cancer* **2003,** *3*, 330.
37. Yu, B. T.; Sun, X.; Zhang, Z. R. *Arch. Pharm. Res.* **2003,** *26*, 1096.
38. Sagnella, S. M.; Gong, X.; Moghaddam, M. J.; Conn, C. E.; Kimpton, K.; Waddington, L. J.; Krodkiewska, I.; Drummond, C. J. *Nanoscale* **2011,** *3*, 919.
39. Gong, X.; Moghaddam, M. J.; Sagnella, S. M.; Conn, C. E.; Danon, S. J.; Waddington, L. J.; Drummond, C. J. *Colloids and Surfaces B: Biointerfaces* **2011,** *85*, 349.
40. Gong, X.; Moghaddam, M. J.; Sagnella, S. M.; Conn, C. E.; Mulet, X.; Danon, S. J.; Waddington, L. J.; Drummond, C. J. *Soft Matter* **2011,** *7*, 5764.
41. van Borssum Waalkes, M.; van Galen, M.; Morselt, H.; Sternberg, B.; Scherphof, G. L. *Biochim. Biophys. Acta* **1993,** *1148*, 161.
42. Wang, J. X.; Sun, X.; Zhang, Z. R. *Eur. J. Pharm. Biopharm.* **2002,** *54*, 285.
43. Koning, G. A.; Morselt, H. W. M.; Velinova, M. J.; Donga, J.; Gorter, A.; Allen, T. M.; Zalipsky, S.; Kamps, J. A. A. M.; Scherphof, G. L. *Biochimica et Biophysica Acta (BBA) - Biomembranes* **1999,** *1420*, 153.
44. Koning, G. A.; Kamps, J. A.; Scherphof, G. L. *Cancer Detect Prev* **2002,** *26*, 299.

45. Hong, C. I.; Kirisits, A. J.; Nechaev, A.; Buchheit, D. J.; West, C. R. *J. Med. Chem.* **1990,** *33*, 1380.
46. Tokunaga, Y.; Iwasa, T.; Fujisaki, J.; Sawai, S.; Kagayama, A. *Chem. Pharm. Bull.* **1988,** *36*, 3574.
47. Schott, H.; Schwendener, R. A. *Anticancer Drug Des* **1996,** *11*, 451.
48. Sarpietro, M. G.; Ottimo, S.; Giuffrida, M. C.; Rocco, F.; Ceruti, M.; Castelli, F. *Int. J. Pharm.* **2011,** *406*, 69.
49. Hertel, L. W.; Boder, G. B.; Kroin, J. S.; Rinzel, S. M.; Poore, G. A.; Todd, G. C.; Grindey, G. B. *Cancer Res.* **1990,** *50*, 4417.
50. Immordino, M. L.; Brusa, P.; Rocco, F.; Arpicco, S.; Ceruti, M.; Cattel, L. *J Control Release* **2004,** *100*, 331.
51. Castelli, F.; Sarpietro, M. G.; Ceruti, M.; Rocco, F.; Cattel, L. *Mol. Pharm.* **2006,** *3*, 737.
52. Castelli, F.; Sarpietro, M. G.; Rocco, F.; Ceruti, M.; Cattel, L. *J. Colloid Interface Sci.* **2007,** *313*, 363.
53. Jin, Y.; Lian, Y.; Du, L. *Colloids and Surfaces A: Physicochemical and Engineering Aspects* **2012,** *393*, 60.
54. Brusa, P.; Immordino, M. L.; Rocco, F.; Cattel, L. *Anticancer Res.* **2007,** *27*, 195.
55. Chung, W. G.; Sandoval, M. A.; Sloat, B. R.; Lansakara, P. D.; Cui, Z. *J Control Release* **2012,** *157*, 132.
56. Sloat, B. R.; Sandoval, M. A.; Li, D.; Chung, W. G.; Lansakara, P. D.; Proteau, P. J.; Kiguchi, K.; DiGiovanni, J.; Cui, Z. *Int. J. Pharm.* **2011,** *409*, 278.
57. Jin, Y.; Lian, Y.; Du, L.; Wang, S.; Su, C.; Gao, C. *Int. J. Pharm.* **2012,** *430*, 276.
58. Sandoval, M. A.; Sloat, B. R.; Lansakara-P, D. S. P.; Kumar, A.; Rodriguez, B. L.; Kiguchi, K.; DiGiovanni, J.; Cui, Z. *J. Control. Rel.* **2012,** *157*, 287.
59. Zhu, S.; Li, X.; Lansakara, P. D.; Kumar, A.; Cui, Z. *J. Pharm. Pharmacol.* **2013,** *65*, 236.
60. Lansakara, P. D.; Rodriguez, B. L.; Cui, Z. *Int. J. Pharm.* **2012,** *429*, 123.
61. Desmaële, D.; Gref, R.; Couvreur, P. *J. Control. Rel.* **2012,** *161*, 609.
62. Couvreur, P.; Stella, B.; Reddy, L. H.; Hillaireau, H.; Dubernet, C.; Desmaële, D.; Lepêtre-Mouelhi, S.; Rocco, F.; Dereuddre-Bosquet, N.; Clayette, P.; Rosilio, V.; Marsaud, V.; Renoir, J.-M.; Cattel, L. *Nano Lett.* **2006,** *6*, 2544.
63. Couvreur, P.; Reddy, L. H.; Mangenot, S.; Poupaert, J. H.; Desmaele, D.; Lepetre-Mouelhi, S.; Pili, B.; Bourgaux, C.; Amenitsch, H.; Ollivon, M. *Small* **2008,** *4*, 247.

64. Reddy, L. H.; Dubernet, C.; Mouelhi, S. L.; Marque, P. E.; Desmaele, D.; Couvreur, P. *J. Control. Rel.* **2007,** *124*, 20.
65. Rejiba, S.; Reddy, L. H.; Bigand, C.; Parmentier, C.; Couvreur, P.; Hajri, A. *Nanomedicine* **2011,** *7*, 841.
66. Reddy, L. H.; Khoury, H.; Paci, A.; Deroussent, A.; Ferreira, H.; Dubernet, C.; Decleves, X.; Besnard, M.; Chacun, H.; Lepetre-Mouelhi, S.; Desmaele, D.; Rousseau, B.; Laugier, C.; Cintrat, J.-C.; Vassal, G.; Couvreur, P. *Drug Metab. Dispos.* **2008,** *36*, 1570.
67. Reddy, L. H.; Ferreira, H.; Dubernet, C.; Mouelhi, S. L.; Desmaele, D.; Rousseau, B.; Couvreur, P. *Anti-Cancer Drugs* **2008,** *19*, 999.
68. Reddy, L. H.; Marque, P.-E.; Dubernet, C.; Mouelhi, S.-L.; Desmaele, D.; Couvreur, P. *J. Pharmacol. Exp. Ther.* **2008,** *325*, 484.
69. Reddy, L. H.; Renoir, J.-M.; Marsaud, V.; Lepetre-Mouelhi, S.; Desmaële, D.; Couvreur, P. *Mol. Pharm.* **2009,** *6*, 1526.
70. Bildstein, L.; Marsaud, V.; Chacun, H.; Lepetre-Mouelhi, S.; Desmaele, D.; Couvreur, P.; Dubernet, C. *Soft Matter* **2010,** *6*, 5570.
71. Bildstein, L.; Dubernet, C.; Marsaud, V.; Chacun, H.; Nicolas, V.; Gueutin, C.; Sarasin, A.; Benech, H.; Lepetre-Mouelhi, S.; Desmaele, D.; Couvreur, P. *J. Control. Rel.* **2010,** *147*, 163.
72. Bildstein, L.; Pili, B.; Marsaud, V.; Wack, S.; Meneau, F.; Lepetre-Mouelhi, S.; Desmaele, D.; Bourgaux, C.; Couvreur, P.; Dubernet, C. *Eur. J. Pharm. Biopharm.* **2011,** *79*, 612.
73. Bekkara-Aounallah, F.; Gref, R.; Othman, M.; Reddy, L. H.; Pili, B.; Allain, V.; Bourgaux, C.; Hillaireau, H.; Lepetre-Mouelhi, S.; Desmaele, D.; Nicolas, J.; Chafi, N.; Couvreur, P. *Adv. Funct. Mater.* **2008,** *18*, 3715.
74. Pili, B.; Reddy, L. H.; Bourgaux, C.; Lepetre-Mouelhi, S.; Desmaele, D.; Couvreur, P. *Nanoscale* **2010,** *2*, 1521.
75. Bui, D. T.; Maksimenko, A.; Desmaele, D.; Harrisson, S.; Vauthier, C.; Couvreur, P.; Nicolas, J. *Biomacromolecules* **2013,** *14*, 2837.
76. Bui, D. T.; Nicolas, J.; Maksimenko, A.; Desmaele, D.; Couvreur, P. *Chem. Commun.* **2014**, DOI: 10.1039/c3cc47427e.
77. Caron, J.; Lepeltier, E.; Reddy, L. H.; Lepêtre-Mouelhi, S.; Wack, S.; Bourgaux, C.; Couvreur, P.; Desmaële, D. *Eur. J. Org. Chem.* **2011,** *2011*, 2615.
78. Caron, J.; Reddy, L. H.; Lepetre-Mouelhi, S.; Wack, S.; Clayette, P.; Rogez-Kreuz, C.; Yousfi, R.; Couvreur, P.; Desmaele, D. *Bioorg. Med. Chem. Lett.* **2010,** *20*, 2761.

79. Arias, J. L.; Reddy, L. H.; Couvreur, P. *Langmuir* **2008,** *24*, 7512.
80. Maksimenko, A.; Mougin, J.; Mura, S.; Sliwinski, E.; Lepeltier, E.; Bourgaux, C.; Lepêtre, S.; Zouhiri, F.; Desmaële, D.; Couvreur, P. *Cancer Lett.*, DOI. 10.1016/j.canlet.2012.08.023.
81. Mura, S.; Zouhiri, F.; Lerondel, S.; Maksimenko, A.; Mougin, J.; Gueutin, C.; Brambilla, D.; Caron, J.; Sliwinski, E.; LePape, A.; Desmaele, D.; Couvreur, P. *Bioconjugate Chem.* **2013**.
82. Harrisson, S.; Nicolas, J.; Maksimenko, A.; Bui, D. T.; Mougin, J.; Couvreur, P. *Angew. Chem., Int. Ed.* **2013,** *52*, 1678.
83. Maksimenko, A.; Dosio, F.; Mougin, J.; Ferrero, A.; Wack, S.; L., H. R.; Weyn, A. A.; Lepeltier, E.; Bourgaux, C.; Stella, B.; Cattel, L.; Couvreur, P. *Proc. Natl. Acad. Sci. U. S. A.* **2013**.
84. Hodoshima, N.; Udagawa, C.; Ando, T.; Fukuyasu, H.; Watanabe, H.; Nakabayashi, S. *Int. J. Pharm.* **1997,** *146*, 81.
85. Versluis, A. J.; Rump, E. T.; Rensen, P. C. N.; van Berkel, T. J. C.; Bijsterbosch, M. K. *J. Pharmacol. Exp. Ther.* **1999,** *289*, 1.
86. Sasaki, H.; Fukumoto, M.; Hashida, M.; Kimura, T.; Sezaki, H. *Chem Pharm Bull (Tokyo)* **1983,** *31*, 4083.
87. Sasaki, H.; Takakura, Y.; Hashida, M.; Kimura, T.; Sezaki, H. *J Pharmacobiodyn* **1984,** *7*, 120.
88. Tokunaga, Y.; Iwasa, T.; Fujisaki, J.; Sawai, S.; Kagayama, A. *Chem Pharm Bull (Tokyo)* **1988,** *36*, 3565.
89. Gabizon, A.; Amitay, Y.; Tzemach, D.; Gorin, J.; Shmeeda, H.; Zalipsky, S. *J. Control. Rel.* **2012,** *160*, 245.
90. Gabizon, A. A.; Tzemach, D.; Horowitz, A. T.; Shmeeda, H.; Yeh, J.; Zalipsky, S. *Clin. Cancer Res.* **2006,** *12*, 1913.
91. Ansell, S. M.; Johnstone, S. A.; Tardi, P. G.; Lo, L.; Xie, S.; Shu, Y.; Harasym, T. O.; Harasym, N. L.; Williams, L.; Bermudes, D.; Liboiron, B. D.; Saad, W.; Prud'homme, R. K.; Mayer, L. D. *J. Med. Chem.* **2008,** *51*, 3288.
92. Lundberg, B. B.; Risovic, V.; Ramaswamy, M.; Wasan, K. M. *J. Control. Rel.* **2003,** *86*, 93.
93. Ma, P.; Rahima Benhabbour, S.; Feng, L.; Mumper, R. J. *Cancer Lett.* **2013,** *334*, 253.
94. Stevens, P. J.; Sekido, M.; Lee, R. J. *Pharm. Res.* **2004,** *21*, 2153.

95. Dosio, F.; Reddy, L. H.; Ferrero, A.; Stella, B.; Cattel, L.; Couvreur, P. *Bioconjugate Chem.* **2010,** *21*, 1349.
96. Caron, J.; Maksimenko, A.; Wack, S.; Lepeltier, E.; Bourgaux, C.; Morvan, E.; Leblanc, K.; Couvreur, P.; Desmaële, D. *Advanced Healthcare Materials* **2013,** *2*, 172.
97. Sarpietro, M. G.; Ottimo, S.; Paolino, D.; Ferrero, A.; Dosio, F.; Castelli, F. *Int. J. Pharm.* **2012,** *436*, 135.
98. Zhigaltsev, I. V.; Winters, G.; Srinivasulu, M.; Crawford, J.; Wong, M.; Amankwa, L.; Waterhouse, D.; Masin, D.; Webb, M.; Harasym, N.; Heller, L.; Bally, M. B.; Ciufolini, M. A.; Cullis, P. R.; Maurer, N. *J. Control. Rel.* **2010,** *144*, 332.
99. Feng, L.; Benhabbour, S. R.; Mumper, R. J. *Advanced Healthcare Materials* **2013,** *2*, 1451.
100. Pedersen, P. J.; Adolph, S. K.; Subramanian, A. K.; Arouri, A.; Andresen, T. L.; Mouritsen, O. G.; Madsen, R.; Madsen, M. W.; Peters, G. n. H.; Clausen, M. H. *J. Med. Chem.* **2010,** *53*, 3782.
101. Arouri, A.; Mouritsen, O. G. *Eur. J. Pharm. Sci.* **2012,** *45*, 408.
102. Pedersen, P. J.; Adolph, S. K.; Andresen, T. L.; Madsen, M. W.; Madsen, R.; Clausen, M. H. *Bioorg. Med. Chem. Lett.* **2010,** *20*, 4456.
103. Linderoth, L.; Peters, G. H.; Madsen, R.; Andresen, T. L. *Angewandte Chemie International Edition* **2009,** *48*, 1823.
104. Vaccaro, M.; Del Litto, R.; Mangiapia, G.; Carnerup, A. M.; D'Errico, G.; Ruffo, F.; Paduano, L. *Chem. Commun.* **2009**, 1404.
105. Dong, Y.; Zhu, Y.; Li, J.; Zhou, Q.-H.; Wu, C.; Oupický, D. *Mol. Pharm.* **2012,** *9*, 1654.
106. Raouane, M.; Desmaele, D.; Gilbert-Sirieix, M.; Gueutin, C.; Zouhiri, F.; Bourgaux, C.; Lepeltier, E.; Gref, R.; Ben Salah, R.; Clayman, G.; Massaad-Massade, L.; Couvreur, P. *J. Med. Chem.* **2011,** *54*, 4067.

Chapitre II

Multifunctional squalene-based prodrug nanoparticles for targeted cancer therapy

Duc Trung Bui, Julien Nicolas, Andrei Maksimenko, Didier Desmaële, and Patrick Couvreur*

Chem. Commun. **2014**. DOI: 10.1039/c3cc47427e

Résumé

Dans ce chapitre, nous avons réussi à préparer des nanoparticules multifonctionnelles à base de Gem-Sq, qui sont à la fois fluorescentes *via* l'utilisation de la rhodamine (pour faire de l'imagerie et du suivi lors des expériences d'internalisation cellulaire) et biotinylées (pour cibler les récepteurs de la biotine hyper-exprimées à la surface de cellules cancéreuses). L'idée a été de préparer les composés conjugués (rhodamine-Sq, Gem-Sq et Biotin-Sq) puis de les co-auto-assembler à la stœchiométrie désirée, par nanoprécipitation en solution aqueuse, pour obtenir les nanoparticules multifonctionnelles (*i.e.*, thérapeutique, fluorescentes et ciblées).

Ces nanoparticules biotinylées ont montré une internalisation *in vitro* dans trois lignées cancéreuses connues pour sur-exprimer le récepteur à la biotine nettement plus importante que leurs homologues non-biotinylées. Du fait de ce ciblage actif à la biotine, nous avons également obtenu une meilleure efficacité thérapeutique.

1. Introduction

The medical application of nanotechnology, often termed nanomedicine, has witnessed a crucial impulse with the development of various types of drug-carriers.[1] The encapsulation of drugs into colloidal nanocarriers (*e.g.*, polymer nanoparticles, micelles, liposomes, etc.) has, indeed, resulted in intensive research and promising achievements in the last decade.[2-5] However, strong limitations still remain which may hamper their further translation to the clinic: (i) the "*burst release*", which corresponds to a rapid release of drug post-administration and can be harmful to patients; (ii) the encapsulation of poorly soluble drugs, exhibiting a high tendency to crystallization and (iii) the poor drug loadings (generally a few percent), that require the use of a large amount of nanocarrier materials, which can lead to prohibitive toxicity *in vivo*.

To resolve these issues, alternative strategies deriving from the prodrug[6] concept have recently been reported and hold great hope due to their ability to suppress the "*burst release*" and to enable easier and more efficient incorporation of drugs into nanocarriers. For instance, drugs can be covalently linked to amphiphilic block copolymers (mainly on the hydrophobic block that composes the core of the nanoparticle,[5] at the junction of the two polymer blocks[7]), or on the side chain of water-soluble polymers.[8-10] In the latter case, fully water-soluble conjugates or small-size aggregates are generally formed. Additionally, it has been shown that hydrophobic polymer chains can also be grown in a controlled fashion from drugs, leading to either hydrophobic polymer prodrugs further stabilized by PEG-based surfactants in case of hydrophobic drugs,[11,12] or amphiphilic polymer prodrugs that can self-assembled into nanoparticles when the drug is hydrophilic.[13,14] In the past few years, a novel approach has emerged, using squalene (Sq) –a lipidic precursor in the cholesterol's biosynthesis widely distributed in nature– as building block for the synthesis of drug-Sq conjugates, that can self-assemble in aqueous solution to form nanoassemblies with high drug payloads (~50 wt.%).[15,16] This approach has been applied to various drugs and has led to promising results *in vivo* against several pathologies.[17-20] However, this novel system is urgently lacking of an efficient targeting strategy that would enhance nanoparticle internalization by cancer cells *via* a receptor-mediated mechanism, thus avoiding potential side effects often faced with passive drug delivery strategies.

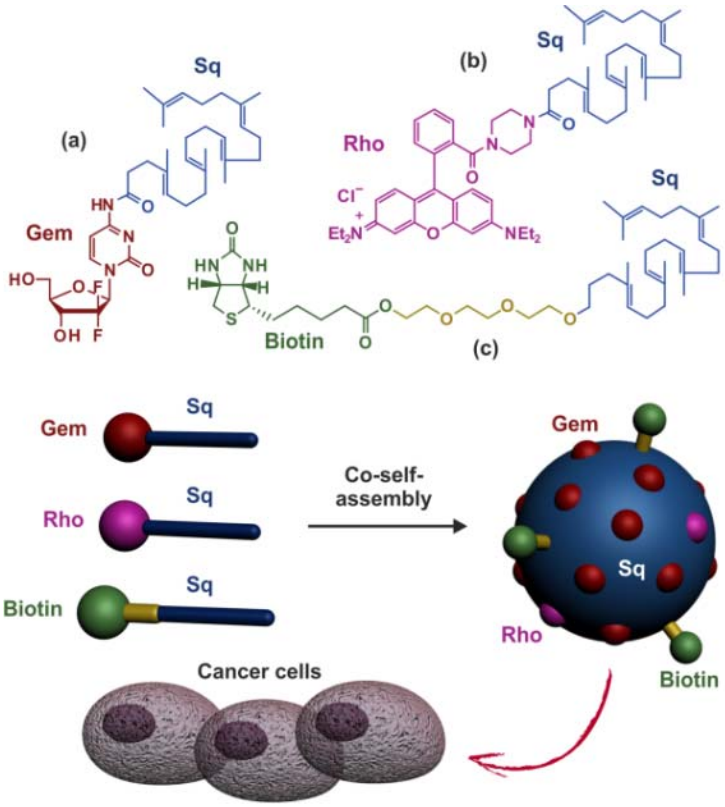

Scheme 1 Structure of gemcitabine-squalene (Gem-Sq, a), rhodamine-squalene (Rho-Sq, b) and biotin-squalene (Biotin-Sq, c), and their co-self-assembly to prepare multifunctional nanoparticles for cancer cell targeting.

Herein, we report an efficient and simple strategy to conceive multifunctional Sq-based nanoparticles (*i.e.*, therapeutic, fluorescent and targeted) based on the co-self-assembly of the different Sq-based functional components (Scheme 1), that is: (i) gemcitabine-squalene (Gem-Sq, a) owing to the demonstrated activity of Gem against a wide range of solid tumors;[21] (ii) rhodamine-squalene (Rho-Sq, b) due to advantageous properties of Rho (*e.g.*, high water-solubility, good photostability, etc.) and the retained fluorescence emission under a broad range of pH of its tertiary amide derivative,[22] and (iii) biotin-squalene (Biotin-Sq, c) in order to selectively target cancer cells *via* biotin receptors overexpressed at the surface of many cancer cells.[23]

2. Results and discussion

Rho-Sq was simply achieved in 90% yield by direct acylation of the piperazine-functionalized rhodamine-B[22] with the chloroformate mixed anhydride of trisnor-squalenic acid.† On the other hand, Biotin-Sq was obtained from conjugation of biotin to trisnorsqualenol through a short hydrophilic triethylene glycol linker (to promote surface ligand display from the

resulting nanoparticles) *via* Mitsunobu reaction.†

Multifunctional nanoparticles **N1*** were prepared by co-self-assembly of Gem-Sq, Biotin-Sq and Rho-Sq (86:9:5 wt.%) in aqueous solution *via* the nanoprecipitation technique. Average diameter, D_z, was 149 ± 3 nm with a narrow particle size distribution (PSD) of ~0.15, and a zeta (ζ) potential value of –25 ± 3 mV. Their colloidal stability was assessed over a period of at least 7 days, during which little variations of their colloidal characteristics were noticed (Fig. 1a). Cryogenic-transmission electron microscopy (Cryo-TEM) showed spherical morphologies and average diameters in good agreement with DLS data (Fig 1b). Interestingly, a thorough inspection of Cryo-TEM images showed internal organization of the nanoparticles, similarly to what has been previously observed with Gem-Sq nanoassemblies[16] (see insert in Fig. 1b).

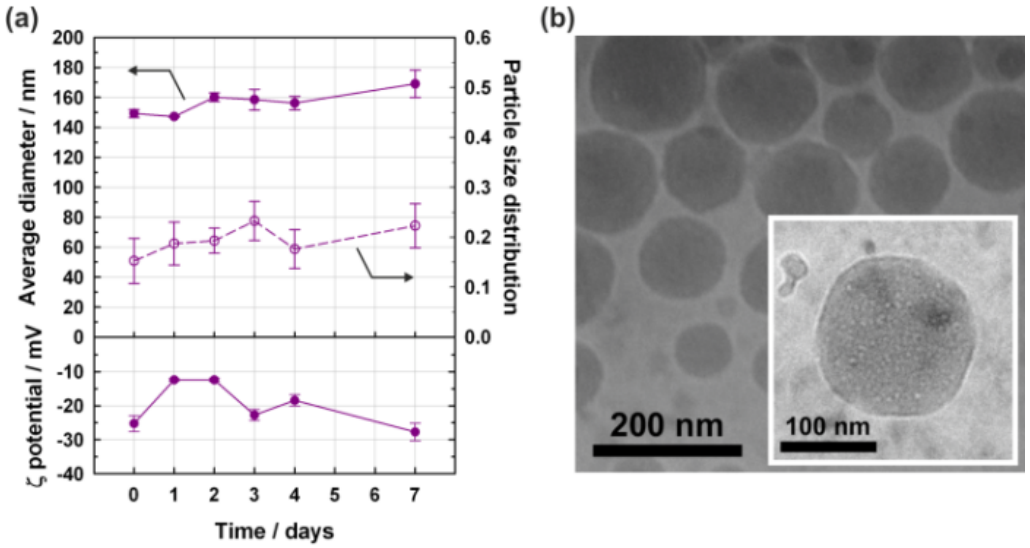

Figure 1 Evolution of the average diameter, the particle size distribution and the zeta (□) potential with time (a), and cryogenic transmission electron microscopy images (b) of Gem-Sq/Biotin-Sq/Rho-Sq (86:9:5 wt.%) multifunctional nanoparticles **N1***.

Three cancer cell lines; human breast adenocarcinoma cells (MCF7), murine lung cancer cells (M109) and human cervix carcinoma cells (HeLa), which overexpress biotin receptors,[23,24] were chosen to evaluate the tumor targeting ability of the multifunctional nanoparticles **N1*** and compared to non-biotinylated Gem-Sq/Rho-Sq nanoparticles **N1** (D_z = 120 nm, PSD = 0.19). After incubation at different time intervals, the cells were collected for analysis of rhodamine B fluorescence by flow cytometry. The results showed a higher cell fluorescence intensity of all three cell lines when biotin-decorated nanoparticles **N1*** were employed, as opposed to the treatment with **N1** (Fig. 2a–c). This demonstrated the surface availability of

biotin and the effectiveness of the targeting. When incubation was achieved for 4 h at 4°C, the cell fluorescence intensity of the all three cell lines was dramatically decreased down to very low values with both types of nanoparticles (Fig. 2d), suggesting an internalization rather governed by endocytosis.

The use of specific endocytosis inhibitors (chlorpromazine, Filipin III and amiloride, respectively associated to clathrin-mediated endocytosis, caveolae-mediated endocytosis and macropinocytosis),[25] suggested that the biotinylated nanoparticles were internalized by endocytosis; clathrin and caveolae-mediated endocytotic pathways being both involved (Fig. S2).† Conversely, non-functionalized nanoparticles were not affected by endocytosis blockers, in agreement with previous literature.[26]

Importantly, in order to demonstrate the integrity of the nanoparticles during *in vitro* experiments (*i.e.*, the absence of colloidal disassembly that would split up Rho-Sq, Gem-Sq and Biotin-Sq), a similar experiment was performed with a double fluorescence labelling by using Rho-Sq and Chol-BODIPY (Table S1).† Incubation of HeLa cells with the resulting dual fluorescent nanoparticles; either targeted **N2*** (Gem-Sq/Biotin-Sq/Rho-Sq/Chol-BODIPY) or not **N2** (Gem-Sq/Rho-Sq/Chol-BODIPY) was monitored by confocal microscopy through both fluorescence channels associated to rhodamine B and BODIPY. Whereas Rho-Sq/Chol-BODIPY dyes alone (**N3**) gave poor cell capture, nanoparticles **N2*** and **N2** led to similar cell internalization patterns two-by-two, whatever the fluorescence channel (*i.e.*, by following each dye individually) (Fig. S1).† Moreover, the improved internalization at 37°C of biotin-functionalized nanoparticles **N2*** compared to non-targeted counterparts **N2** was confirmed for both channels. At 4°C, very low cell internalization was again noted.

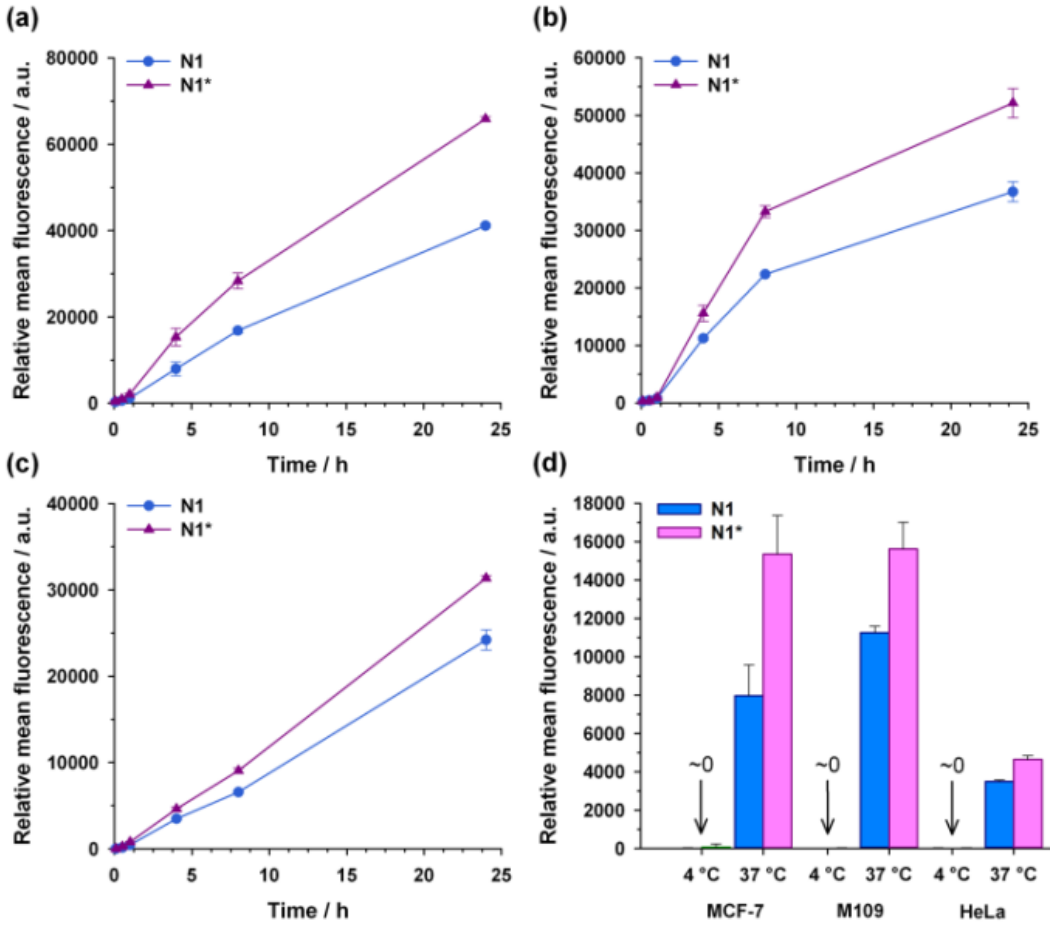

Figure 2 Kinetics of cell capture of non-functionalized (Gem-Sq/Rho-Sq) **N1** and biotin-functionalized (Gem-Sq/Biotin-Sq/Rho-Sq) **N1*** nanoparticles in MCF7 (a), M109 (b) and HeLa (c) cells. Fluorescence of cells after incubation of MCF7, M109 and HeLa cells with nanoparticles **N1** and **N1*** for 4 h at 4°C or 37°C (d).

Further confocal microscopy investigation showed multifunctional nanoparticles **N2*** localized intracellularly as endocellular and perinuclear fluorescent spots, suggesting an endo-lysosomal distribution. Noteworthy is the fact that the nearly perfect co-localization of the two fluorochromes, as attested by the overlay of the red and green fluorescence channels, suggested that the nanoparticles are likely to be still intact after 24 h of incubation (Fig. 3).

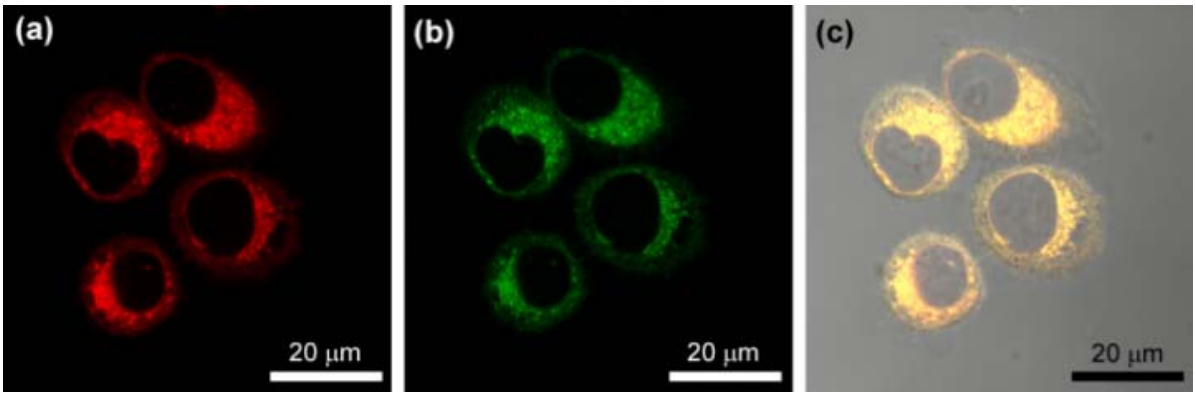

Figure 3 Confocal microscopy images [red (Rho, a) and green (BODIPY, b) fluorescence images] and merge of red and green fluorescence images with Nomarski image (c) after a 24 h incubation of HeLa cells with dual fluorescent Gem-Sq/Biotin-Sq/Rho-Sq/Chol-BODIPY **N2*** nanoparticles.

In order to assess the therapeutic effect of the targeted Sq-based nanoparticles **N1***, they were then tested for their *in vitro* anticancer activity on HeLa, M109 and MCF7 cancer cells by means of the MTT assay and compared to free Gem, Gem-Sq nanoparticles **N4** (D_z = 140 nm, PSD = 0.14) and control Biotin-Sq/Rho-Sq nanoparticles **N5** (see Table S1).† While control nanoparticles **N5** showed no cytotoxicity, targeted nanoparticles **N1*** exhibited superior anticancer activity for all three cell lines compared to Gem-Sq nanoparticles. Although improvement with M109 cells was rather modest, higher cytoxicity was observed on HeLa and MCF-7 cells. For instance, IC_{50} of targeted nanoparticles **N1*** was 330 ± 12 nM for HeLa cells, whereas Gem-Sq nanoparticles displayed an IC_{50} of 710 ± 42 nM. This shows that biotin-functionalized nanoparticles were able to enter cancer cells more efficiently, likely *via* biotin receptors, than non-functionalized nanoparticles. The observation that nanoparticles were less cytotoxic than free Gem was not surprising, due to their prodrug nature (*i.e.*, hydrolysis of the amide bond between Sq and Gem must occur to release of the active Gem), with however, IC_{50} values remaining in the nanomolar range. Note that the small amounts of Biotin-Sq and Rho-Sq in **N1*** are unlikely to alter the Gem release from Gem-Sq nanoparticles in biological media (Fig. 4).[8a]

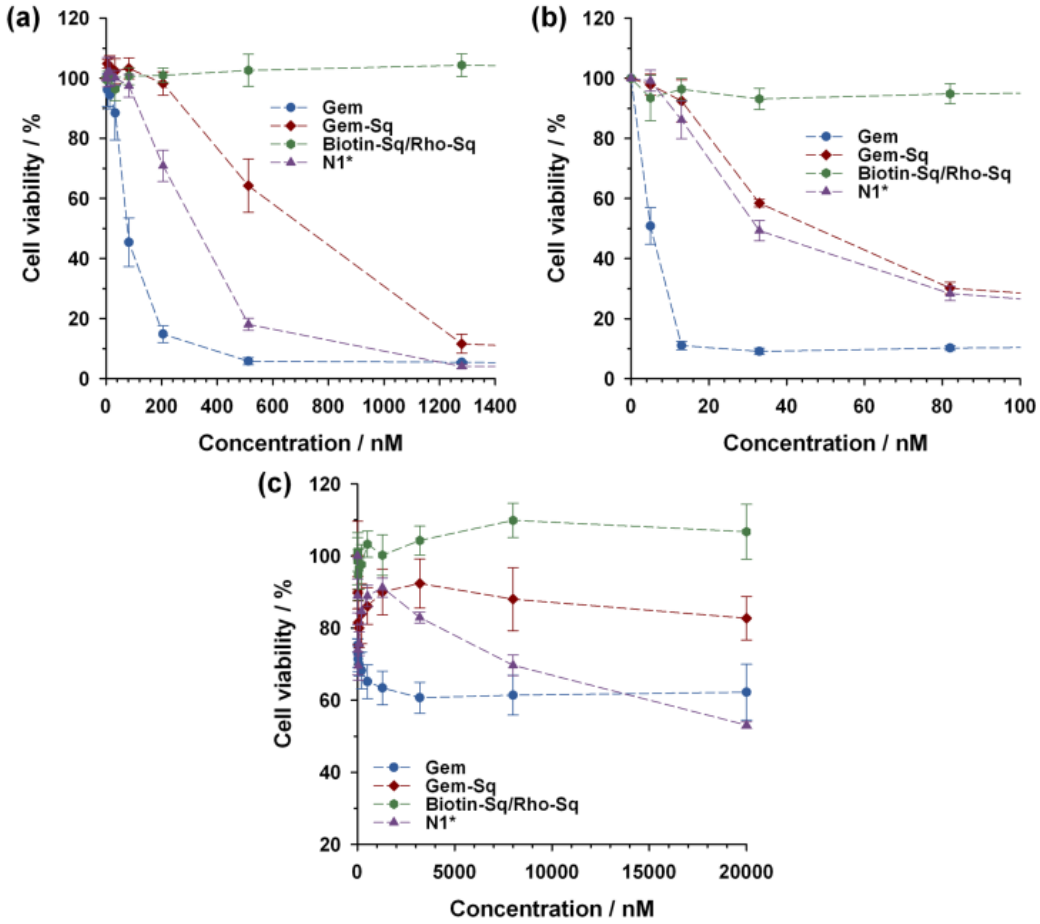

Figure 4 Viability assay (MTT test) on HeLa (a), M109 (b) and MCF-7 (c) cells with increasing concentrations of free Gem, Gem-Sq nanoparticles **N4**, Biotin-Sq/Rho-Sq nanoparticles **N5** and nanoparticles **N1***.

3. Conclusions

For the first time, therapeutic, fluorescent and targeted nanoparticles based on the naturally occurring Sq, using biotin as a cancer cell recognition ligand and rhodamine as a fluorescent moiety, have been prepared. The method is very simple and relied on the concomitant self-assembly of the different Sq-based building blocks to furnish stable multifunctional nanoparticles. They demonstrated improved internalization in different cancer cell lines as well as greater anticancer activity than non-functionalized Gem-Sq nanoparticles. This approach could be easily applied to other anticancer drugs (*e.g.*, nucleoside analogues, antifolic acid compounds, platinum-based compounds, etc.), fluorescent dies (UV-Vis- or near infrared-emitting) or biologically active ligands (*e.g.*, folic acid, anisamide, small peptidic sequences, etc.). Therefore, it paves the way to the design of various multifunctional Sq-based nanoparticles simply by changing the nature of the functional moiety linked to the Sq.

References

1. Farokhzad, O. C.; Langer, R. *ACS Nano* **2009,** 3, 16.
2. Elsabahy, M.; Wooley, K. L. *Chem. Soc. Rev.* **2012,** 41, 2545.
3. Torchilin, V. *Pharm. Res.* **2007,** 24, 1.
4. Samad, A.; Sultana, Y.; Aqil, M. *Curr. Drug Delivery* **2007,** 4, 297.
5. Nicolas, J.; Mura, S.; Brambilla, D.; Mackiewicz, N.; Couvreur, P. *Chem. Soc. Rev.* **2013,** 42, 1147.
6. Albert, A. *Nature* **1958,** 182, 421.
7. Bensaid, F.; Thillaye du Boullay, O.; Amgoune, A.; Pradel, C.; Harivardhan Reddy, L.; Didier, E.; Sablé, S.; Louit, G.; Bazile, D.; Bourissou, D. *Biomacromolecules* **2013,** 14, 1189.
8. Kopeček, J.; Kopečková, P. *Adv. Drug Delivery Rev.* **2010,** 62, 122.
9. Duncan, R. *Nat. Rev. Cancer* **2006,** 6, 688.
10. Vicent, M. J.; Duncan, R. *Trends Biotechnol.* **2006,** 24, 39.
11. Tong, R.; Cheng, J. *Angew. Chem., Int. Ed.* **2008,** 47, 4830.
12. Tong, R.; Cheng, J. *J. Am. Chem. Soc.* **2009,** 131, 4744.
13. Harrisson, S.; Nicolas, J.; Maksimenko, A.; Bui, D. T.; Mougin, J.; Couvreur, P. *Angew. Chem., Int. Ed.* **2013,** 52, 1678.
14. Bui, D. T.; Maksimenko, A.; Desmaele, D.; Harrisson, S.; Vauthier, C.; Couvreur, P.; Nicolas, J. *Biomacromolecules* **2013,** 14, 2837.
15. Couvreur, P.; Stella, B.; Reddy, L. H.; Hillaireau, H.; Dubernet, C.; Desmaële, D.; Lepêtre-Mouelhi, S.; Rocco, F.; Dereuddre-Bosquet, N.; Clayette, P.; Rosilio, V.; Marsaud, V.; Renoir, J.-M.; Cattel, L. *Nano Lett.* **2006,** 6, 2544.
16. Couvreur, P.; Reddy, L. H.; Mangenot, S.; Poupaert, J. H.; Desmaele, D.; Lepetre-Mouelhi, S.; Pili, B.; Bourgaux, C.; Amenitsch, H.; Ollivon, M. *Small* **2008,** 4, 247.
17. Arias, J. L.; Reddy, L. H.; Othman, M.; Gillet, B.; Desmae□le, D.; Zouhiri, F.; Dosio, F.; Gref, R.; Couvreur, P. *ACS Nano* **2011,** 5, 1513.
18. Reddy, L. H.; Khoury, H.; Paci, A.; Deroussent, A.; Ferreira, H.; Dubernet, C.; Decleves, X.; Besnard, M.; Chacun, H.; Lepetre-Mouelhi, S.; Desmaele, D.; Rousseau, B.; Laugier, C.; Cintrat, J.-C.; Vassal, G.; Couvreur, P. *Drug Metab. Dispos.* **2008,** 36, 1570.
19. Reddy, L. H.; Marque, P.-E.; Dubernet, C.; Mouelhi, S.-L.; Desmaele, D.; Couvreur, P. *J. Pharmacol. Exp. Ther.* **2008,** 325, 484.

20. Sémiramoth, N.; Meo, C. D.; Zouhiri, F.; Saïd-Hassane, F.; Valetti, S.; Gorges, R.; Nicolas, V.; Poupaert, J. H.; Chollet-Martin, S.; Desmaële, D.; Gref, R.; Couvreur, P. *ACS Nano* **2012,** 6, 3820.
21. Hertel, L. W.; Boder, G. B.; Kroin, J. S.; Rinzel, S. M.; Poore, G. A.; Todd, G. C.; Grindey, G. B. *Cancer Res.* **1990,** 50, 4417.
22. Nguyen, T.; Francis, M. B. *Org. Lett.* **2003,** 5, 3245.
23. Russell-Jones, G.; McTavish, K.; McEwan, J.; Rice, J.; Nowotnik, D. *J. Inorg. Biochem.* **2004,** 98, 1625.
24. Lee, E. S.; Na, K.; Bae, Y. H. *Nano Lett.* **2005,** 5, 325.
25. Hillaireau, H.; Couvreur, P. *Cell. Mol. Life Sci.* **2009,** 66, 2873.
26. Bildstein, L.; Marsaud, V.; Chacun, H.; Lepetre-Mouelhi, S.; Desmaele, D.; Couvreur, P.; Dubernet, C. *Soft Matter* **2010,** 6, 5570.

Supplementary Information

1. Materials

Tetrahydrofuran (THF) was distilled from sodium/benzophenone ketyl. Dimethylformamide (DMF) and dichloromethane (DCM) were distilled from calcium hydride, under a nitrogen atmosphere. All reactions involving air- or water-sensitive compounds were routinely conducted with a flame-dried glassware under a positive pressure of nitrogen. Diisopropyl azodicarboxylate (94%) was purchased from Acros Organics. Sodium hydride (95%), Filipin III (>85%), chlorpromazine (98%), DMA (5-(*N*,*N*-dimethyl) amiloride hydrochloride, triethylene glycol (99%), methanol (99.8%) and 3-[4,5-dimethylthiazol-2-yl]-3,5-diphenyl tetrazolium bromide (MTT) were purchased from Sigma-Aldrich Chemical Co., France. Gemcitabine, squalene, biotin (98%), triphenylphosphine (99%), ethyl chloroformate (97%), 4-dimethylaminopyridine (DMAP, 99%) and imidazole (99%) were purchased from Alfa-Aesar (A Johnson Matthey Co., France). RPMI 1640 GlutaMAX I, DMEM GlutaMAX I and fetal bovine serum were purchased from Dulbecco (Invitrogen, France). Penicillin and streptomycin solution were purchased from Lonza (Verviers, Belgium). Chemicals obtained from commercial suppliers were used without further purification. Rhodamine-B piperazine and trisnorsqualenyl methanesulfonate were synthesized as published elsewhere.[1,2]

2. Analytical methods

2.1 Nuclear magnetic resonance spectroscopy (NMR).

NMR spectroscopy was performed in 5 mm diameter tubes at 25 °C. ^{1}H and ^{13}C NMR spectroscopy were performed on a Bruker Avance 400 spectrometer at 400 MHz (^{1}H) or 100 MHz (^{13}C). The chemical shift scale was calibrated on the basis of the solvent peak. Recognition of methyl, methylene, methine, and quaternary carbon nuclei in ^{13}C NMR spectra rested on the *J*-modulated spin-echo sequence. ^{19}F NMR spectroscopy was performed on a Bruker 200 spectrometer at 188 MHz.

2.2 Transmission electron microscopy (TEM).

The morphology of the different nanoassemblies was examined by cryogenic transmission electron microscopy (Cryo-TEM). Briefly, 5 µL of the nanoparticle suspension (5 $mg.mL^{-1}$) was deposited on a Lacey Formvar/carbon 300 mesh copper microscopy grid (Ted Pella). Most of the drop was removed with a blotting filter paper and the residual thin film remaining

within the holes was vitrified by plunging into liquid ethane. Samples were then observed using a JEOL 2100HC microscope.

2.3 Dynamic light scattering (DLS) and zeta potential.

Nanoparticle diameters (D_z) and zeta potentials (ζ) were measured by dynamic light scattering (DLS) with a Nano ZS from Malvern (173° scattering angle) at a temperature of 25 °C. The surface charge of the nanoparticles was investigated by ζ-potential (mV) measurement at 25 °C, after dilution with 1 mM NaCl, using the Smoluchowski equation. Measurements were performed in triplicate following dilution of the nanoparticle suspensions in water.

3. Synthesis methods

3.1 Synthesis of 2-(2-(2-(((4*E*,8*E*,12*E*,16*E*)-4,8,13,17,21-pentamethyldocosa-4,8,12,16,20-oxy)ethoxy)ethoxy)ethanol (3). pentaen-1-yl)

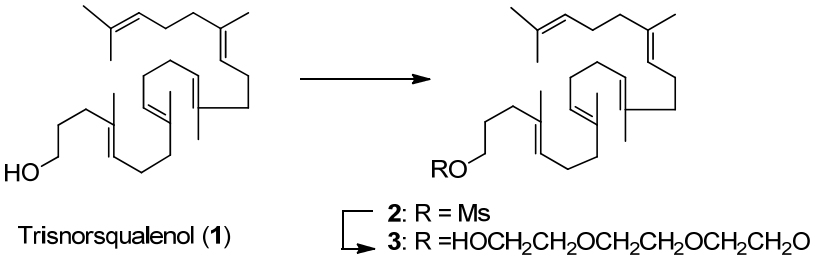

To an ice-cooled suspension of sodium hydride (190 mg, 7.5 mmol) in anhydrous THF (10 mL) was added dropwise a solution of triethylene glycol (1.13 g, 7.5 mmol). After 30 min at 0 °C, the hydrogen evolution has totally ceased and a solution of trisnorsqualenyl methanesulfonate (**2**) (700 mg, 1.5 mmol) in anhydrous THF (5 mL) was added dropwise. After being stirred at 20 °C for 1 day, the volatiles were removed under reduced pressure. The residue was taken up in water (10 mL) and extracted with ethyl acetate (4 × 20 mL). The combined organic layers were washed with brine, dried over $MgSO_4$ and concentrated under reduced pressure. The crude product was then purified by flash chromatography (SiO_2, petroleum ether/AcOEt 1:1) to give trisnorsqualenyl triethylene-glycol ether (**3**) (300 mg, 40%) as a colorless viscous oil. ^{1}H NMR (400 MHz, $CDCl_3$, δ in ppm) 5.18−5.05 (5H, m, *H*C=C(CH_3)CH_2), 3.74−3.70 (2H, m, HOC*H*$_2$$CH_2$), 3.69−3.55 (10H, m, HOCH_2C*H*$_2$, OC*H*$_2$C*H*$_2$O), 3.42 (2H, t, *J* = 6.8 Hz, OC*H*$_2$$CH_2$$CH_2$), 2.11−1.93 (16H, m, =C(CH_3)C*H*$_2$C*H*$_2$CH=), 1.67 (2H, m, CH_2C*H*$_2$$CH_2$C($CH_3$)), 1.67 (3H, s, HC=C(C*H*$_3$)$_2$), 1.59 (15H, s, HC=C(C*H*$_3$)); ^{13}C NMR (100 MHz, $CDCl_3$, δ in ppm) 135.2 (C, HC=*C*(CH_3)CH_2), 135.2 (C, HC=*C*(CH_3)CH_2), 135.0 (C, HC=*C*(CH_3)CH_2), 134.4 (C, HC=*C*(CH_3)CH_2), 131.3

(C, C=*C*(CH_3)$_2$), 124.7 (CH, H*C*=C(CH_3)$_2$), 124.5 (CH, H*C*=C(CH_3)CH_2), 124.4 (3CH, H*C*=C(CH_3)CH_2), 72.7 (CH_2, HO*C*H_2*C*H_2O), 71.2 (CH_2, O*C*H_2CH_2CH_2), 70.7 (CH_2, O*C*H_2*C*H_2O), 70.7 (CH_2, O*C*H_2*C*H_2O), 70.5 (CH_2, O*C*H_2*C*H_2O), 70.2 (CH_2, O*C*H_2*C*H_2O), 61.9 (CH_2, HO*C*H_2*C*H_2), 39.8 (3CH_2, =C(CH_3)*C*H_2CH_2CH=), 36.0 (CH_2, CH_2CH_2*C*H_2C(CH_3), 28.4 (2CH_2, =CH*C*H_2*C*H_2CH=), 27.9 (CH_2, CH_2*C*H_2CH_2C(CH_3), 26.9 (CH_2, =C(CH_3)CH_2*C*H_2CH=), 26.8 (2CH_2, =C(CH_3)CH_2*C*H_2CH=), 25.8 (CH_3, CH_2C=C(*C*H_3)$_2$), 17.8 (CH_3, CH_2C=C(*C*H_3)$_2$), 16.2 (2CH_3, =C(*C*H_3)CH_2), 16.1 (CH_3, =C(*C*H_3)CH_2), 16.0 (CH_3, =C(*C*H_3)CH_2); MS (+APCI) *m/z* (%): 519.5 (100) $[M + H]^+$.

3.2 Synthesis of 2-(2-(2-(((4*E*,8*E*,12*E*,16*E*)-4,8,13,17,21-pentamethyldocosa-4,8,12,16,20-pentaen-1-yl)oxy)ethoxy)ethoxy)ethyl 5-(2-oxohexahydro-1H-thieno[3,4-d]imidazol-4-yl)pentanoate (Biotin-Sq, 4).

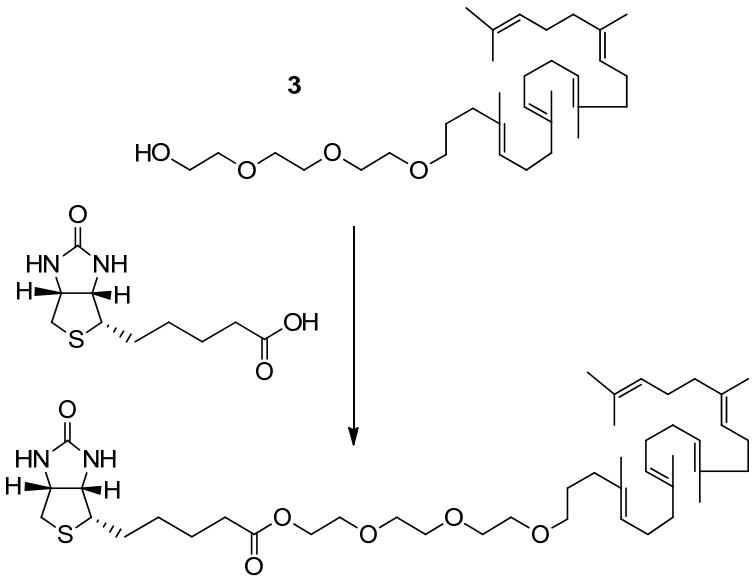

To an ice-cooled solution of biotin (145 mg, 0.59 mmol) and triphenylphosphine (156 mg, 0.59 mmol) in anhydrous DMF (8 mL) was added dropwise diisopropyl azodicarboxylate (127 mg, 7.5 mmol). The reaction mixture was stirred for 1 h and a solution of trisnorsqualenyl tri(ethylene glycol) ether (**3**) (200 mg, 0.39 mmol) in anhydrous DMF (2 mL) was added dropwise. After being stirred at 20 °C for 3 days, the volatiles were removed under reduced pressure. The residue was taken up in water (5 mL) and extracted with dichloromethane (3 × 10 mL). The combined organic layers were washed with brine, dried over $MgSO_4$ and concentrated under reduced pressure. The crude was then purified by flash chromatography (SiO_2, CH_2Cl_2/methanol 95:5) to give trisnorsqualenyl tri(ethylene glycol)

biotin ester (Biotin-Sq, **4**) (87 mg, 30%) as a colorless viscous oil. ^{1}H NMR (400 MHz, CD_3OD, δ in ppm) 5.18−5.06 (5H, m, *H*C=C(CH_3)CH_2), 4.49 (1H, ddd, *J* = 7.9 Hz, *J* = 5.0 Hz, *J* = 0.8 Hz, HNC*H*CH_2S), 4.31 (1H, dd, *J* = 7.9 Hz, *J* = 4.5 Hz, Hz, HNC*H*CHS), 4.24−4.19 (2H, m, $CO_2CH_2CH_2$), 3.72−3.68 (2H, m, $CO_2CH_2CH_2O$), 3.65−3.60 (6H, m, OCH_2CH_2O), 3.59−3.54 (2H, m, OCH_2CH_2O), 3.44 (2H, t, *J* = 6.6 Hz, $OCH_2CH_2CH_2$), 3.20 (1H, m, SC*H*CH_2), 2.93 (1H, dd, *J* = 12.8 Hz, *J* = 5.0 Hz, HNCHCH_2S), 2.70 (1H, d, *J* = 12.8 Hz, HNCHCH_2S), 2.37 (2H, t, *J* = 7.3 Hz, $CH_2CH_2CO_2$), 2.14−1.93 (18H, m, =C(CH_3)CH_2CH_2CH=, $OCH_2CH_2CH_2$(CH_3)C=), 1.80−1.55 (6H, m, SCHCH_2CH_2, $CH_2CH_2CO_2$), 1.67 (3H, s, HC=C(CH_3)$_2$), 1.61 (15H, s, HC=C(CH_3)), 1.47 (2H, q, *J* = 8.0 Hz, $CH_2CH_2CH_2CO_2$); ^{13}C NMR (100 MHz, CD_3OD) δ 175.2 (C, $CH_2CO_2CH_2$), 166.1 (C, NHCONH)*, 136.0 (2C, HC=C(CH_3)CH_2), 135.8 (C, HC=C(CH_3)CH_2), 135.5 (C, HC=C(CH_3)CH_2), 132.0 (C, C=C(CH_3)$_2$), 125.7 (CH, HC=C(CH_3)$_2$), 125.6 (2CH, HC=C(CH_3)CH_2), 125.5 (2CH, HC=C(CH_3)CH_2), 71.9 (CH_2, $OCH_2CH_2CH_2$), 71.62 ($2CH_2$, OCH_2CH_2O), 71.57 (CH_2, OCH_2CH_2O), 71.2 (CH_2, OCH_2CH_2O), 70.2 (CH_2, $CO_2CH_2CH_2O$), 64.6 (CH_2, $CO_2CH_2CH_2O$), 63.4 (CH, NHCHCHCH_2), 61.6 (CH, NHCHCH_2S), 57.0 (CH, NHCHCHCH_2), 41.0 (CH_2, NHCHCH_2S), 40.9 (CH_2, =C(CH_3)CH_2CH_2CH=), 40.8 ($2CH_2$, =C(CH_3)CH_2CH_2CH=), 37.1 (CH_2, $CH_2CH_2CH_2C(CH_3)$, 34.7 (CH_2, $CH_2CH_2CO_2$), 29.7 (CH_2, $CH_2CH_2CH_2CO_2$), 29.5 (CH_2, SCHCH_2CH_2), 29.2 ($2CH_2$, =CHCH_2CH_2CH=), 29.1 (CH_2, $CH_2CH_2CH_2C(CH_3)$, 27.8 (CH_2, =C(CH_3)CH_2CH_2CH=), 27.6 (CH_2, =C(CH_3)CH_2CH_2CH=), 27.6 (CH_2, =C(CH_3)CH_2CH_2CH=), 25.9 (CH_2, $CH_2CH_2CO_2$), 25.9 (CH_3, CH_2C=C(CH_3)$_2$), 17.8 (CH_3, CH_2C=C(CH_3)$_2$), 16.2 ($2CH_3$, =C(CH_3)CH_2), 16.1 (CH_3, =C(CH_3)CH_2), 16.1 (CH_3, =C(CH_3)CH_2); MS (+APCI) *m*/*z* (%): 745.6 (100) $[M + H]^+$.

*: HMBC detected.

3.3 Synthesis of rhodamine B 4-(1,1',2-trisnorsqualenoyl)piperazine (Rho-Sq, 7).

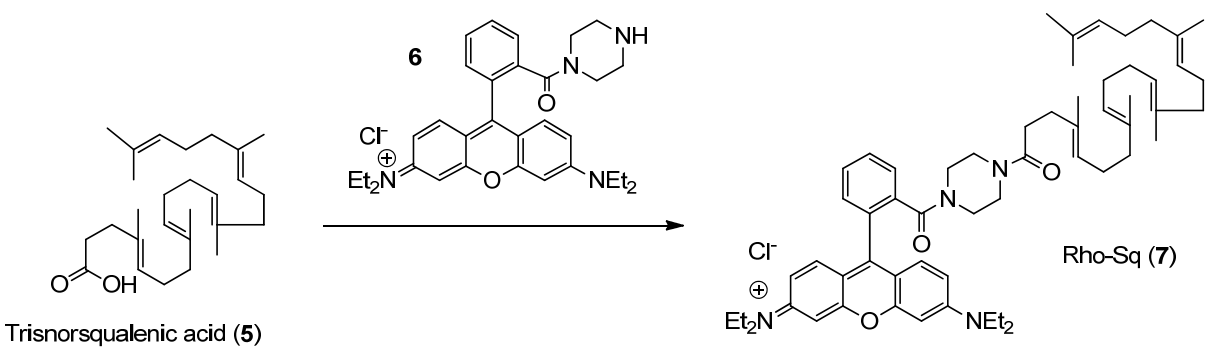

To a solution of trisnorsqualenic acid (**5**) (120 mg, 0.3 mmol) in anhydrous THF (2 mL) was added Et_3N (90 µL, 0.6 mmol). The mixture was cooled at 0 °C and a solution of ethyl chloroformate (30 µL, 0.33 mmol) in THF (1 mL) was added dropwise. The mixture was stirred for 30 min at 0 °C and a solution of rhodamine B piperazine (**6**) (181 mg, 0.33 mmol) in THF (1 mL) was added dropwise. After being stirred at 20 °C for 1 day, the volatiles were removed under reduced pressure. The residue was taken up in sat. $NaHCO_3$ aqueous solution (4 mL) and extracted with CH_2Cl_2 (3 × 15 mL). The combined organic layers were washed with brine, dried over $MgSO_4$ and concentrated under reduced pressure. The crude was then purified by flash chromatography (SiO_2, CH_2Cl_2/Methanol 90:10) to give rhodamine B 4-(1,1',2-trisnorsqualenoyl)piperazine (**7**) (231 mg, 90%) as a dark purple waxy solid. ^{1}H NMR (400 MHz, $CDCl_3$, δ in ppm) 7.78 (2H, m, H-4', H-5'), 7.70 (1H, dd, J = 6.6 Hz, J = 3.9 Hz, H-3'), 7.52 (1H, m, H-6'), 7.29 (2H, d, J = 9.5 Hz, H-1, H-8), 7.08 (2H, dd, J = 9.5 Hz, J = 2.4 Hz, H-2, H-7), 6.97 (2H, d, J = 2.4 Hz, H-4, H-5), 5.03−5.20 (5H, m, *H*C=C(CH_3)CH_2), 3.69 (8H, q, J = 7.1 Hz, $H_3CC\mathit{H}_2N$), 3.32−3.48 (8H, m, $NC\mathit{H}_2C\mathit{H}_2N$), 2.48−2.39 (2H, m, $NOCC\mathit{H}_2CH_2$), 2.24−2.16 (2H, m, $NOCCH_2C\mathit{H}_2$), 2.13−1.95 (16H, m, =C(CH_3)$C\mathit{H}_2C\mathit{H}_2$CH=), 1.66 (3H, s, HC=C($C\mathit{H}_3$)$_2$), 1.60 (3H, s, HC=C($C\mathit{H}_3$)), 1.59 (12H, s, HC=C($C\mathit{H}_3$)), 1.31 (12H, t, J = 7.1 Hz, H_3CCH_2N); ^{13}C NMR (100 MHz, CD_3OD, δ in ppm) 173.7 (C, N*C*OCH_2CH_2), 169.5 (C, Ar*C*ON), 159.3 (2C, C-4a, C-4b), 157.2 (2C, *C*NEt_2), 157.0 (C, C-9), 136.5 (2C, C-1', C-2'), 136.1 (C, HC=*C*(CH_3)CH_2), 135.9 (2C, HC=*C*(CH_3)CH_2), 134.8 (C, HC=*C*(CH_3)CH_2), 133.2 (2CH, C-1, C-8), 132.2 (C, C=*C*(CH_3)$_2$), 131.8 (CH, C-6'), 131.4 (CH, C-4' or C-5'), 131.3 (CH, C-4' or C-5'), 128.9 (CH, C-3), 126.3 (CH, H*C*=C(CH_3)$_2$, 125.7 (CH, H*C*=C(CH_3)CH_2), 125.5 (CH, H*C*=C(CH_3)CH_2), 125.4 (2CH, H*C*=C(CH_3)CH_2), 115.4 (2CH, C-2, C-7), 114.9 (2C, C-8a, C-9a), 97.4 (2CH, C-4, C-5), 48.1 (CH_2, N*C*H_2*C*H_2N)*, 46.9 (4CH_2, $H_3CC\mathit{H}_2N$), 46.2 (CH_2, N*C*H_2*C*H_2N)*, 42.5 (2CH_2, N*C*H_2*C*H_2N)*, 40.9 (CH_2, =C(CH_3)*C*H_2CH_2CH=), 40.8 (CH_2, =C(CH_3)*C*H_2CH_2CH=), 40.7 (CH_2, =C(CH_3)*C*H_2CH_2CH=), 36.1 (CH_2, $OCCH_2C\mathit{H}_2C(CH_3)$=), 29.2 (2$CH_2$, =CH*C*$H_2$*C*$H_2$CH=), 27.8 ($CH_2$, =C($CH_3$)$CH_2$*C*$H_2$CH=), 27.6 (2$CH_2$, =C($CH_3$)$CH_2$*C*$H_2$CH=), 25.9 ($CH_3$, C=C(*C*$H_3$)$_2$), 17.8 ($CH_3$, CH_2C=C(*C*H_3)$_2$), 16.2 (3CH_3, =C(*C*H_3)CH_2), 12.8 (4CH_3, $H_3C\mathit{C}H_2N$); MS (+APCI) *m*/*z* (%): 909.6 (16) [M – Cl + H_2O]$^+$, 893.9 (100) [M – Cl]$^+$.

*: HMBC detected.

3.4 Nanoparticle preparation

Nanoparticles were prepared by the nanoprecipitation technique. Nanoparticles **N1*** at 1 $mg.mL^{-1}$ were prepared as follows. Stock solutions of Gem-Sq (1 mg) in 0.1 mL of THF, Biotin-Sq (1 mg) in 0.1 mL of methanol and Rho-Sq (1 mg) in 0.1 mL of methanol were prepared. A mixed solution of Gem-Sq/Biotin-Sq/Rho-Sq (86:9:5 wt.%) was then prepared and 0.1 mL of this solution was added dropwise under vigorous stirring (500 rpm) to 1 mL of MilliQ water. Formation of the nanoparticles occurred spontaneously and stirring was continued for 3 min. The suspension was then transferred into a weighted round bottom flask and the solvents were evaporated at ambient temperature using a Rotavapor. Other nanoparticles were identically prepared and weight ratios were adjusted accordingly.

Table S1. Average Diameters and Particle Size Distributions (PSD) for the Different Nanoparticles Employed in this Study.

Expt.	Composition (x:y:z wt.%)	D_z (nm)	PSD[a]
N1*	Gem-Sq/Biotin-Sq/Rho-Sq (86:9:5)	149	0.15
N1	Gem-Sq/Rho-Sq (95:5)	120	0.19
N2*	Gem-Sq/Biotin-Sq/Rho-Sq/Chol-BODIPY (85:9:5:1)	94	0.20
N2	Gem-Sq/Rho-Sq/Chol-BODIPY (94:5:1)	101	0.17
N3	Rho-Sq/Chol-BODIBY (80:20)	98	0.17
N4	Gem-Sq	140	0.14
N5	Biotin-Sq/Rho-Sq (77:33)	261	0.18

[a]Particle size distribution determined by the DLS apparatus.

4. Biological activity

4.1 Cell lines and cell culture

Human breast adenocarcinoma cells (MCF-7) and human cervix carcinoma cells (HeLa) were obtained from the American Type Culture Collection. Murin lung tumor cells (M109) were obtained from the University of Florida, USA. All cell lines were maintained as recommended. Briefly, M109 cells were cultured in RPMI 1640 medium. MCF-7 and Hela cells were grown in Dulbecco's minimal essential medium (DMEM). All media were supplemented with 10% heat-inactivated foetal bovine serum (FBS) (56°C, 30 min), penicillin

(100 U.mL^{-1}) and streptomycin (100 µg.mL^{-1}). Cells were maintained in a humid atmosphere at 37 °C with 5% CO_2.

4.2 Cell internalization

To quantitatively measure the cell internalization of the nanoparticles, Hela, M109 and MCF-7 cells were cultured on 12-well plates for 24 h to achieve 60-80 % confluence. The different nanoparticle samples were then added at the concentration of 1 µM to each well. After incubation, the cells were collected at different time intervals for measurement of rhodamine B fluorescence. Cells were incubated for 4 h at 4 °C or 37 °C. The fluorescence from individual cells was examined using a flow cytometer C6 (**Accuri Cytometers Ltd., UK**). For fluorescence detection of nanoparticles, excitation was carried out with the 488-nm line of an argon laser, and emission fluorescence was measured between 560 and 606 nm. 10000 cells were measured in each sample. All experiments were set up in triplicate to determine means and SDs. For the experiment with the dual fluorescently labelled nanoparticles, emission of fluorescence was performed at 560 nm (rhodamine B) and 515 nm (BODIPY).

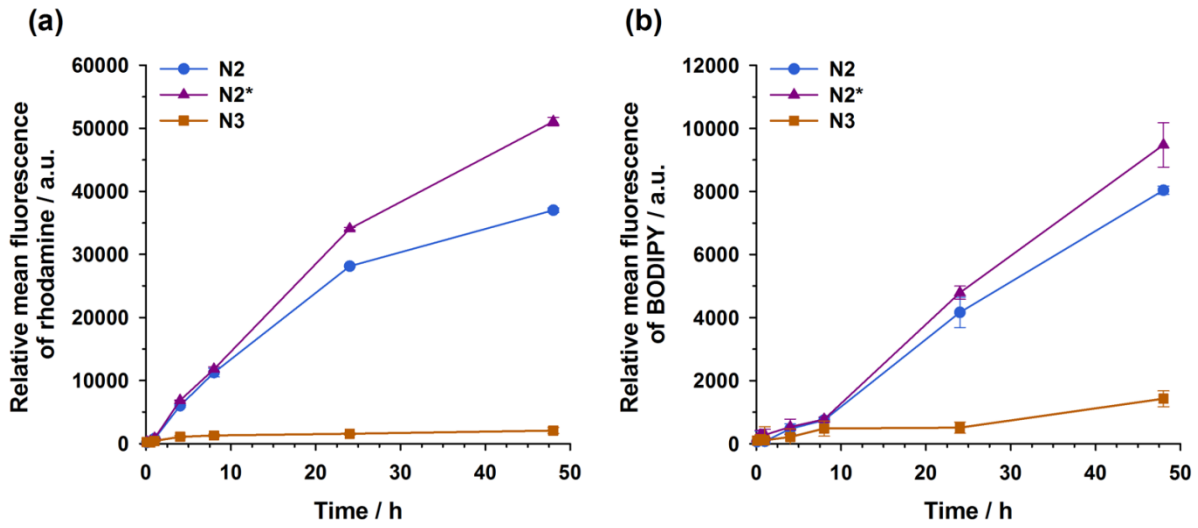

Figure S1. Kinetics of cell capture of non-functionalized (Gem-Sq/Rho-Sq/Chol-BODIPY) **N2** and biotin-functionalized (Gem-Sq/Biotin-Sq/Rho-Sq/Chol-BODIPY) **N2*** nanoparticles in HeLa cells at 37 °C monitored at 560 nm (a) and 515 nm (b).

For confocal microscopy experiment, Hela cells were cultured on a coverslip in a culture dish for 24 h to achieve approximately 40 % confluence. Cells were then incubated with different kinds of nanoparticles at the concentration of 10 µM at 37 °C for different time periods. After

incubation, the cells were washed with Dulbecco's PBS five times and imaged using a confocal laser scanning microscope LSM 510 META (Zeiss, Germany) equipped with a 1 mW Helium Neon laser and a Plan-Apochromat 63X objective lens (Numerical Aperture / 1.4, oil immersion). Excitation was carried out with the 488-nm line of an argon laser, and emission was performed at 560 nm (rhodamine B) and 515 nm (BODIPY).

4.3 *In vitro* anticancer activity

MTT [3-(4,5-dimethylthiazol-2-yl)-2,5-diphenyl tetrazolium bromide] was used to test the cytotoxic activity of the nanoparticles. Briefly, cells (5×10^3/well) were seeded in 96-well plates. After overnight incubation, the cells were exposed to different kinds of nanoparticles at a concentration of 1 $mg.mL^{-1}$ for 72 h. The medium was then removed and 100 µL of MTT solution (0.5 $mg.mL^{-1}$ in DMEM containing 10% FBS) were added to each well. The plates were incubated for 2 h at 37 °C and 100 µL of 20% SDS solution were then added to each well for 24 h at 37 °C. Absorbance was measured at 570 nm using a plate reader (Metertech Σ 960, Fisher Bioblock, Illkirch, France). The percentage of surviving cells was calculated as the absorbance ratio of treated to untreated cells. The inhibitory concentration 50% (IC_{50}) of the treatments was determined from the dose-response curve. All experiments were set up in quadruplicate to determine means and SDs.

4.4 Endocytosis in the presence of inhibitors

Hela cells were cultured in 24-well plates for 24 h to achieve 60-80 % confluence. The cells were then treated with endocytosis inhibitors (filipin III at 5 $\mu g.mL^{-1}$, chlorpromazine at 11 $\mu g.mL^{-1}$, and DMA (5-(*N,N*-dimethyl)amiloride hydrochloride) at 40 µM) for 30 min before their incubation with 1 µM of nanoparticles (either Sq-Gem/Chol-BODIPY at 99:1 wt.% or Sq-Gem/Biotin-Sq/Chol-BODIPY at 89:10:1 wt.%) for 6 h at 37°C. Cells were then washed with Dulbecco's PBS two times and treated with 0.25% trypsin for 10 min at 37°C. The fluorescence from individual cells was examined using a flow cytometer C6 (Accuri Cytometers Ltd., UK). For fluorescence detection of nanoparticles, excitation was carried out with the 488-nm line of an argon laser, and emission fluorescence was collected at 515 nm. 10000 cells were measured in each sample.

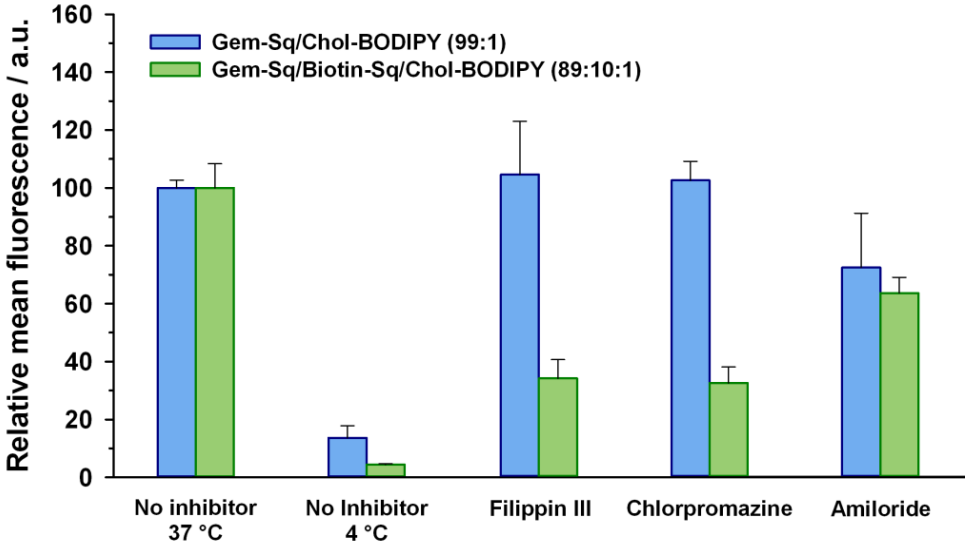

Figure S2. Internalization in Hela cells of Gem-Sq/Chol-BODIPY (99:1 wt.%) and (Gem-Sq/Biotin-Sq/Chol-BODIPY (89:10:1 wt.%) nanoparticles in the presence of endocytosis inhibitors by means of flow cytometry.

5. References

1. Nguyen, T.; Francis, M. B. *Org. Lett.* **2003,** 5, 3245.
2. Bekkara-Aounallah, F.; Gref, R.; Othman, M.; Reddy, L. H.; Pili, B.; Allain, V.; Bourgaux, C.; Hillaireau, H.; Lepetre-Mouelhi, S.; Desmaele, D.; Nicolas, J.; Chafi, N.; Couvreur, P. *Adv. Funct. Mater.* **2008,** 18, 3715.

Chapitre III

Polymer prodrug nanoparticles based on naturally occurring isoprenoid for anticancer therapy

Bui Duc Trung, Andrei Maksimenko, Didier Desmaële, Simon Harrisson, Christine Vauthier, Patrick Couvreur, Julien Nicolas[*]

Biomacromolecules **2013**, *14*, 2837–2847

Résumé

Dans ce chapitre, nous nous sommes proposé de résoudre le problème de la PEGylation observé avec les conjugués de Gem-Sq. Pour ce faire, nous avons développé une nouvelle famille de prodrogues macromoléculaires capables de s'auto-assembler sous la forme de nanoparticules. Afin de résister à la PEGylation via l'addition de Sq-PEG durant la nanoprécipitation de la Gem-Sq, l'idée a été de coupler à la Gem un polymère à base de squalène pour augmenter l'hydrophobie du « segment squalène ». Pour ce faire, nous avons utilisé la méthode « drug-induced polymerization » en faisant croitre de manière contrôlée par la technique RAFT (polymérisation radicalaire contrôlée par transfert de chaîne réversible par addition-fragmentation) le polymère à partir de la Gem.

En pratique, nous avons couplé la Gem à un agent RAFT puis polymérisé le squalène methacrylate (SqMA) pour obtenir une petite librairie de composés conjugués de type Gem-PSqMA de masses molaires variables. Ces derniers ont donné par auto-assemblage des nanoparticules stables avec des activités anticancéreuses importantes sur différentes lignées cellulaires. Pour conférer des propriétés de furtivité à ces nanoparticules, leur PEGylation a été entreprise avec succès et confirmé par XPS et par des tests d'activation du complément. Il a également été montré que les nanoparticules PEGylées pouvaient être internalisées dans les cellules cancéreuses de façon plus importante que leurs homologues non PEGylées.

1. Introduction

Drug-loaded polymer nanoparticles or micelles are promising drug delivery systems for the treatment of severe diseases such as cancer, infections and neurodegenerative disorders.[1-5] Encapsulation in nanoparticles allows the drug to be protected from metabolization and/or rapid clearance from the body, while protecting healthy tissues from the drug's inherent cytotoxicity. These nanocarriers are typically obtained by drug encapsulation during the self-assembly of amphiphilic copolymers in aqueous solution. Due to the flexibility offered by macromolecular synthesis methods, a plethora of polymeric nanocarriers have been engineered so far and evaluated against different pathologies *in vitro* and *in vivo*.[1,6] Although promising results have been witnessed, most of these drug delivery systems face strong limitations which may hamper their further translation to the clinic and eventually to the market: (i) the "*burst release*", in which a large fraction of adsorbed drug is quickly released post-administration, can lead to prohibitive toxicity *in vivo*; (ii) the encapsulation of poorly soluble drugs exhibiting a high tendency to crystallization often requires the use of additional organic co-solvents during nanocarrier preparation; (iii) the poor drug loading, generally only a few percent, usually necessitates a high concentration of nanocarrier to obtain a noticeable therapeutic effect, which can itself be harmful to patients.

Alternative strategies, derived from the prodrug concept, may alleviate some of the above-mentioned drawbacks witnessed with polymeric nanoparticulate systems. For instance, drugs have been covalently linked to preformed amphiphilic copolymers, leading to a sustained anticancer drug release from the nanoparticles by hydrolysis.[7-12] Alternatively, Stenzel and co-workers have reported block copolymer micelles with pendant bifunctional chelators for platinum drugs, which are released by chlorine-ion mediated ligand exchange.[13-15] There are also many reports on the conjugation of hydrophobic drugs to the side chain of water-soluble polymers, resulting in fully water-soluble conjugates or small-size aggregates.[16-23]

Polymers can also be grown directly from drugs. Cheng and co-workers employed hydroxy-containing anticancer drugs (*e.g.*, paclitaxel, doxorubicin, docetaxel, camptothecin) as initiators for the ring opening polymerization of lactide (LA)[24-26] or phenyl *O*-carboxyanhydride (Phe-OCA)[27] using Zn- or Mg-based catalysts. Co-self-assembly of the resulting conjugates with PLGA-*b*-PEG or P(Phe-OCA)-*b*-PEG, respectively, furnished stabilized nanoparticles of drug-polymer conjugates with controlled drug release profiles.

We recently demonstrated that well-defined amphiphilic macromolecular prodrugs prepared by nitroxide-mediated polymerization (NMP)[28] of isoprene (polyisoprene being biocompatible)[29] from an anticancer drug initiator, form stable, narrowly dispersed nanoparticles with high drug payloads and remarkable *in vitro* and *in vivo* anticancer activity.[30] This method is, in principle, applicable to any kind of controlled/living radical polymerization (CLRP) technique and drug/polymer pair, provided that the drug and polymer have substantially different solubilities for self-stabilization purposes.

Recently, squalene (Sq), a lipidic precursor in cholesterol biosynthesis that is widely distributed in nature, has been employed as building block for the synthesis of molecular prodrugs, which self-assemble in aqueous solution to form supramolecular nanostructures.[31] This approach has been applied to various drugs and has led to promising results *in vivo* against several pathologies,[32-36] but is limited by the rigidity of the synthetic pathway (*e.g.*, no structural variation of the squalene moiety, poor modulation of the conjugate hydrophilic-lipophilic balance) as well as colloidal disassembly upon PEGylation.[37]

By combining the use of natural isoprenoids as drug delivery vehicle components and '*grafting from*' drugs under CLRP conditions, we propose a general approach to well-defined macromolecular prodrug nanoparticles based on squalene for anticancer therapy. For this purpose, a methacrylate monomer based on squalene (SqMA) was designed and polymerized by reversible addition fragmentation chain transfer (RAFT)[38] in the presence of a RAFT agent bearing gemcitabine (Gem), a nucleoside analogue with demonstrated activity against a wide range of solid tumors (*e.g.*, colon, lung, pancreatic, breast, bladder and ovarian cancers).[39] This furnished narrow polydispersity Gem-PSqMA polymers of tunable molar masses with chain-end Gem and pending Sq moieties (Figure 1). The resulting nanoparticles exhibited significant anticancer activity *in vitro* on various cancer cell lines. Preliminary structure-activity relationships could be extracted by modulating the polymer chain length. In order to confer stealth properties, a robust PEGylation strategy was also reported (Figure 1) and accounted for a significant reduction of complement activation compared to non-PEGylated counterparts. Finally, the influence of PEGylation on nanoparticle cytotoxicity and cell internalization is discussed. Importantly, this study: (i) broadens the range of the newly created family of macromolecular prodrug nanoparticles; (ii) clearly shows the versatility of the synthetic concept; (iii) establishes an easier and more flexible pathway toward squalene-based nanoassemblies with improved *in vitro* anticancer activities and (iv) demonstrates their first successful PEGylation.

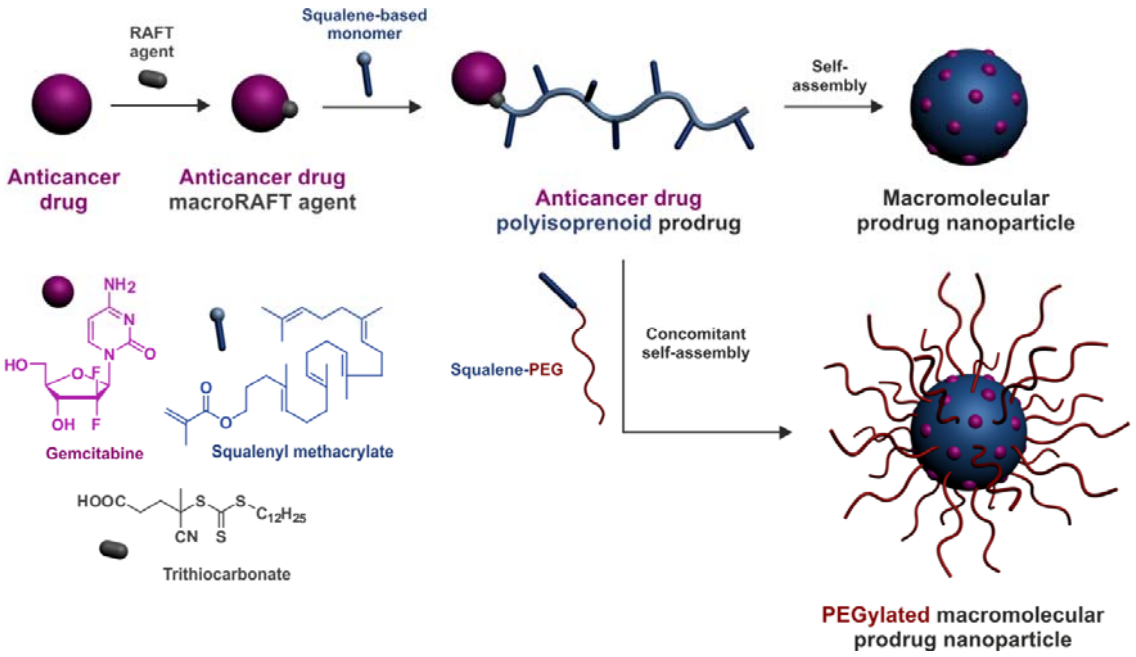

Figure 1. Design of macromolecular prodrug nanoparticles based on squalene as a naturally occurring isoprenoid, *via* reversible addition fragmentation chain transfer (RAFT) technique for anticancer therapy.

2. Experimental Part

2.1. Materials

Tetrahydrofuran (THF) was distilled from sodium/benzophenone ketyl. Dimethylformamide (DMF) and dichloromethane (DCM) were distilled from calcium hydride, under a nitrogen atmosphere. All reactions involving air- or water-sensitive compounds were routinely conducted in glassware which was flame-dried under a positive pressure of nitrogen. Gemcitabine (98%) was purchased from Sequoia Research Products Ltd. Squalene (98%), 4,4'-azobis(4-cyanopentanoic acid) (98%), 1,4-dioxane (99%), 4-cyano-4-[(dodecylsulfanylthiocarbonyl) sulfanyl] pentanoic acid (97%), methanol (99.8%) and 3-[4,5-dimethylthiazol-2-yl]-3,5-diphenyl tetrazolium bromide (MTT) were purchased from Sigma-Aldrich Chemical Co., France. Squalene-poly(ethylene glycol) (Sq-PEG) was synthesized from 1,1',2-trisnor-squalenoic acid and poly(ethylene glycol) monomethyl ether (M_n = 2 000 g.mol^{-1}) as published elsewhere.[37] Ethyl chloroformate (97%), 4-dimethylaminopyridine (99%), imidazole (99%) and tetrabutylammonium fluoride (98%) were purchased from Alfa-Aesar (A Johnson Matthey Co., France). RPMI 1640 GlutaMAX I, DMEM GlutaMAX I, F12-K and fetal bovine serum were purchased from Dulbecco (Invitrogen, France). Penicillin and streptomycin solution were purchased from Lonza (Verviers, Belgium). Chemicals

obtained from commercial suppliers were used without further purification. BODIPY-cholesterol was purchased from Invitrogen Life Technologies and used as received.

2.2. Analytical techniques

Nuclear Magnetic Resonance Spectroscopy (NMR). The ^{1}H and ^{13}C NMR spectra were recorded on Bruker Avance 300 (300 MHz and 75 MHz, respectively) or Bruker Avance 400 (400 MHz and 100 MHz, respectively) spectrometers. The ^{19}F NMR spectra were recorded on Bruker AC 200 F (188 MHz). Recognition of methyl, methylene, methine, and quaternary carbon nuclei in ^{13}C NMR spectra rests on the *J*-modulated spin-echo sequence. Mass spectra were recorded on a Bruker Esquire-LC spectrometer.

Infrared (IR) spectroscopy. IR spectra were obtained as solid or neat liquid on a Fourier Transform Bruker Vector 22 spectrometer. Only significant absorptions are listed. Optical rotations were measured on a Perkin-Elmer 241 Polarimeter at 589 nm.

Elemental analysis. Elemental analyses were performed by the Service de microanalyse, Centre d'Etudes Pharmaceutiques, Châtenay-Malabry, France, with a Perkin Elmer 2400 analyzer.

Size Exclusion Chromatography (SEC). SEC was performed at 30 °C with two columns from Polymer Laboratories (PL-gel MIXED-D; 300 × 7.5 mm; bead diameter 5 mm; linear part 400 to 4×10^5 g.mol^{-1}) and a differential refractive index detector (SpectraSystem RI-150 from Thermo Electron Corp.). The eluent was chloroform at a flow rate of 1 mL.min^{-1} and toluene was used as a flow-rate marker. The calibration curve was based on poly(methyl methacrylate) (PMMA) standards (peak molar masses, M_p = 625–625 500 g.mol^{-1}) from Polymer Laboratories. This technique allowed M_n (the number-average molar mass), M_w (the weight-average molar mass), and M_w/M_n (the dispersity, $Đ$) to be determined.

Dynamic Light Scattering (DLS) and Zeta Potential. Nanoparticle diameters (D_z) and zeta potentials (ζ) were measured by dynamic light scattering (DLS) with a Nano ZS from Malvern (173° scattering angle) at a temperature of 25 °C. The surface charge of the nanoparticles was investigated by ζ-potential (mV) measurement at 25 °C after dilution with 1 mM NaCl, using the Smoluchowski equation. Measurements were performed in triplicate following dilution of the NP suspensions in water.

Cryomicroscopy experiments (Cryo-TEM). The morphology of the different nanoassemblies was examined by cryo-TEM. Briefly, 5 µL of the nanoparticle suspension (1 mg.mL^{-1}) was deposited on a Lacey Formvar/carbon 300 mesh copper microscopy grid (Ted Pella). Most of the drop was removed with a blotting filter paper and the residual thin film

remaining within the holes was vitrified by plunging into liquid ethane. Samples were then observed using a JEOL 2100HC microscope.

X-ray photoelectron spectroscopy (XPS). XPS was used to determine the surface composition of the nanoparticles. A Thermo Electron Escalab 250 spectrometer with monochromated AlKα radiation (1486.6 eV) was used. The analyzer pass energy was 100 eV for survey spectra and 20 eV for high resolution spectra. The spectrometer was calibrated against Au $4f_{7/2}$ at 84.1 eV. O 1s, C 1s, F 1s, N 1s and S 2p core levels were analysed. The photoelectron take-off angle (angle of the surface with the direction in which the photoelectrons are analyzed) was 90°. Curve fitting of the spectra was performed using Thermo Electron software. For calculation of the surface composition, the inelastic mean free paths calculated by Tanuma *et al*.[40] and photoemission cross-sections calculated by Scofield were used.

2.3. Synthetic pathways

*4-Amino-1-[4-(tert-butyl-dimethyl-silanyloxy)-5-(tert-butyl-dimethyl-silanyloxymethyl)-3,3-difluoro-tetrahydro-furan-2-yl]-1H-pyrimidin-2-one (**2**).* To a mixture of gemcitabine hydrochloride (**1**, 2.00 g, 6.7 mmol), *tert*-butyldimethylsilyl chloride (2.54 g, 16.8 mmol) and imidazole (1.37 g, 20.2 mmol) in 40 mL of distilled DMF, was added dropwise triethylamine (Et_3N, 0.75 g, 7.4 mmol). The mixture was stirred at 25 °C for 24 h. The DMF was removed under reduced pressure and the residue was treated with sat. $NaHCO_3$ aqueous solution, extracted with ethyl acetate. The combined organic layers were washed with brine, dried over $MgSO_4$ and concentrated under reduced pressure. The residue was purified by flash chromatography over silica gel eluting with AcOEt to give **2** (3.15 g, 95%) as a white solid. Mp: 119-120 °C; $[\alpha]_D^{26}$ + 2.19 (*c* = 1, MeOH); ^{1}H NMR (400 MHz, $CDCl_3$) δ 8.25 (1H, br s, N*H*), 7.60 (1H, d, *J* = 7.6 Hz, H-6), 6.30 (1H, dd, *J* = 10.8, 4.5 Hz, H-1'), 5.80 (1H, d, *J* = 7.6 Hz, H-5), 4.29 (1H, td, *J* = 11.9, 8.2 Hz, H-3'), 3.97 (1H, d, *J* = 11.8 Hz, H-5'), 3.86 (1H, br d, *J* = 8.2 Hz, H-4'), 3.78 (1H, dd, *J* = 11.8, 2.0 Hz, H-5'), 0.92 (9H, s, (CH_3)$_3$CSi), 0.89 (9H, s, (CH_3)$_3$CSi), 0.12 (3H, s, (CH_3)$_2$Si), 0.10 (9H, s (CH_3)$_2$Si) ppm; ^{13}C NMR (100 MHz, $CDCl_3$) δ 166.1 (C, C-4), 155.8 (C, C-2), 140.6 (CH, C-6), 122.2 (CF_2, t, $J_{C\text{-}F}$ = 260.7 Hz, C-2'), 95.4 (CH, C-5), 84.3 (CH, dd, $J_{C\text{-}F}$ = 40.0, 23.4 Hz, C-1'), 81.0 (CH, d, $J_{C\text{-}F}$ = 9.0 Hz, C-4'), 70.0 (CH, dd, $J_{C\text{-}F}$ = 28.1,18.1 Hz, C-3'), 60.3 (CH_2, C-5'), 26.0 (3 CH_3, (*C*H_3)$_3$CSi), 25.7 (3 CH_3, (*C*H_3)$_3$CSi), 18.4 (C, (CH$_3$)$_3$*C*Si), 18.1 (C, (CH$_3$)$_3$*C*Si),), −4.6 (CH_3, (*C*H_3)$_2$Si), −5.2 (CH_3, (*C*H_3)$_2$Si), −5.3 (CH_3, (*C*H_3)$_2$Si), −5.4 (CH_3, (*C*H_3)$_2$Si) ppm; ^{19}F NMR (188 MHz, $CDCl_3$) δ -113.83 (d, $J_{F\text{-}F}$ = 238 Hz, 1F), -115.79 (d, $J_{F\text{-}F}$ = 238 Hz, 1F) ppm; IR (neat) : 2956

(m), 2929 (m), 2857 (m), 1636 (s), 1472 (m),1403 (s), 1362 (s), 1254 (s), 1206 (s), 1148 (s), 1088 (m), 955 (s), 833 (m), 780 (m), 731 (m), 676 (m) cm^{-1}; MS (-ESI) *m*/*z*(%): 490 (100) [M^+−H]; Anal. Calcd for $C_{21}H_{39}F_2N_3O_4Si_2$: C 51.29, H 7.99, N 8.55. Found: C 51.15, H 8.11, N 8.48.

*Gemcitabine-RAFT agent (TBSGem-RAFT, **4**).* To a solution of 4-cyano-4-[(dodecylsulfanylthiocarbonyl)-sulfanyl]pentanoic acid (**3**) (605 mg, 1.5 mmol) in anhydrous THF (5 mL) was added Et_3N (180 mg, 1.8 mmol). The mixture was cooled at 0 °C and a solution of ethyl chloroformate (108 mg, 1.4 mmol) in THF (2 mL) was added dropwise. The mixture was stirred for 30 min at 0 °C and a solution of GemTBS **2** (490 mg, 1 mmol) in DMF (3 mL) was added dropwise. After being stirred at 20 °C for 2 days, the volatiles were removed under reduced pressure. The residue was taken up in sat. $NaHCO_3$ aqueous solution and extracted with ethyl acetate. The combined organic layers were washed with brine, dried over $MgSO_4$ and concentrated under reduced pressure. The crude was then purified by flash chromatography (SiO_2, petroleum ether/AcOEt 4:1) to give trithiocarbonate **4** (450 mg, 50%) as a viscous yellow oil. ^{1}H NMR (400 MHz, $CDCl_3$) the presence of two diastereomers induced the splitting of some signals δ 10.73 (1H, s, CON*H*), 8.13 (1H, d, *J* = 7.6 Hz, H-6), 7.46 (1H, d, *J* = 7.6 Hz, H-5), 6.29 (1H, dd, *J* = 10.8, 4.5 Hz, H-1'), 4.34 (1H, td, *J* = 11.8, 8.3 Hz, H-3'), 4.03 (1H, d, *J* = 11.7 Hz, H-5'), 3.96 (1H, d, *J* = 8.3 Hz , H-4'), 3.81 (1H, d, *J* = 11.7 Hz, H-5'), 3.35-3.30 (2H, m, SCS_2CH_2), 3.10-2.20 (4H, m, $HNCOCH_2CH_2$(Me)(CN)S), 1.85 (3H, s, $CH_2C(CH_3)CN$), 1.60-1.65 (2H, m, $SCS_2CH_2CH_2$), 1.48-1.15 (18H, m, $SCS_2CH_2CH_2(CH_2)_9CH_3$), 0.95 (9H, s, $(CH_3)_3CSi$), 0.90 (9H, s, $(CH_3)_3CSi$), 0.87 (3H, t, *J* = 7.9 Hz, $SCS_2(CH_2)_{11}CH_3$), 0.13 (3H, s, $(CH_3)_2Si$), 0.10 (9H, s, $(CH_3)_2Si$) ppm; ^{13}C NMR (100 MHz, $CDCl_3$) the presence of two diastereomers induced the splitting of some signals δ 217.3 (C, *C*=S), 172.2 (C, CONH), 163.4 (C, C-4), 155.0 (C, C-2), 144.3 (CH, , C-6), 122.1 (CF_2, t, $J_{C\text{-}F}$ = 260.8 Hz, C-2'), 119.4 and 119.3 (C, *C*N), 97.5 (CH, C-5), 85.0 (CH, dd, $J_{C\text{-}F}$ = 28.0, 17.0 Hz, C-1'), 81.6 (CH, d, $J_{C\text{-}F}$ = 9.0 Hz, C-4'), 69.5 (CH, dd, $J_{C\text{-}F}$ = 28.1, 18.0 Hz, C-3'), 60.1 (CH_2, C-5'), 46.5(C, $(CH_3)C$(CN)), 37.1 (CH_2, SCS_2CH_2), 33.3 and 33.2 (CH_2, $HNCOCH_2CH_2$), 32.4 (CH_2, $HNCOCH_2CH_2$), 32.0 (CH_2, $CH_2CH_2CH_3$), 29.8-29.1 (m, 7 CH_2), 27.8 (CH_2, $SCS_2CH_2CH_2$), 26.0 (3 CH_3, $(CH_3)_3CSi$), 25.6 (3 CH_3, $(CH_3)_3CSi$), 24.6 and 24.5 ($(H_3C)C$(CN)), 22.8 (CH_2, $CH_2CH_2CH_3$), 18.5 (C, $(CH_3)_3CSi$), 18.1 (C, $(CH_3)_3CSi$), 14.2 (CH_3, CH_2CH_3), -4.6 (CH_3, $(CH_3)_2Si$); -5.1 (CH_3, $(CH_3)_2Si$), -5.3 (2CH_3, $(CH_3)_2Si$) ppm; ^{19}F NMR (188 MHz, $CDCl_3$) δ −117.87 (d, $J_{F\text{-}F}$ = 238.8 Hz, 1F), −116.07 (d, $J_{F\text{-}F}$ = 238.8 Hz, 1F) ppm; MS (+ESI) *m*/*z*(%): 878 (7) [M+1], 565

(75), 492 (100) [M−$C_{19}H_{31}NOS_3$]; Anal. Calcd for $C_{40}H_{70}F_2N_4O_5S_3Si_2$: C 54.76, H 8.04, N 6.39. Found : C 55.08, H 8.00, N 6.31.

1,1',2-Trisnor-squalenyl methacrylate (squalenyl methacrylate, SqMA, ***5****).* To a solution of 1,1'2-trisnor-squalenol (6.50 g, 16.9 mmol) in anhydrous DCM (80 mL) cooled at 0 °C were added Et_3N (5.12 g, 50.7 mmol) and a catalytic amount of DMAP. The mixture was stirred at 0 °C for 5 min and methacryloyl chloride (3.53 g, 33.8 mmol) was added dropwise. After being stirred at room temperature for 12 h, sat. NH_4Cl aqueous solution (20 mL) was added. The organic layer was separated and the aqueous phase was extracted with DCM. The combined organic phase was washed with brine before, dried over $MgSO_4$ and concentrated under reduced pressure. The crude product was then purified by flash chromatography over silica gel (petroleum ether/ Et_2O, 95:5) to give methacrylate ester **5** (6.0 g, 75%) as a colorless oil. ^{1}H NMR (400 MHz, $CDCl_3$) δ 6.10 (1H, s, H_2C=C(CH_3)CO_2), 5.54 (1H, s, H_2C=C(CH_3)CO_2), 5.10-5.14 (5H, m, HC=C(CH_3)CH_2), 4.12 (2H, t, J = 4.5 Hz, =C(CH_3)CO_2CH_2), 2.14-1.92 (19H, m, =C(CH_3)CH_2CH_2CH=), 1.94 (3H, s, H_2C=C(CH_3)CO_2), 1.77 (1H, quint, J = 6.0 Hz, =C(CH_3)$CO_2CH_2CH_2$), 1.68 (3H, s, HC=C(CH_3)CH_2), 1.60 (15H, s, HC=C(CH_3)CH_2) ppm; ^{13}C NMR (100 MHz, $CDCl_3$) δ (100 MHz, $CDCl_3$): 167.5 (C, CO), 136.71 (C, H_2C=*C*(CH_3)CO_2), 135.3 (C, HC=*C*(CH_3)CH_2), 135.1 (C, HC=*C*(CH_3)CH_2), 135.0 (C, HC=*C*(CH_3)CH_2), 133.8 (C, HC=*C*(CH_3)CH_2), 131.4 (C, C=*C*(CH_3)$_2$), 125.3 (CH_2, H_2C=C(CH_3)CO_2), 125.3 (CH, HC=C(CH_3)CH_2), 124.6 (2CH, HC=C(CH_3)CH_2), 124.4 (2CH, HC=C(CH_3)CH_2), 64.5 (CH_2, CO_2CH_2), 39.9 ($2CH_2$, =C(CH_3)CH_2CH_2CH=), 39.8 (CH_2, =C(CH_3)CH_2CH_2CH=), 36.0 (CH_2, =C(CH_3)CH_2CH_2CH=), 28.4 (CH_2, =C(CH_3)CH_2CH_2CH=), 27.0 (CH_2, =C(CH_3)CH_2CH_2CH=), 26.9 (CH_2, =C(CH_3)CH_2CH_2CH=), 26.8 ($2CH_2$, =C(CH_3)CH_2CH_2CH=), 25.8 (CH_3, CH_2C=C(*C*H_3)$_2$), 18.5 (CH_3, H_2C=C(*C*H_3)CO_2), 17.8 (CH_3, CH_2C=C(*C*H_3)$_2$), 16.2 ($3CH_3$, =C(*C*H_3)CH_2), 16.0 (CH_3, =C(*C*H_3)CH_2) ppm; Anal. Calcd for $C_{31}H_{50}O_2$: C 81.88, H 11.08. Found: C 79.74, H 10.42.

*Gemcitabine-poly(squalene methacrylate) (****7****).* Squalenyl methacrylate (**5**) (273 mg, 0.6 mmol), TBSGem-RAFT **4** (87.6 mg, 0.1 mmol) and of 4,4'-azobis(4-cyanopentanoic acid) (2 mg, 6 μmol) were dissolved in 1 mL of 1,4-dioxane. The mixture was degassed by 3 freeze-pump-thaw cycles and stirred at 80 °C for 3 h. After cooling, the polymer was precipitated in methanol 3 times to give silylated polymer **6** (187 mg, 54% conversion) as a viscous yellow oil. The crude product was then reacted with TBAF (1M in THF, 0.17 ml, 0.17 mmol) in 2 mL of THF for 1 h at 20 °C. The deprotected polymer was then precipitated in methanol to give **7** (133 mg, 80%) as a viscous yellow oil. ^{1}H NMR (400 MHz, $CDCl_3$) δ 8.00

(m, H-6), 7.49 (m, H-5), 6.21 (m, H-1'), 5.01-5.21 (m, *H*C=C(CH_3)CH_2), 4.20-3.75 (m, $CO_2CH_2CH_2$), 2.15-1.85 (m, =C(CH_3)CH_2CH_2CH=), 1.68 (s, =C(CH_3)CH_2CH_2CH=), 1.60 (s, =C(CH_3)CH_2CH_2CH=), 1.60-0.85 (m, $SCS_2CH_2CH_2(CH_2)_9CH_3$), 0.77 (m, $SCS_2(CH_2)_{11}CH_3$) ppm; ^{19}F NMR (188 MHz, $CDCl_3$) δ: -116.19 ppm.

2.4. Nanoparticle formation

The nanoparticles were formed using the nanoprecipitation technique. A solution of the above mentioned corresponding polymers (1 mg) in 0.1 mL of THF was added dropwise, under stirring (500 rpm) into 1 mL of MilliQ water. Precipitation of the nanoassemblies occurred spontaneously. Stirring was continued for 3 min. The suspension was then transferred into a weighted round bottom flask and THF was evaporated at ambient temperature using a Rotavapor. The composite nanoassemblies of Gem-PSqMA/Sq-PEG at a final concentration of 1 mg mL^{-1} were prepared in the same way by conanoprecipitation of Gem-PSqMA with Sq-PEG using THF as organic solvent with different ratio of Gem-PSqMA/Sq-PEG (1:0; 1:0.4; 1:1.2; 1:2; 1:4.1; 0:1; mol:mol).

2.5. Biological activity

Complement activation. The complement activation of different nanoparticles was determined by studying the conversion of C3 into C3b by 2D immunoelectrophoresis using a polyclonal antibody to human C3.[41] Human serum was obtained after calcifying plasma from healthy donors and stored at -80°C until use, veronal-buffered saline containing 0.15 mM Ca^{2+} and 0.5 mM Mg^{2+} ions (VBS^{2+}) was prepared in lab as described by Kazatchkine *et al.*[42] Complement C3 antiserum rose in goat was purchased from Sigma, Saint Quentin Fallavier, France. Gem-PSqMA and Gem-PSqMA/Sq-PEG (1:0.8; mol:mol) nanoparticles were prepared by the nanoprecipitation technique. To ensure a valid comparison of the different nanoparticles, each sample was diluted with MilliQ water to obtain a surface area of hydrated particles per unit volume corresponding to 1000 $cm^2.mL^{-1}$. The nanoparticle suspensions (100 µL) were incubated under gentle agitation for 1 h at 37 °C with 50 µL human serum and 50 µL of VBS^{2+}. After incubation, 7 µL of each sample was subjected to a first electrophoresis (600 V, 16 mA, 100 W, 70 min) on 1% agarose gel slab. The 2-D electrophoresis was carried out on Gelbond® films in agarose gel plates containing a polyclonal antibody to human C3, recognizing both C3 and C3b. The films were stained with Coomassie blue to reveal the presence of C3 and C3b and the heights of these peaks, as shown on the immunoelectrophoretic plate, were measured. The activation of complement was expressed as

the ratio of the area of C3b detected on the plate to the sum of the areas of C3 and C3b (C3b/(C3+C3b)). Serum diluted in VBS^{2+} was used to control for the spontaneous activation of complement occurring in the experimental conditions used (~17%).

Cell lines and cell culture. Human leukemia cell line CCRF-CEM, murine leukemia cell line P388S, human pancreatic cancer cell line MiaPaCa-2 and human lung carcinoma cell line A549 were obtained from the American Type Culture Collection. Murine leukemia cell line L1210 WT was kindly provided by Dr. Lars Petter Jordheim (Université Claude Bernard Lyon I, Lyon, France). All cell lines were maintained as recommended. Briefly, A549 cells were maintained in F12-K medium. CCRF-CEM, L1210 WT were cultured in RPMI 1640 medium. MiaPaCa-2 cells were grown in Dulbecco's minimal essential medium (DMEM). All media were supplemented with 10% heat-inactivated fetal bovine serum (FBS) (56 °C, 30 min), penicillin (100 $U.mL^{-1}$) and streptomycin (100 $\mu g.mL^{-1}$). Medium for MiaPaCa-2 cell line was supplemented additionally with 2.5% heat-inactivated horse serum (Gibco) (56 °C, 30 min). Cells were maintained in a humid atmosphere at 37 °C with 5% CO_2.

Cell prolife ration assay. MTT [3-(4,5-dimethylthiazol-2-yl)-2,5-diphenyl tetrazolium bromide] was used to test cytotoxicity of gemcitabine-poly(squalene methacrylate) (Gem-PSqMA) prodrug nanoassemblies and cell viability. Briefly, cells ($5x10^3$/well) were seeded in 96-well plates. After overnight incubation, the cells were then exposed to a series of concentrations of Gem-PSqMA (**7a**, **7b**, **7c** and **7e**), PSqMA, Gem-PSqMA **7b**/Sq-PEG (1:2; mol:mol), or free Gem or for 72 h (incubation time was 120 h for MiaPaCa-2 cells). After drug exposure, the medium was removed and 100 µL of MTT solution (0.5 $mg.mL^{-1}$ in DMEM containing 10% FBS) was added to each well. The plates were incubated for 2 h at 37 °C and 100 µL of 20% SDS solution was then added to each well for 24 h at 37 °C. Absorbance was measured at 570 nm using a plate reader (Metertech Σ 960, Fisher Bioblock, Illkirch, France). The percentage of surviving cells was calculated as the absorbance ratio of treated to untreated cells. The inhibitory concentration 50% (IC_{50}) of the treatments was determined from the dose-response curve by noting the concentration at which the curve passes through the 50% inhibition level. All experiments were performed in quadruplicate to determine means and SDs.

Cell Internalization. To quantitatively measure the cell capture of the nanoparticles, MiaPaCa-2 cells were cultured on 12-well plates for 24 h to achieve 60-80 % confluence. Gem-PSqMA (**7b**) or Gem-PSqMA **7b**/Sq-PEG (1:2; mol:mol) co-nanoprecipitated with 0.5 wt.% of BODIPY-cholesterol were then added at the concentration of 1 µM to each well. After incubation, the cells were collected at different time intervals for measurement of

BODIPY fluorescence. To investigate the mechanism of cell internalization, the cells were incubated 4 h at 4 °C or 37 °C. The fluorescence from individual cells was examined using a flow cytometer C6 (Accuri Cytometers Ltd., UK). For the detection of BODIPY fluorescence, excitation was with the 488-nm line of an argon laser, and the emission of fluorescence was measured at 515 nm; 10000 cells were measured in each sample.

MiaPaCa-2 cells were cultured on a coverslip in a culture dish for 24 h to achieve approximately 40 % confluence. Cells were then incubated with Gem-PSqMA (**7b**) or Gem-PSqMA **7b**/Sq-PEG (1:2; mol:mol) co-nanoprecipitated with 0.5 wt.% of BODIPY-cholesterol, at the concentration of 10 μM at 37 °C for different time periods. After treatment, the cells were washed with Dulbecco's PBS five times and imaged using a confocal microscope (Zeiss) with a x60 oil-immersion objective. The following wavelengths were used: excitation at 488 nm and detection through a 515 nm filter for BODIPY.

3. Results and discussion

3.1. Synthesis and characterization of gemcitabine-poly(squalenyl methacrylate) (Gem-PSqMA) conjugates

The RAFT technique offers unmatched flexibility in the construction of advanced macromolecular architectures, especially for biomedical applications.[43] A gemcitabine end-functional poly(squalenyl methacrylate) was synthesized from the polymerization of squalenyl methacrylate (SqMA, **5**) under conventional radical initiation in the presence of a Gem-based trithiocarbonate RAFT agent (Figure 2). SqMA (**5**) was prepared from 1,1',2-trisnor-squalene alcohol by acylation with methacryloyl chloride.[44] The trithiocarbonate RAFT moiety (4-cyano-4-[(dodecylsulfanylthiocarbonyl) sulfanyl] pentanoic acid, **3**) was then linked to the C-4 amino group of the Gem (**1**) cytosine ring. However, the direct condensation of **1** with **3** was unselective and low yielding. A more rewarding route involved TBS protection of the 3',5'-OH groups (TBSGem, **2**), followed by conventional acylation of the C-4 amino group with the mixed anhydride derived from **3** and ethyl chloroformate to afford the protected Gem-functionalized RAFT agent (TBSGemRAFT, **4**).

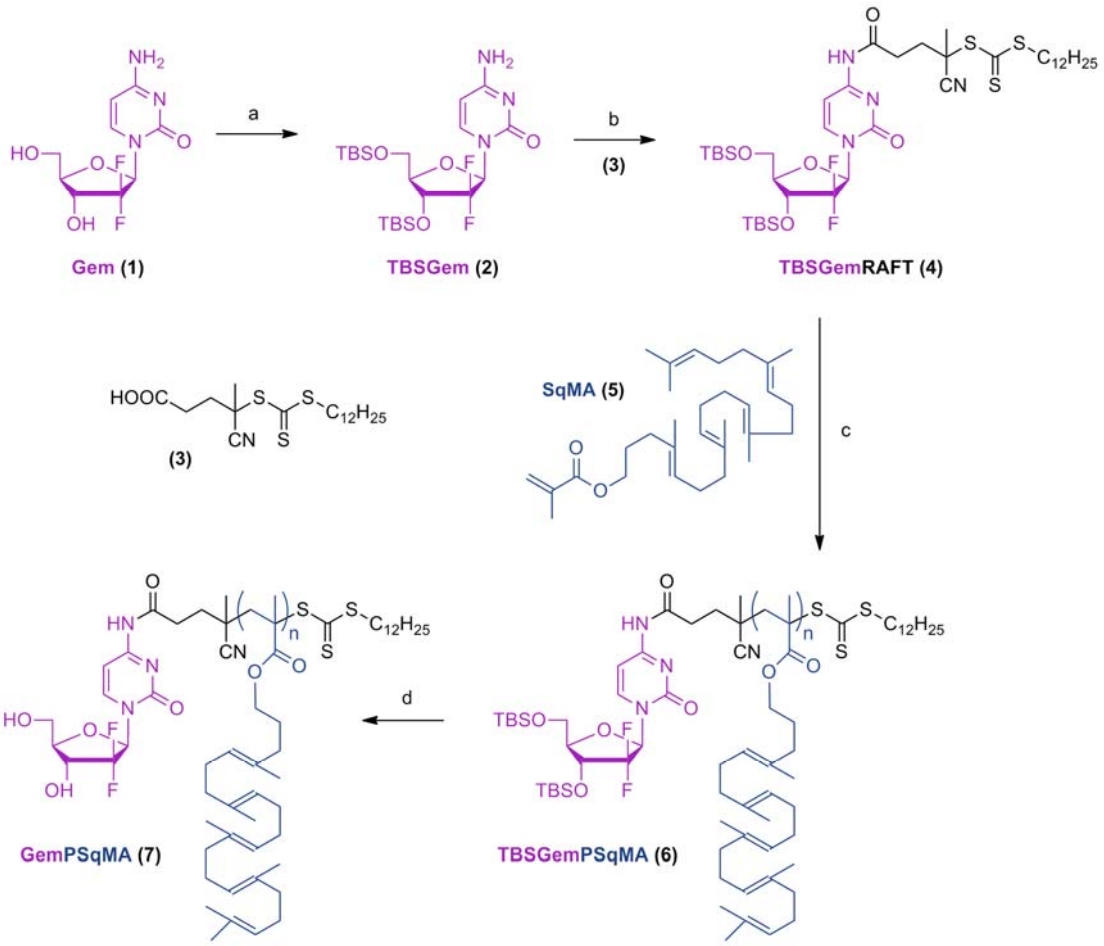

Figure 2. Synthetic pathway of gemcitabine-poly(squalenyl methacrylate) (Gem-PSqMA) conjugates by RAFT polymerization. *Reagents and conditions:* (a) TBSCl, imidazole, 24 h, Et_3N, DMF, 95%; (b) 4-cyano-4-[(dodecylsulfanylthiocarbonyl) sulfanyl] pentanoic acid (**3**), $ClCO_2Et$, Et_3N, THF, DMF, 48 h, 55%; (c) squalenyl methacrylate (SqMA, **5**), 4,4'-azobis(4-cyanopentanoic acid), 1,4-dioxane, 80°C, 1-3 h; (d) TBAF, 1 h.

The RAFT polymerization of **5** in the presence of **4** was then performed in 1,4-dioxane at 80°C under 4,4'-azobis(4-cyanopentanoic acid) radical initiation and furnished low dispersity Gem-PSqMA conjugates (Table 1 and Figure 2). By varying the $[\mathbf{5}]_0$:$[\mathbf{4}]_0$ initial concentration ratio and/or the reaction time, a small library of Gem-PSqMA exhibiting variable chain length (**7a–e**) was obtained. The Gem-PSqMA structure and the presence of Gem was confirmed through ^1H and ^{19}F NMR (Figure 3). Its distribution across polymer chains of all molar masses was also confirmed by SEC with RI and UV detection (Figure S1). The number-average molar masses (M_n) determined by conventional SEC were in the 3720–6800 g.mol^{-1} range with dispersities ($Đ$) between 1.18 and 1.28. By ^1H NMR, M_n ranged from 4380 to 11300 g.mol^{-1}, which corresponds to DP_n varying from ~8 to ~28. As long as deprotection of

TBS did not alter the macromolecular characteristics of the polyisoprenoid block nor the Gem functionality (as confirmed by SEC with dual RI and UV detections), this discrepancy may be explained by the conventional calibration used for SEC. Therefore, M_n values deriving from ^{1}H NMR will be used in subsequent calculations. A consequence of the synthetic strategy of growing PSqMA from the Gem-based RAFT agent is that the weight fraction of Gem in the resulting conjugate can be fine-tuned by adjusting the polymer chain length *via* the polymerization time and/or the initial stoichiometry of the reactants. In this study, Gem weight fractions of 2.5 to 7.2 wt.% were selected. Note that the drug payload could be easily increased simply by reducing the polymer chain length.

Table 1. Macromolecular and Colloidal Characteristics of Gemcitabine-Poly(Squalenyl Methacrylate) (Gem-PSqMA) Conjugates.

Gem-PSqMA (**7**)	$[SqMA]_0$:$[TBSGemRAFT]_0$	Polym. time (h)	$M_{n,SEC}$ (g.mol^{-1})[a]	$Đ$[a]	$DP_{n,SEC}$[b]	$M_{n,NMR}$ (g.mol^{-1})[c]	$DP_{n,NMR}$[d]	$D_z \pm SD$[d]	PSD[d]	%Gem (wt.%)[e]
7a	6:1	1	3720	1.18	~7	4380	~8	138 ± 1	0.169	7.2
7b	6:1	2	4620	1.19	~9	4840	~9	142 ± 6	0.114	6.4
7c	6:1	3	5030	1.20	~10	6850	~14	156 ± 2	0.123	4.1
7d	8:1	3	5950	1.27	~12	9660	~20	138 ± 1	0.107	2.9
7e	10:1	3	6800	1.28	~14	11300	~23	122 ± 3	0.129	2.5

[a]Determined by size exclusion chromatography (SEC) and calibrated with poly(methyl methacrylate) standards. [b]Calculated by SEC according to $DP_{n,SEC} = (M_{n,SEC} – MW_{deprotected\ \mathbf{4}})/MW_{\mathbf{5}}$. [c]Determined by ^{1}H NMR using peaks *s* and *q* (see Figure 3).[d]Calculated by ^{1}H NMR according to $DP_{n,NMR} = (M_{n,NMR} – MW_{deprotected\ \mathbf{4}})/MW_{\mathbf{5}}$. [e]Weight fraction of Gem calculated according to $\%Gem = MW_{Gem}/(DP_{n,NMR} \times MW_{\mathbf{5}})$.

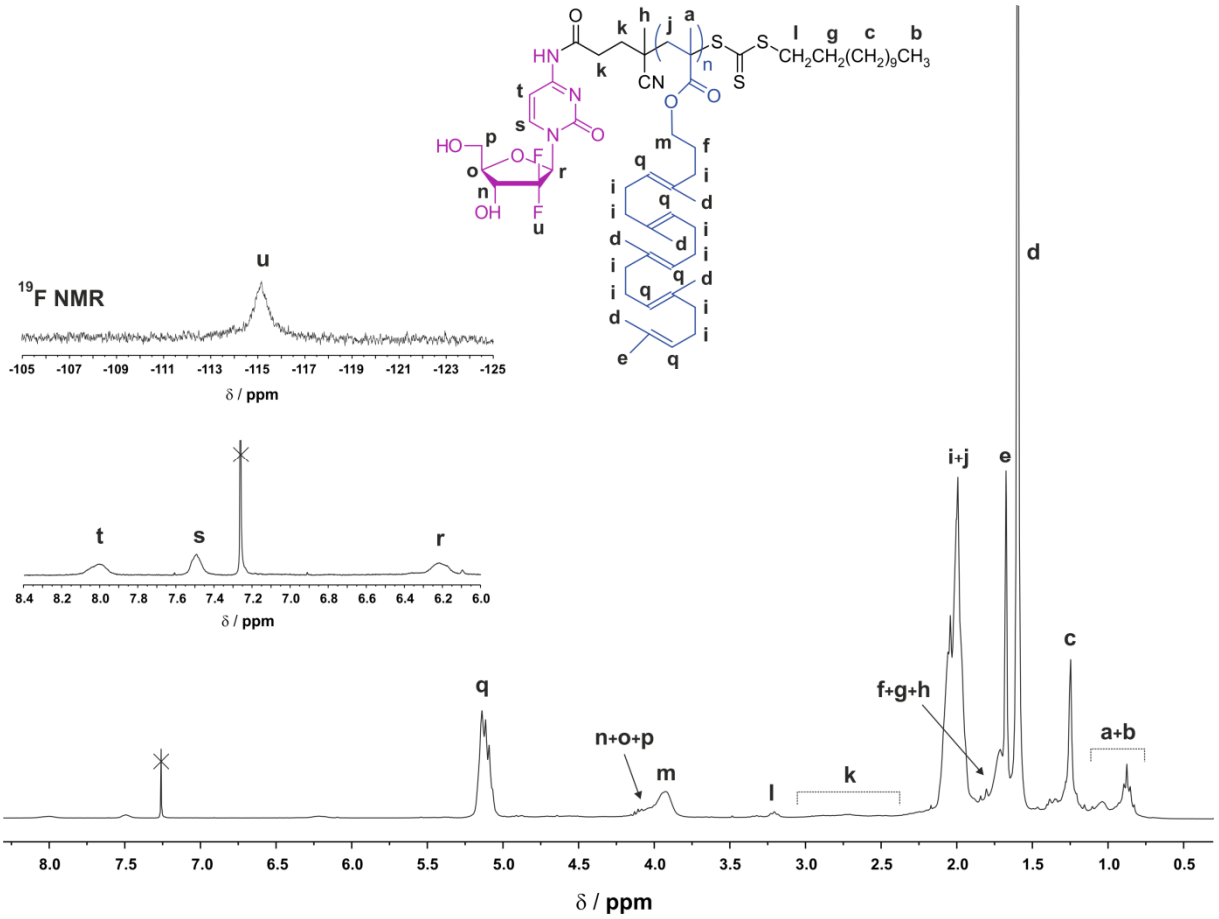

Figure 3. ^{1}H NMR spectrum (300 MHz, $CDCl_3$) of Gem-PSqMA (**7a**). Inserts: zoom of the ^{1}H NMR spectrum in the 6.0–8.4 ppm region (bottom); zoom of the ^{19}F NMR spectrum in the -105 – -125 ppm region (top).

3.2. Preparation of nanoparticles

Gem-PSqMA macromolecular prodrug nanoparticles were obtained by self-assembly of Gem-PSqMA conjugates in aqueous solution *via* the nanoprecipitation technique. This was performed without any additional stabilizer, due to the amphiphilic nature of the conjugate. Nanoparticles, whose colloidal stability was assessed for a period of at least 4 weeks, were obtained for all polymer chain lengths. Average diameters were in the 122-138 nm range (Table 1), which is suitable for drug delivery through intravenous administration. Particle size distributions were all below 0.17 as determined by DLS (Figure 4a and Table 1). No clear dependence of the nanoparticle size on the polymer chain length was observed. Nanoparticles were further characterized by cryogenic transmission electron microscopy (cryo-TEM) and showed spherical morphologies and colloidal characteristics, in good agreement with DLS data (Figure 4b).

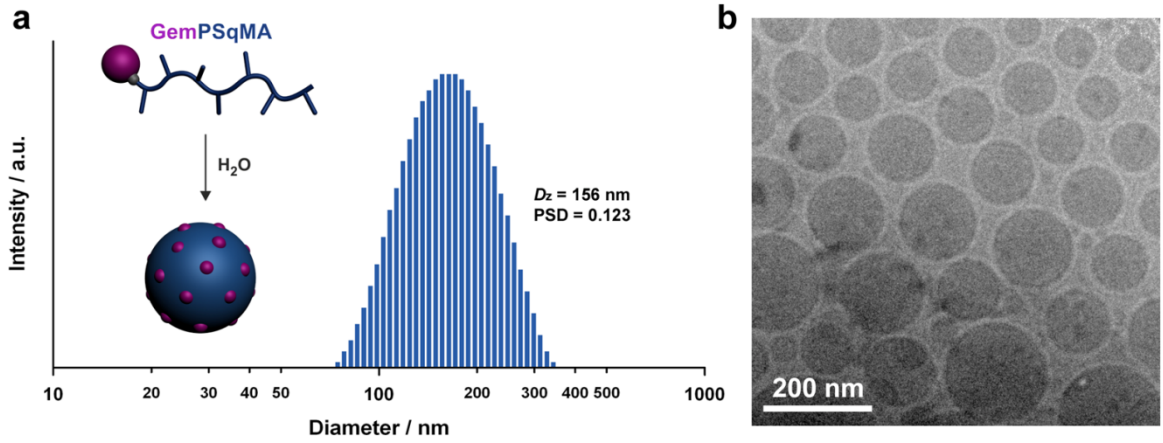

Figure 4. Dynamic light scattering data giving the average diameter in intensity (a) and cryogenic transmission electron microscopy (b) of nanoparticles **7c**.

In order to confer stealth features to Gem-PSqMA nanoparticles, their PEGylation was also undertaken. PEG coating at the surface of nanoparticulate systems gives rise to several key benefits such as longer systemic circulation time,[45] low complement activation and lower toxicity *in vivo* as compared to non-PEGylated counterparts. For this purpose, a PEG-Sq derivative bearing a 2000 g.mol^{-1} PEG chain was synthesized[37] and co-self-assembled with Gem-PSqMA (**7d**) at different molar ratios (Gem-PSqMA:Sq-PEG; 1:0; 1:0.4; 1:1.2; 1:2; 1:4.1; 0:1; mol:mol). Due to the structural similarity between the Sq moiety and PSqMA, PEG-Sq is expected to anchor at the surface of Gem-PSqMA nanoparticles. For all Gem-PSqMA:Sq-PEG molar ratios, stable nanoparticles were obtained with constant average diameters in the 130-140 nm range and narrow particle size distributions (Figure S2). This is a major improvement over molecular Sq-based prodrug nanoassemblies for which PEGylation by Sq-PEG resulted in destruction of the nanoparticulate system due to swelling of the inverted hexagonal phases.[37] However, it is likely that the entangled polymer chains of the Gem-PSqMA nanoparticles form a denser and less hydrophilic nanoparticle core, resulting in more stable nanoparticles upon PEGylation.

The presence of PEG at the surface of Gem-PSqMA nanoparticles was demonstrated by the combination of X-ray photoelectron spectroscopy (XPS) and complement activation assay. The XPS spectrum of Gem-PSqMA/Sq-PEG (1:2.2 mol:mol) nanoparticles differed from the Gem-PSqMA spectrum (Figure 5a–d, Table S1 and Figure S3–4). The C_{1s} and O_{1s} envelopes showed substantial changes of binding energy intensities of their main components. For instance, C_{C-C} (282.0 eV) decreased from 77.6 to 71.1%, whereas C_{C-O} (283.5 eV) and

$O_{\underline{O}\text{-}C}$ (529.6 eV) increased from 4.9 to 11.7% and 10.0 to 11.5%, respectively, demonstrating the PEG coverage. This was confirmed by the decrease of N_{1s} (397.7 eV, from 0.7 to 0.5%), F_{1s} (685.2 eV, from 0.7 to 0.2%) and S_{2p} (160.3 eV, from 1.6 to 0.5%) peaks belonging to the GemRAFT moiety, which was buried in the core of the nanoparticles upon PEGylation with Sq-PEG.

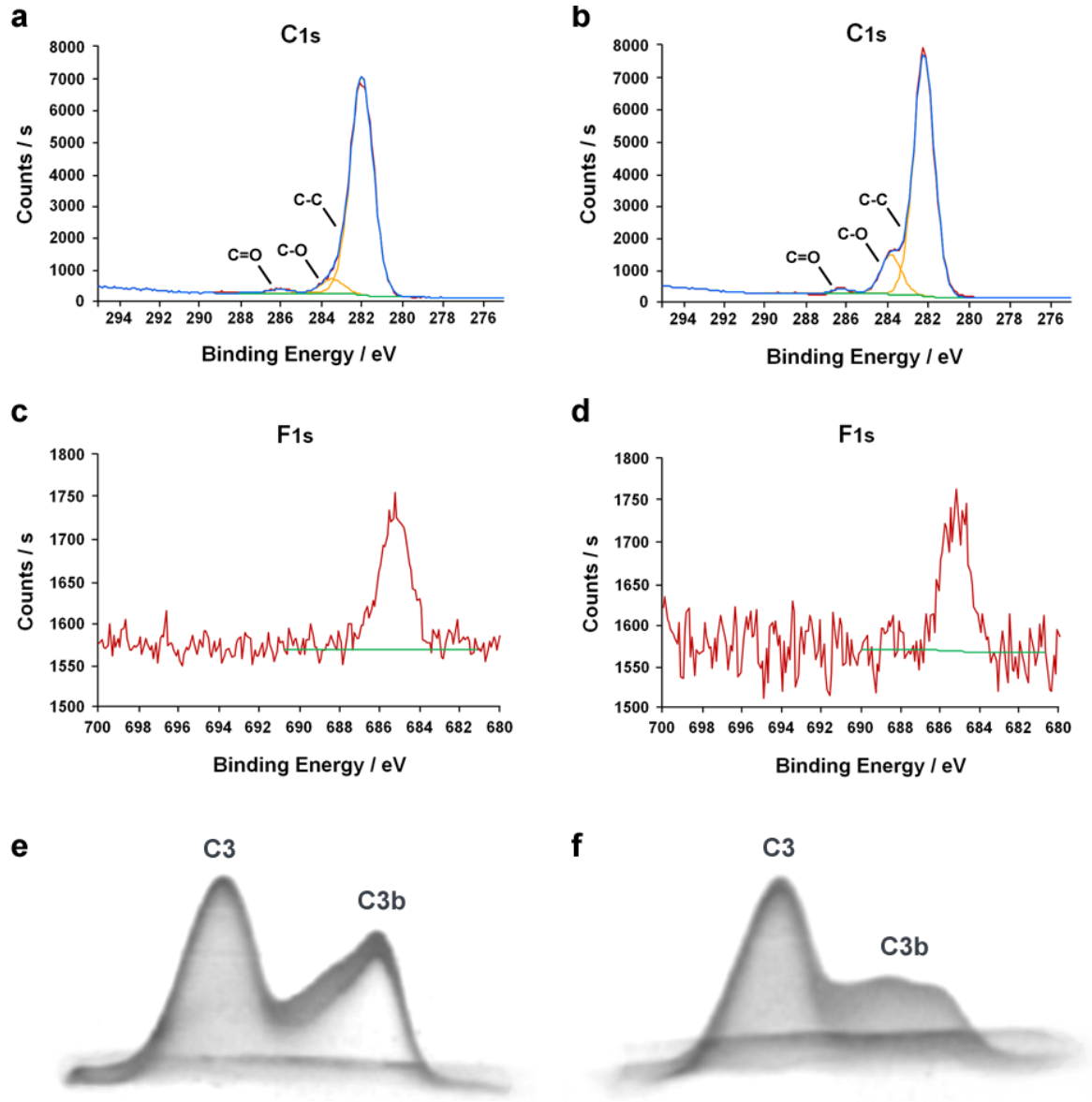

Figure 5. Carbon C_{1s} (a and b) peak envelopes and Fluorine F_{1s} (c and d) peaks of X-ray photon spectroscopic analysis from Gem-PSqMA **7c** (a and c) and Gem-PSqMA **7c**/Sq-PEG (1:2.2; mol:mol) (b and d) nanoparticles. 2-D electroimmunophoretic profile of complement activation for Gem-PSqMA **7c** (e) and Gem-PSqMA **7c**/Sq-PEG (1:0.8; mol:mol) (f).

Complement activation experiments were performed to confirm the effective PEG coating at the surface of Gem-PSqMA nanoparticles. The complement system and especially protein C3 are strongly involved in the opsonization process.[42] The protein C3 has a central role in triggering the immune system response against foreign bodies, leading to short blood lifetime and rapid accumulation in organs of the mononuclear phagocyte system, including the liver and the spleen. The capacity of Gem-PSqMA and Gem-PSqMA/Sq-PEG nanoparticles to activate the complement was investigated in human serum in the presence of nanoparticles. The cleavage of protein C3 into C3b fragment was evidenced by 2-D immunoelectrophoresis by measuring the height of the peaks corresponding to C3 and C3b (Figure 5e–f).[41] Whereas 50% of C3 present in the serum was activated by Gem-PSqMA nanoparticles (**7c**), Gem-PSqMA/Sq-PEG nanoparticles (**7c**:Sq-PEG; 1:0.8; mol:mol; D_z = 140 nm, PSD = 0.146) led to complement activation of only 22%, which was only slightly above the spontaneous activation of the serum measured under identical experimental conditions (17 ± 2 %).

3.3. *In Vitro* Anticancer efficacy

Gem-PSqMA conjugate nanoparticles (**7a–c** and **e**) were then tested for their *in vitro* anticancer activity on various cancer cell lines: i) murine leukemia (L1210 WT); ii) human pancreatic cancer (MiaPaCa-2); iii) human lung carcinoma (A549); iv) human leukemia (CCRF-CEM) and v) murine leukemia (P388S), in order to investigate whether these novel macromolecular prodrug nanoparticles present anti-cancer activities despite their macromolecular/bulky structure and potential anticancer activity modification upon subtle variation of the Gem-PSqMA chain length.

From Figure 6 and Table S2, respectively presenting the variation of cell viability as a function of the concentration of the studied compound and the resulting half maximal inhibitory concentrations (IC_{50}), it appears that Gem-PSqMA nanoparticles exhibited significant anti-cancer activities on all tested cell lines, whereas PSqMA nanoparticles (D_z = 111 nm, PSD = 0.19) were not cytotoxic. As expected owing to their prodrug nature, all nanoparticles were less cytotoxic than free Gem, while IC_{50} values remained in the nanomolar range (Table S2). In addition, for all cell lines, it appeared that the anticancer activity was not significantly influenced by the polymer chain length, despite the coverage of a rather broad range of M_ns (*e.g.*, M_n = 4380 g.mol^{-1} for **7a** vs. 11300 g.mol^{-1} for **7e**). Indeed, from Table S2 presenting IC_{50}s of Gem-PSqMA nanoparticles, anticancer activity was maintained whatever the polymer chain length. This preliminary structure/anticancer activity relationship, readily performed due to the controlled/living polymerization process employed here, is of prime

importance as it provides insight into the mechanism of action of the bioconjugates and so aids the design of optimal drug delivery systems.

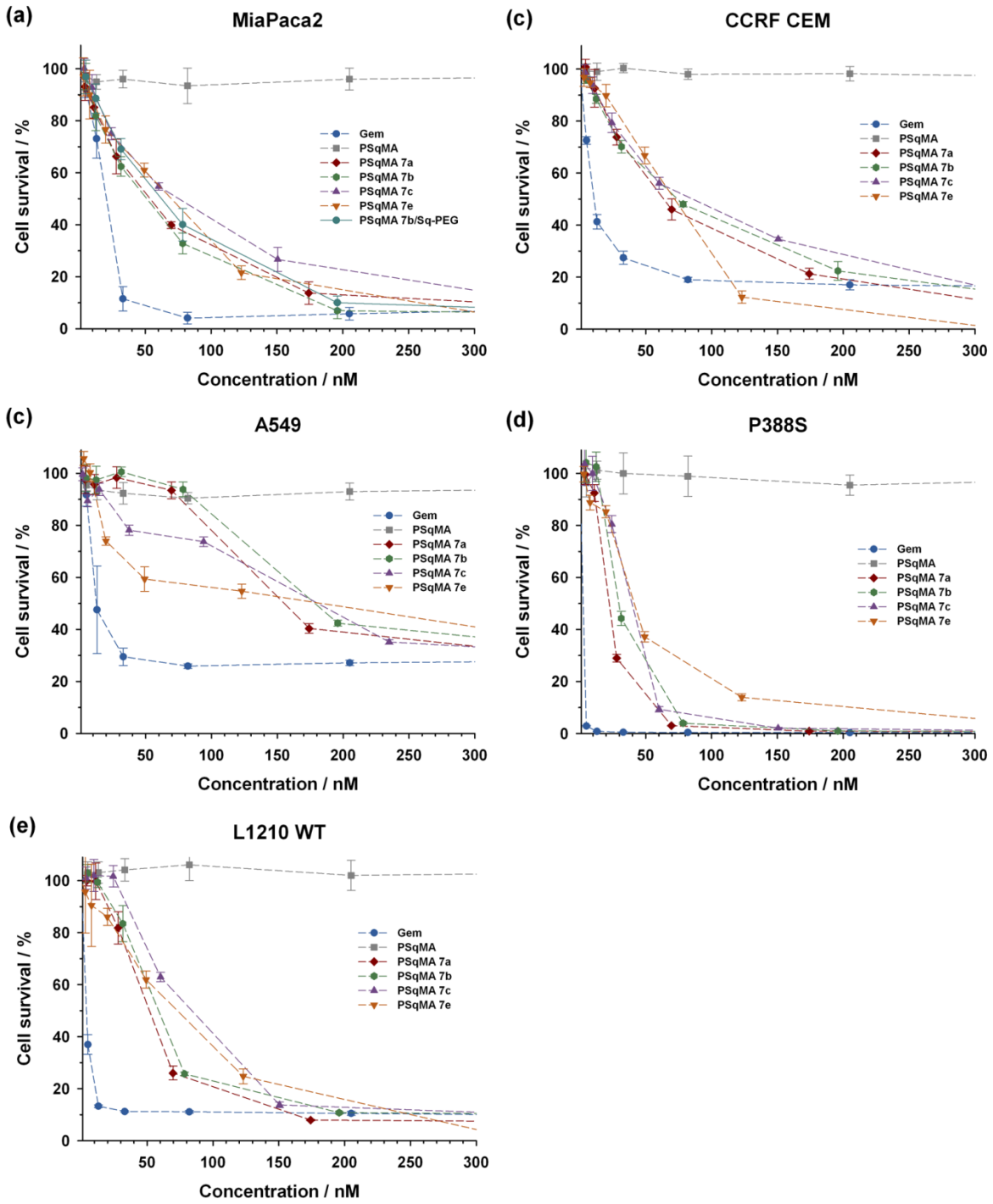

Figure 6. Viability assay (MTT test) on MiaPaca2 (a), CCRF CEM (b), A549 (c), P388S (d) and L1210 WT (e) cell lines with various concentrations of free Gem, PSqMA nanoparticles, Gem-PSqMA nanoparticles (**7a-c** and **e**) and or-PSqMA **7b**/Sq-PEG nanoparticles (1:2; mol:mol).

Interestingly, the PEGylation of Gem-PSqMA nanoparticles **7b** with Sq-PEG (1:2; mol:mol) did not significantly affect its cytotoxic activity (Figure 6a) as its IC_{50} was still of the same order of magnitude than the non-PEGylated counterpart (66 ± 4 nM and 51 ± 4 nM, respectively).

3.4. Cell internalization

To have a better insight concerning the biological fate of Gem-PSqMA and Gem-PSqMA/Sq-PEG nanoparticles, their ability to be internalized by cancerous cells was investigated using the MiaPaca2 cell line. In order to study the kinetics of internalization, fluorescent BODIPY-tagged nanoparticles were incubated with MiaPaca2 cells and cell fluorescence was analyzed by a combination of flow cytometry and confocal microscopy, and compared to untreated cells. After 5 min of incubation, confocal images revealed a faint cell fluorescence signal with both kinds of nanoparticles (Figure 7a). However, after 4 h, a more pronounced internalization was obtained with PEGylated PSqMA nanoparticles as opposed to non-PEGylated ones. This was confirmed by flow cytometry experiments which showed a marked difference of cell internalization in MiaPaca2 cells (Figure 7b), with for instance, a 5-fold increase of internalization of PEGylated nanoassemblies at 4 h. Furthermore, when incubation was achieved for 4 h at 4°C, the cell fluorescence intensity was dramatically decreased for both types of nanoparticles (Figure 7c), suggesting that internalization was likely governed by endocytosis.

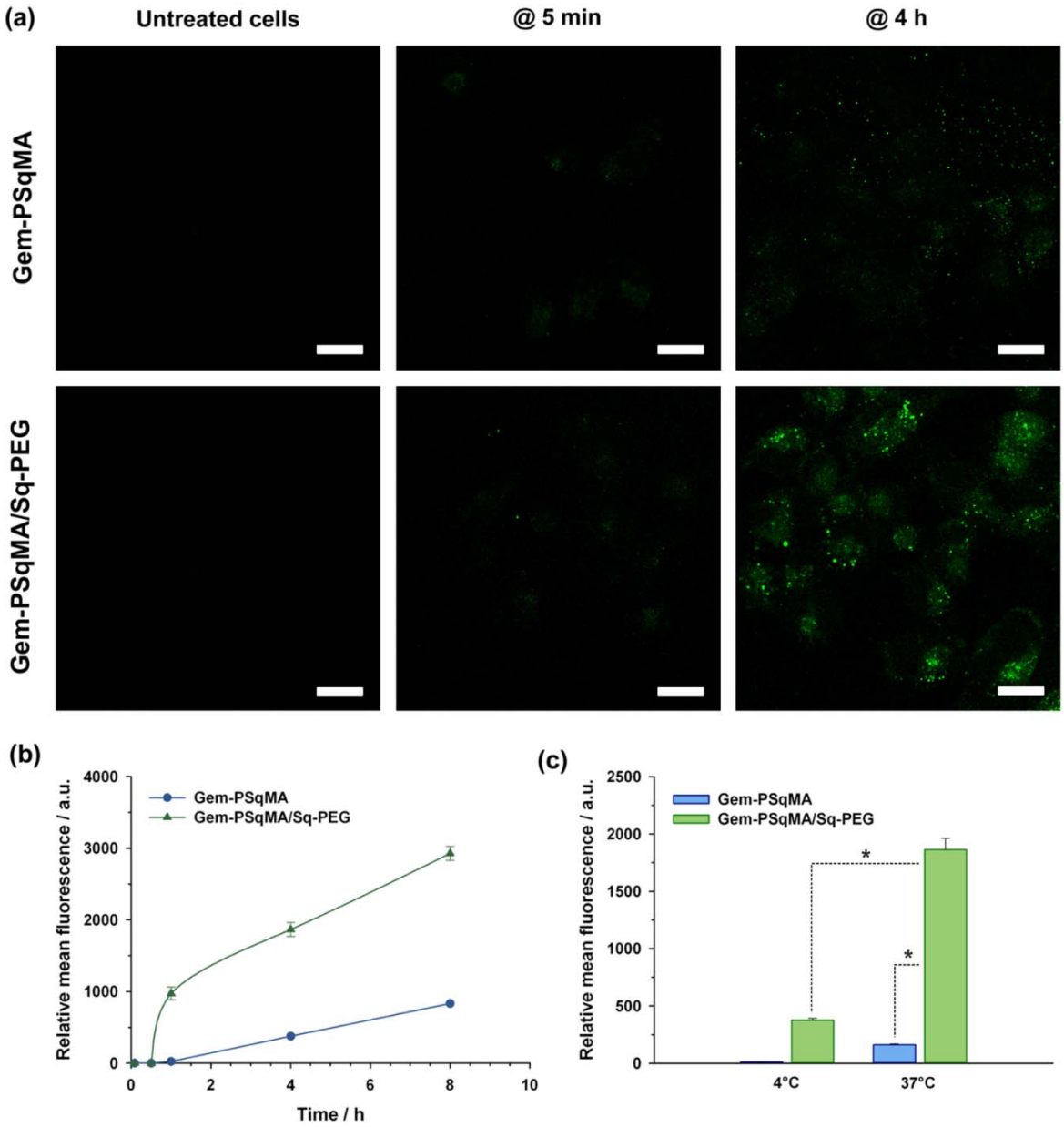

Figure 7. Confocal fluorescence microscopy images of MiaPaca2 cells incubated with BODIPY-labelled Gem-PSqMA **7b** and Gem-PSqMA **7b**/Sq-PEG (1:2; mol:mol) nanoparticles, after 5 min and 4 h of incubation at 37 °C. Scale bars = 20 μm (a). Kinetics of cellular uptake of BODIPY-labelled Gem-PSqMA **7b** and Gem-PSqMA **7b**/Sq-PEG (1:2; mol:mol) nanoparticles in MiaPaca2 cells exposed to 1 μM of nanoparticles (b). Internal fluorescence in cells after 4 h of MiaPaca2 exposure to 1 μM of nanoparticles at 4°C and 37 °C (c). Statistical differences are expressed by * ($p < 0.001$).

The marked difference of cell internalization between Gem-PSqMA and Gem-PSqMA/Sq-PEG nanoparticles may be related to their different surface chemistry. The presence of

flexible and hydrophilic PEG chains at the surface of nanoparticulate systems induces long-circulating feature due to their ability to avoid opsonin adsorption, leading to immune system response/complement activation. Another consequence of the presence of surface PEG is a modification of the surface potential which can impact electrostatic interaction between nanoparticles and biological entities and/or membranes. Gem-PSqMA nanoparticles exhibited a strongly negative zeta potential of –63.8 mV, whereas Gem-PSqMA/Sq-PEG led to a higher zeta potential of only –16.6 mV. Thus, electrostatic repulsions between Gem-PSqMA nanoparticles and biological membranes, both negatively charged, may hamper their uptake by the cells, which was not the case with Gem-PSqMA/Sq-PEG nanoparticles, thanks to the charge shielding ensured by the PEG surface coating combined to their stealth feature.

4. Conclusions

In this study is reported a general pathway for the synthesis of a novel class of well-defined macromolecular prodrug nanoparticles by the RAFT technique, starting from a novel squalene derivative monomer. By appropriate functionalization of the RAFT agent with Gem as anticancer drug, the polymerization of squalene-methacrylate led to well-defined macromolecular prodrugs comprising one Gem at the extremity of each polymer chain. Furthermore, the controlled/living polymerization process employed here permitted tunable Gem payloads to be obtained, due to adjustable polymer chain lengths. The amphiphilic nature of the resulting conjugates allowed them to self-assemble into narrowly dispersed nanoparticles with significant anticancer activity *in vitro* on various cancer cell lines. To confer stealth properties on these nanoparticles, their PEGylation was successfully undertaken, as confirmed by XPS and complement activation assay. This novel route towards efficient anticancer nanoparticles is simple, robust and versatile as it could be readily extended to many hydrophilic drugs, either against cancer or for the treatment of other diseases just by changing the nature of the drug, thus leading to a general synthetic approach in the field of drug delivery.

References

1. Nicolas, J.; Mura, S.; Brambilla, D.; Mackiewicz, N.; Couvreur, P. *Chem. Soc. Rev.* **2013,** 42, 1147.
2. Elsabahy, M.; Wooley, K. L. *Chem. Soc. Rev.* **2012,** 41, 2545.
3. Farokhzad, O. C.; Langer, R. *ACS Nano* **2009,** 3, 16.

4. Brambilla, D.; Le Droumaguet, B.; Nicolas, J.; Hashemi, S. H.; Wu, L.-P.; Moghimi, S. M.; Couvreur, P.; Andrieux, K. *Nanomedicine: NBM* **2011,** 7, 521.
5. Hans, M. L.; Lowman, A. M. *Curr. Opin. Solid State Mater. Sci.* **2002,** 6, 319.
6. Kamaly, N.; Xiao, Z.; Valencia, P. M.; Radovic-Moreno, A. F.; Farokhzad, O. C. *Chem. Soc. Rev.* **2012,** 41, 2971.
7. Bensaid, F.; Thillaye du Boullay, O.; Amgoune, A.; Pradel, C.; Harivardhan Reddy, L.; Didier, E.; Sablé, S.; Louit, G.; Bazile, D.; Bourissou, D. *Biomacromolecules* **2013,** 14, 1189.
8. Bae, Y.; Fukushima, S.; Harada, A.; Kataoka, K. *Angew. Chem., Int. Ed.* **2003,** 42, 4640.
9. Bae, Y.; Jang, W.-D.; Nishiyama, N.; Fukushima, S.; Kataoka, K. *Mol. BioSyst.* **2005,** 1, 242.
10. Bae, Y.; Kataoka, K. *Adv. Drug Delivery Rev.* **2009,** 61, 768.
11. Wang, Z.; Chui, W.-K.; Ho, P. C. *Pharm. Res.* **2009,** 26, 1162.
12. Wang, J.; Liu, W.; Tu, Q.; Wang, J.; Song, N.; Zhang, Y.; Nie, N.; Wang, J. *Biomacromolecules* **2010,** 12, 228.
13. Huynh, V. T.; Chen, G.; Souza, P. d.; Stenzel, M. H. *Biomacromolecules* **2011,** 12, 1738.
14. Huynh, V. T.; de Souza, P.; Stenzel, M. H. *Macromolecules* **2011,** 44, 7888.
15. Huynh, V. T.; Quek, J. Y.; de Souza, P. L.; Stenzel, M. H. *Biomacromolecules* **2012,** 13, 1010.
16. Greenwald, R. B.; Choe, Y. H.; McGuire, J.; Conover, C. D. *Adv. Drug Delivery Rev.* **2003,** 55, 217.
17. Minko, T.; Kopečková, P.; Pozharov, V.; Kopeček, J. *J. Control. Rel.* **1998,** 54, 223.
18. Bissett, D.; Cassidy, J.; de Bono, J. S.; Muirhead, F.; Main, M.; Robson, L.; Fraier, D.; Magne, M. L.; Pellizzoni, C.; Porro, M. G.; Spinelli, R.; Speed, W.; Twelves, C. *Br. J. Cancer* **2004,** 91, 50.
19. Seymour, L. W.; Ferry, D. R.; Kerr, D. J.; Rea, D.; Whitlock, M.; Poyner, R.; Boivin, C.; Hesslewood, S.; Twelves, C.; Blackie, R.; Schatzlein, A.; Jodrell, D.; Bissett, D.; Calvert, H.; Lind, M.; Robbins, A.; Burtles, S.; Duncan, R.; Cassidy, J. *Int. J. Oncol.* **2009,** 34, 1629.
20. Yang, D.; Liu, X.; Jiang, X.; Liu, Y.; Ying, W.; Wang, H.; Bai, H.; Taylor, W. D.; Wang, Y.; Clamme, J.-P.; Co, E.; Chivukula, P.; Tsang, K. Y.; Jin, Y.; Yu, L. *J. Control. Rel.* **2012,** 161, 124.

21. Soepenberg, O.; de Jonge, M. J. A.; Sparreboom, A.; de Bruin, P.; Eskens, F. A. L. M.; de Heus, G.; Wanders, J.; Cheverton, P.; Ducharme, M. P.; Verweij, J. *Clin. Cancer Res.* **2005,** 11, 703.
22. Numbenjapon, T.; Wang, J.; Colcher, D.; Schluep, T.; Davis, M. E.; Duringer, J.; Kretzner, L.; Yen, Y.; Forman, S. J.; Raubitschek, A. *Clin. Cancer Res.* **2009,** 15, 4365.
23. Chen, X.; Parelkar, S. S.; Henchey, E.; Schneider, S.; Emrick, T. *Bioconjugate Chem.* **2012,** 23, 1753.
24. Tong, R.; Cheng, J. *Angew. Chem., Int. Ed.* **2008,** 47, 4830.
25. Tong, R.; Cheng, J. *J. Am. Chem. Soc.* **2009,** 131, 4744.
26. Tong, R.; Cheng, J. *Macromolecules* **2012,** 45, 2225.
27. Yin, Q.; Tong, R.; Xu, Y.; Baek, K.; Dobrucki, L. W.; Fan, T. M.; Cheng, J. *Biomacromolecules* **2013,** 14, 920.
28. Nicolas, J.; Guillaneuf, Y.; Lefay, C.; Bertin, D.; Gigmes, D.; Charleux, B. *Prog. Polym. Sci.* **2013,** 38, 63.
29. Yang, H.-C.; Silverman, J.; Wozniak, J. J. Low temperature heat shrinkable polymer material. US 4596728, 1986, US 4596728.
30. Harrisson, S.; Nicolas, J.; Maksimenko, A.; Bui, D. T.; Mougin, J.; Couvreur, P. *Angew. Chem., Int. Ed.* **2013,** 52, 1678.
31. Couvreur, P.; Stella, B.; Reddy, L. H.; Hillaireau, H.; Dubernet, C.; Desmaële, D.; Lepêtre-Mouelhi, S.; Rocco, F.; Dereuddre-Bosquet, N.; Clayette, P.; Rosilio, V.; Marsaud, V.; Renoir, J.-M.; Cattel, L. *Nano Lett.* **2006,** 6, 2544.
32. Arias, J. L.; Reddy, L. H.; Othman, M.; Gillet, B.; Desmae□le, D.; Zouhiri, F.; Dosio, F.; Gref, R.; Couvreur, P. *ACS Nano* **2011,** 5, 1513.
33. Couvreur, P.; Reddy, L. H.; Mangenot, S.; Poupaert, J. H.; Desmaele, D.; Lepetre-Mouelhi, S.; Pili, B.; Bourgaux, C.; Amenitsch, H.; Ollivon, M. *Small* **2008,** 4, 247.
34. Reddy, L. H.; Khoury, H.; Paci, A.; Deroussent, A.; Ferreira, H.; Dubernet, C.; Decleves, X.; Besnard, M.; Chacun, H.; Lepetre-Mouelhi, S.; Desmaele, D.; Rousseau, B.; Laugier, C.; Cintrat, J.-C.; Vassal, G.; Couvreur, P. *Drug Metab. Dispos.* **2008,** 36, 1570.
35. Reddy, L. H.; Marque, P.-E.; Dubernet, C.; Mouelhi, S.-L.; Desmaele, D.; Couvreur, P. *J. Pharmacol. Exp. Ther.* **2008,** 325, 484.
36. Sémiramoth, N.; Meo, C. D.; Zouhiri, F.; Saïd-Hassane, F.; Valetti, S.; Gorges, R.; Nicolas, V.; Poupaert, J. H.; Chollet-Martin, S.; Desmaële, D.; Gref, R.; Couvreur, P. *ACS Nano* **2012,** 6, 3820.

37. Bekkara-Aounallah, F.; Gref, R.; Othman, M.; Reddy, L. H.; Pili, B.; Allain, V.; Bourgaux, C.; Hillaireau, H.; Lepetre-Mouelhi, S.; Desmaele, D.; Nicolas, J.; Chafi, N.; Couvreur, P. *Adv. Funct. Mater.* **2008,** 18, 3715.
38. Moad, G.; Rizzardo, E.; Thang, S. H. *Aust. J. Chem.* **2009,** 62, 1402.
39. Hertel, L. W.; Boder, G. B.; Kroin, J. S.; Rinzel, S. M.; Poore, G. A.; Todd, G. C.; Grindey, G. B. *Cancer Res.* **1990,** 50, 4417.
40. Tanuma, S.; Powell, C. J.; Penn, D. R. *Surf. Interface Anal.* **1994,** 21, 165.
41. Bertholon, I.; Vauthier, C.; Labarre, D. *Pharm. Res.* **2006,** 23, 1313.
42. Kazatchkine, M. D.; Carreno, M. P. *Biomaterials* **1988,** 9, 30.
43. Boyer, C.; Bulmus, V.; Davis, T. P.; Ladmiral, V.; Liu, J.; Perrier, S. *Chem. Rev.* **2009,** 109, 5402.
44. Sen, S. E.; Prestwich, G. D. *J. Med. Chem.* **1989,** 32, 2152.
45. Gref, R.; Minamitake, Y.; Peracchia, M. T.; Trubetskoy, V.; Torchilin, V.; Langer, R. *Science* **1994,** 263, 1600.

Supplementary Information

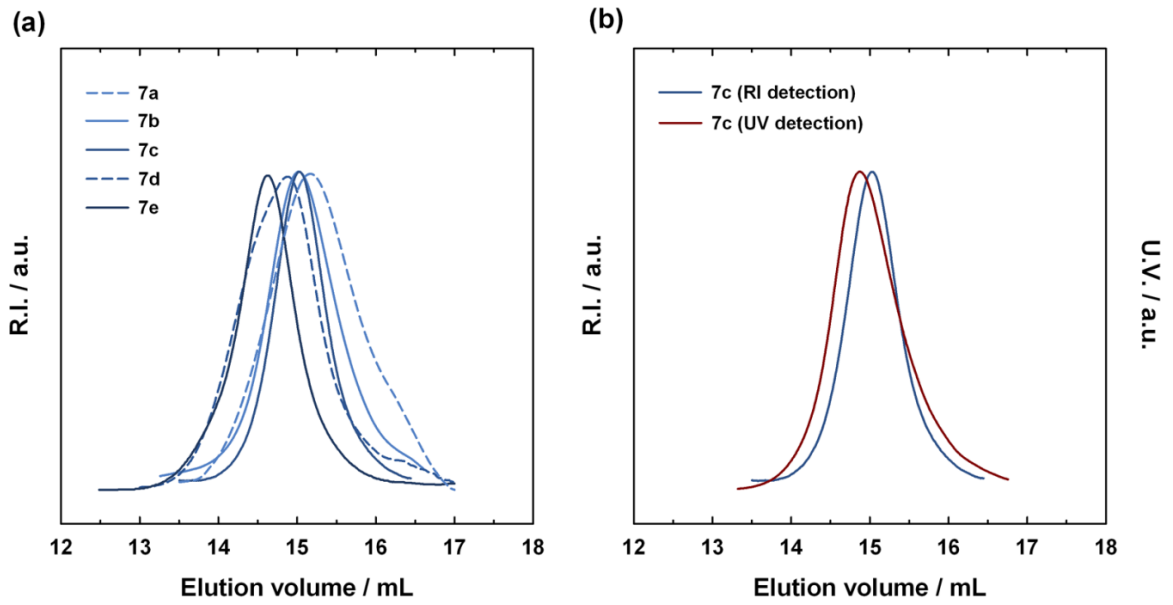

Figure S1. Normalized size exclusion chromatograms ($CHCl_3$, 1 $mL.min^{-1}$) of gemcitabine-poly(squalene methacrylate) conjugates (**7a-e**) after deprotection by RI detection (a). Normalized size exclusion chromatograms ($CHCl_3$, 1 $mL.min^{-1}$) of gemcitabine-poly(squalene methacrylate) conjugate (**7c**) after deprotection by RI and UV (@ 254 nm) detection (b).

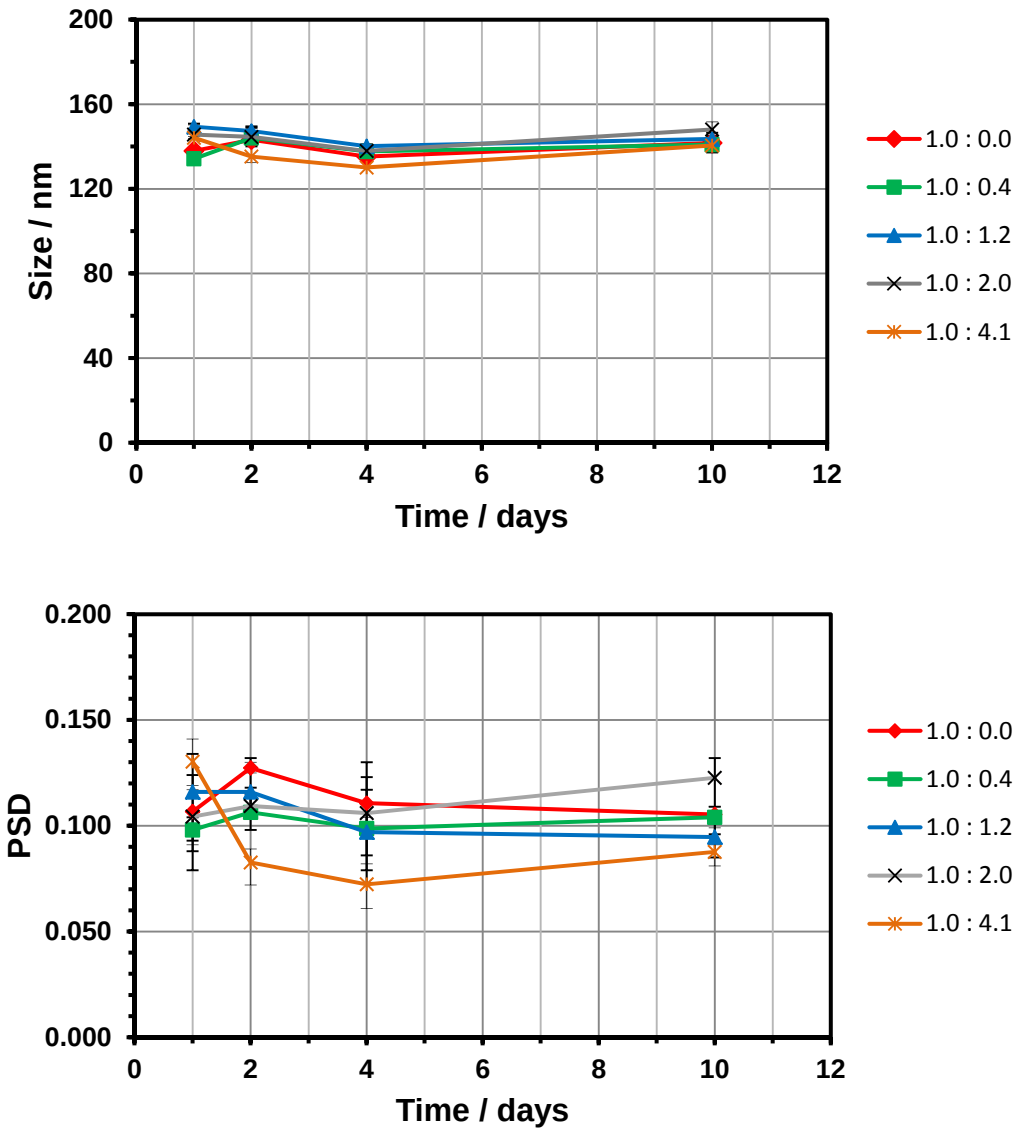

Figure S2. Dynamic light scattering data giving the average diameter in intensity (D_z) (a) and the particle size distribution (PSD) (b) of Gem-PSqMA **7d**/Sq-PEG nanoparticle suspensions for various Gem-PSqMA **7d**/Sq-PEG ratios (1:0; 1:0.4; 1:1.2; 1:2; 1:4.1; mol:mol). The values are represented as mean ± standard deviation of three independent formulations.

Table S1. X-ray Photoelectron Spectroscopic (XPS) Analysis of the Different C1s, O1s, N1s, F1s and S2p Peak Fitting Intensities of Gem-PSqMA and Gem-PSqMA/Sq-PEG Nanoparticles.

Nanoparticles	C1s envelope ratio[a] (%)			O1s envelope ratio[a] (%)		N1s envelope ratio (%)	F1s envelope ratio (%)	S2p envelope ratio (%)	
	C-C	C-O	C=O	O-C	O=C			S-	S=
Gem-PSqMA	77.6	4.9	1.3	10.0	3.2	0.7	0.7	1.6	-
Gem-PSqMA/Sq-PEG	71.1	11.7	1.4	11.5	2.9	0.5	0.2	0.5	0.2

[a] The different percentages were calculated from fitted peaks areas.

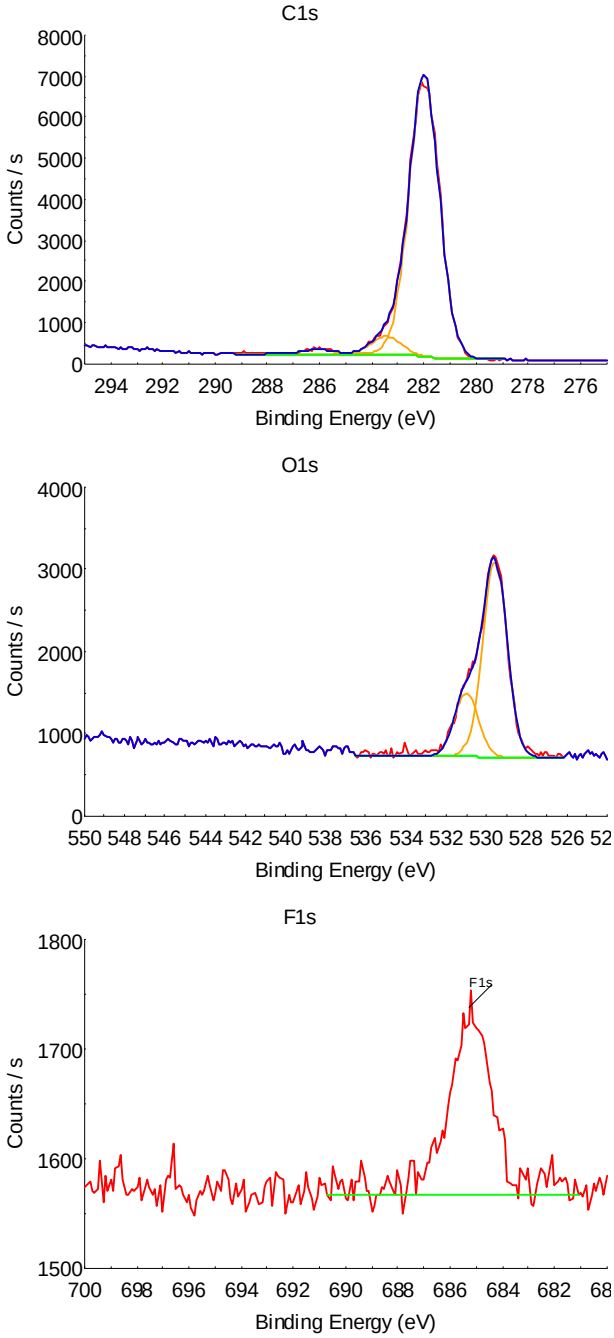
C1s
8000
7000
6000
5000
4000
3000
2000
1000
0
Counts / s
294 292 290 288 286 284 282 280 278 276
Binding Energy (eV)
O1s
4000
3000
2000
1000
0
Counts / s
550 548 546 544 542 540 538 536 534 532 530 528 526 52
Binding Energy (eV)
F1s
1800
1700
1600
1500
Counts / s
F1s
700 698 696 694 692 690 688 686 684 682 68
Binding Energy (eV)

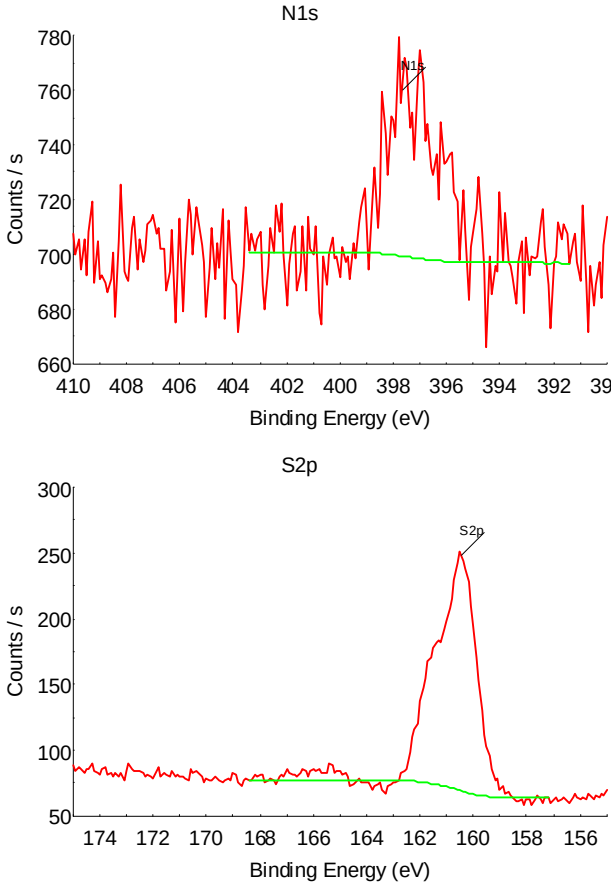

Figure S3. Carbon C1s envelope, Oxygen O1s envelope, Nitrogen N1s peak, Fluorine F1s peak and Sulfur S2p peaks of X-ray photon spectroscopic analysis (XPS) from Gem-PSqMA nanoparticles.

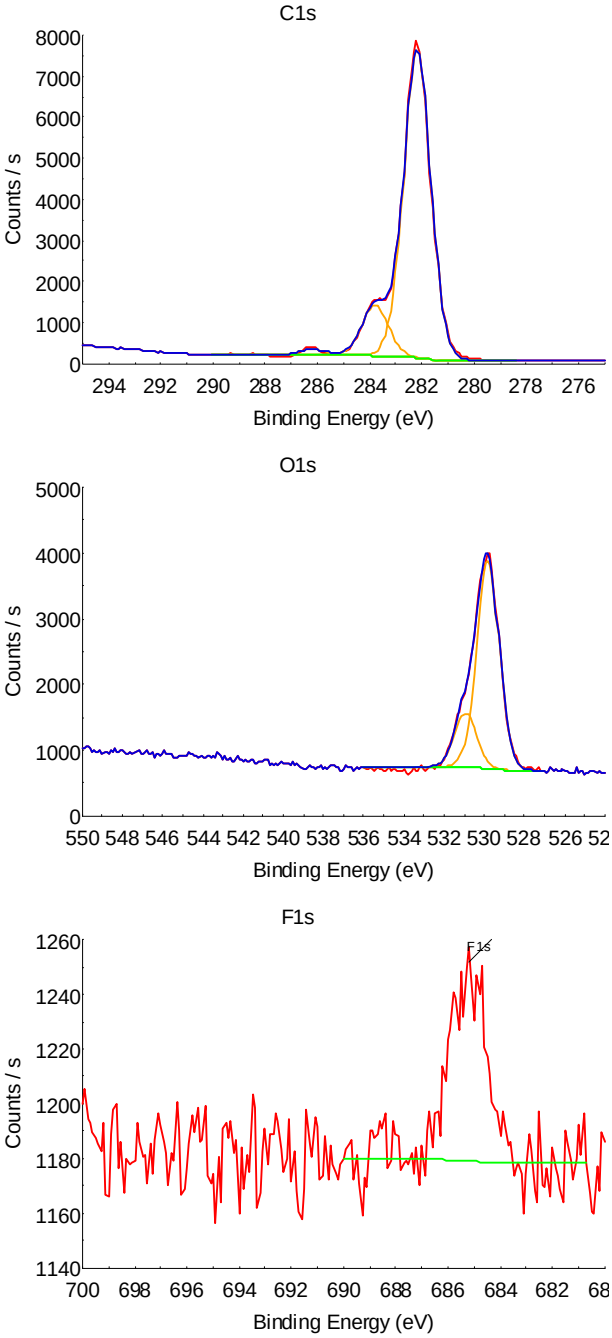
C1s
Counts / s
8000
7000
6000
5000
4000
3000
2000
1000
0
294 292 290 288 286 284 282 280 278 276
Binding Energy (eV)
O1s
Counts / s
5000
4000
3000
2000
1000
0
550 548 546 544 542 540 538 536 534 532 530 528 526 52
Binding Energy (eV)
F1s
F 1s
Counts / s
1260
1240
1220
1200
1180
1160
1140
700 698 696 694 692 690 688 686 684 682 68
Binding Energy (eV)

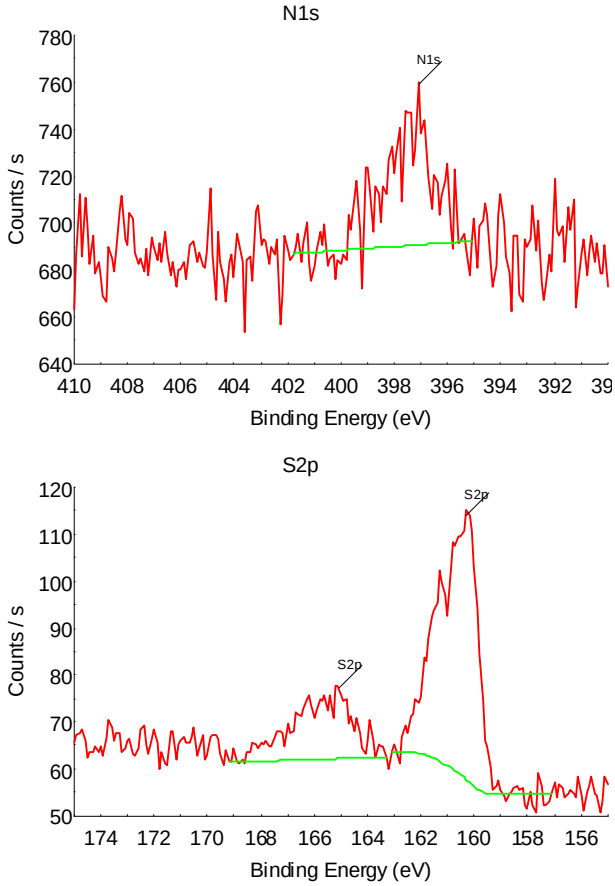

Figure S4. Carbon C1s envelope, Oxygen O1s envelope, Nitrogen N1s peak, Fluorine F1s peak and Sulfur S2p peaks of X-ray photon spectroscopic analysis (XPS) from Gem-PSqMA/PEG-Sq nanoparticles (1:2.2; mol:mol).

Table S2. Half Maximal Inhibitory Concentration (IC_{50}) of Cell Proliferation by Gemcitabine-Poly(Squalene Methacrylate) Nanoparticles on Various Cancer Cell Lines Determined by Cell Viability Assay (expressed as IC_{50} ± SD in nM).

Cell line	Gem	**7e**	**7c**	**7b**	**7a**	PSqMA[a]
MiaPaca2	20 ± 3	68 ± 5	76 ± 6	51 ± 4	54 ± 3	>20000
A549	15 ± 2	180 ± 6	180 ± 4	179 ± 6	155 ± 5	>20000
L1210 WT	4 ± 1	72 ± 4	84 ± 2	58 ± 2	52 ± 1	7800
CCRF CEM	11 ± 1	71 ± 6	85 ± 2	74 ± 1	63 ± 3	7100
P388S	3 ± 1	40 ± 1	39 ± 1	30 ± 1	23 ± 1	1500

[a] DP_n ~6.

Chapitre IV

Nanoparticles with *In Vivo* Anticancer Activity from Polymer Prodrug Amphiphiles Prepared by Living Radical Polymerization

Simon Harrisson, Julien Nicolas, Andrei Maksimenko, Duc Trung Bui, Julie Mougin, and Patrick Couvreur*

Angew. Chem., Int. Ed. **2013**, *125*, 1722-1726

Résumé

Dans cette étude, auquel je n'ai que partiellement participé, nous avons conçu une nouvelle classe de nanoparticules de prodrogues macromoléculaires à forte activité anticancéreuse *in vitro* et *in vivo*. Afin de simplifier le chemin synthétique, nous avons fonctionnalisé la Gem par une alcoxyamine, qui est amorceur de polymérisation radicalaire contrôlée par les nitroxides (NMP), pour en faire croitre dans une seconde étape de courtes chaines de polyisoprènes (PI). Le PI a été choisi comme polymère hydrophobe du fait de ses propriétés intéressantes telles que sa dégradabilité chimie et enzymatique, ainsi que sa biocompatibilité et sa similarité structurelle avec les isoprenoids naturels (vitamine E, squalène, rétinol, etc.).

Une petite librairie de conjugués de type Gem-PI a été préparée et les nanoparticules correspondantes ont démontré une activité anticancéreuse *in vitro* importante sur plusieurs lignées cellulaires cancéreuses ; activité d'autant plus élevée que la longueur de la chaine de PI était augmentée. Par ailleurs, ces nanoparticules se sont également avérées efficaces *in vivo* sur des souris porteuses de tumeurs solides avec la même influence de la longueur du PI sur l'activité anticancéreuse.

1. Introduction

Drug-loaded polymer nanoparticles are a promising approach to the treatment of severe diseases, such as cancer, infections and neurodegenerative disorders.[1-5] These nanoconstructs are obtained from the encapsulation of a drug during self-assembly of amphiphilic copolymers in aqueous solution.[6] In the field of cancer, although this approach has led to numerous encouraging results and proofs of concept *in vitro*,[7,8] important limitations still remain which may explain the lower number of successful *in vivo* studies: i) the "*burst release*", in which a large fraction of chemotherapeutic agent is quickly released post-administration, can be harmful to patients; ii) the encapsulation of poorly soluble drugs, exhibiting a high tendency to crystallization and iii) maximum achievable drug loadings are generally only a few percent, requiring the use of a large amount of nanocarrier, which can lead to prohibitive toxicity *in vivo*.

In order to overcome these imposing obstacles, inspiration can be taken from the prodrug approach, whereby the drug is covalently linked to a (macro)molecule. The inactive prodrug is further metabolized *in vivo* into an active metabolite.[9] This strategy improves drug solubility, prolongs *in vivo* circulation, and reduces adverse effects, the last feature being of paramount importance in many chemotherapy treatments. In the particular case of polymeric prodrugs, the standard approach is to link hydrophobic drugs to a preformed hydrophilic polymer (*e.g.*, poly(ethylene glycol),[10] poly(*N*-(2-hydroxypropyl)methacrylamide),[11-14] poly(L-glutamic acid),[15] dextran,[16] cyclodextrins,[17,18] or poly(methacryloyloxyethyl phosphorylcholine)[19]), resulting in fully water-soluble conjugates or small-size aggregates.[20-22] Likewise, prodrugs prepared *via* conjugation to amphiphilic copolymers have alleviated some of the drawbacks of nanoparticles.[23-27]

We report in this study the facile design of a new class of efficient anticancer nanocarriers with high drug payloads made of well-defined polymer-drug conjugate amphiphiles obtained by nitroxide-mediated polymerization (NMP),[28-30] comprising a hydrophobic polymer block and a hydrophilic drug tail. Like atom transfer radical polymerization (ATRP)[31,32] and reversible addition-fragmentation chain transfer (RAFT),[33] NMP is a living radical polymerization (LRP) technique that enables well-defined macromolecular architectures to be synthesized and that has recently known some success in the bioconjugation area.[34-38] The new strategy we propose relies on the controlled growth of a hydrophobic oligomer from an anticancer drug-bearing macroalkoxyamine initiator, in order to position one chemotherapeutic at the extremity of each polymer chain (Scheme 1). Due to

the amphiphilic nature of the resulting drug-polymer conjugates, they spontaneously self-assemble in aqueous solution to form stable, narrowly-dispersed nanoparticles, which show significant anticancer activity both *in vitro* on various cancer cell lines as well as *in vivo* on tumor-bearing mice. For the first time, nanoparticles with *in vivo* anticancer activity have been obtained from the self-assembly of hydrophilic drug-hydrophobic polymer prodrugs. It also opens a new area for LRP techniques in the biomedical field as this general methodology can be extended to many other hydrophilic drug/hydrophobic polymer combinations.

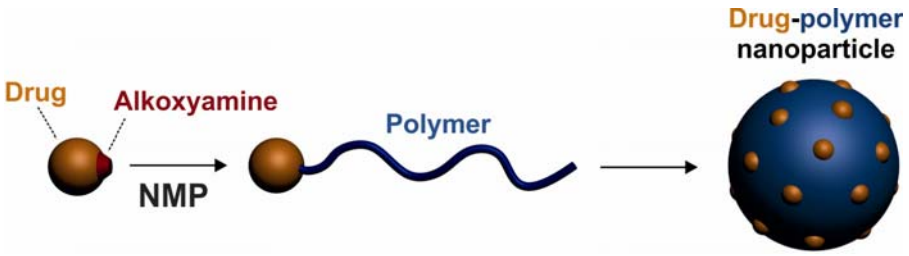

Scheme 1. Strategy to achieve well-defined polymer-drug conjugate nanoparticles by nitroxide-mediated polymerization (NMP).

2. Results and discussions

Polyisoprene (PI) has been chosen as hydrophobic polymer for its interesting properties such as chemical[39,40] and enzymatic[41] degradability, as well as its biocompatibility[42] and its structural similarity with natural polyisoprenoids. Isoprene is the basic structural motif of naturally occurring, biocompatible terpenes (*e.g.*, coenzyme Q10, retinol, vitamin E, etc.). We therefore considered that synthetic PI of controlled structure may also have interesting biomedical applications, especially as a nanocarrier. The anticancer drug gemcitabine (Gem), a nucleoside analogue with demonstrated activity against a wide range of solid tumors (*e.g.*, colon, lung, pancreatic, breast, bladder and ovarian cancers),[43] was selected as a drug model. Nucleoside analogues are a class of therapeutic agents with significant anticancer or antiviral properties, but also serious limitations that often restrict their use, such as short plasma half-life, rapid metabolism, the induction of resistance, and the advent of severe side effects.[44] The employed strategy is expected to protect Gem from rapid deamination by deoxycytidine deaminase,[45] leading to greater *in vivo* anticancer activity than free Gem.

Gem-PI conjugates were prepared by NMP of isoprene under SG1 control,[46] utilizing a Gem-functional alkoxyamine initiator (**3**), which was obtained by coupling unprotected Gem (**1**) to the AMA-SG1 alkoxyamine[47,48] (**2**) under PyBOP-linkage chemistry (Figure 1).

Polymerization of isoprene in the presence of **3** allowed for the preparation of a small library of Gem-PI conjugates (**4a-d**, Table 1), of controlled molar mass with a terminal gemcitabine functionality attached to the polymer chain *via* a hydrolysable amide linkage.

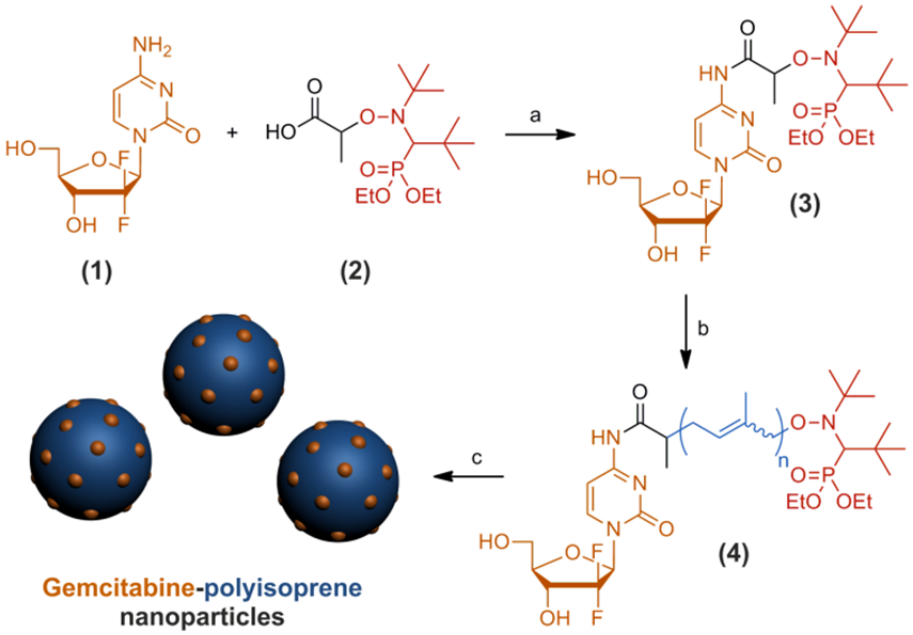

Figure 1. Design of gemcitabine-polyisoprene conjugate nanoparticles. *Reagents and conditions*: (a) PyBOP, DIPEA, DMF, 25 °C, 24 h; (b) isoprene, pyridine, 115°C, 2–16 h; (c) nanoprecipitation (THF:H_2O, 1:2).

A similar pathway employing a TBDMS-protected Gem derivative was also investigated but led to ~20–30% loss of Gem during the deprotection step (see Supporting Information). The alternative of attaching Gem to a previously formed polymer was rejected due to the difficulty of purifying the mixture of products, byproducts and unreacted PI which would result. By contrast, the only components of the "*grafting from*" approach employed here are the functionalized polymer, solvent and unreacted monomer; the latter two being removed by evaporation. Gem-PI conjugates with number-average molar mass (M_n) between 840 and 2510 g.mol^{-1} and dispersities ($Đ$) of 1.3-1.4 were prepared (Table 1). The presence of gemcitabine was confirmed through proton and fluorine NMR, as well as by ESI MS, and its distribution across polymer chains of all molar masses was confirmed by size exclusion chromatography (SEC) with UV detection (see Supporting Information).

Table 1. Characterization of Gemcitabine-Polyisoprene Conjugates and Nanoparticles.

Entry	M_n[a] (g.mol^{-1})	$Đ$[a]	size[b] (nm)	PSD[b]	ζ[c] (mV)	%Gem[d] (wt.%)
4a	840	1.35	159 ± 4	0.10 ± 1	–77 ± 3	31.2
4b	1190	1.29	137 ± 3	0.10 ± 2	–70 ± 5	22.1
4c	1560	1.28	133 ± 4	0.11 ± 2	–66 ± 5	16.9
4d	2510	1.40	138 ± 1	0.11 ± 1	–68 ± 4	10.5

[a] Determined by SEC, calibrated with PS standards and converted to PI using Mark–Houwink–Sakurada parameters.[46] [b] Determined by DLS. [c] Zeta potential. [d] %Gem = $MW_{Gem}/M_{n,PI}$.

The use of **3**, a very polar initiator, in the polymerization of isoprene, a non-polar monomer, presented some difficulties. Attempts to perform the polymerization in bulk isoprene gave poor control over molar mass and broad molar mass distributions due to the poor solubility of the initiator in isoprene. More polar solvents, such as DMF, DMSO or even acetone do not dissolve PI. Improved results were obtained when the polymerization was performed as a 50% solution in pyridine. Pyridine dissolves sugars as a result of its ability to form hydrogen bonds, but is sufficiently non-polar to be able to dissolve PI.[49] The resulting polymerizations exhibited a linear relationship between conversion and M_n which was close to theory, and reached 30% conversion after 16 h of reaction at 115°C (Figures S1 and S2, Supporting Information).

Due to the amphiphilic nature of the Gem-PI conjugates, the corresponding nanoparticles were prepared by self-assembly from a THF solution of Gem-PI into water, followed by evaporation of THF *in vacuo*. The resulting suspensions (2.5 mg.mL^{-1}) contained nanoparticles of 130-160 nm in diameter, which is in the suitable window for drug delivery through intravenous administration, with narrow particle size distributions (PSD ~0.1) and remarkable colloidal stability of up to one month. Some dependence of nanoparticle size on molar mass was observed, with the lowest molar mass PI giving consistently larger nanoparticles than the other samples (Figure S9a,b). Surface charges of the particles ranged from –66 to –77 mV, indicating significant electrostatic stabilization of the nanoparticles, and were correlated with the nanoparticle sizes (Figure S9c,d). Nanoparticle sizes, size distributions and zeta potentials were reproducible, with three independent preparations giving nearly identical results for each sample. A small library of non-functionalized PI

nanoparticles with similar macromolecular and colloidal characteristics was also prepared under identical experimental conditions (**5a-e** in Tables S2, S6 and Figure S5, Supporting Information). Gem-PI and PI nanoparticles were further characterized by cryogenic transmission electron microscopy (Figure 2) and showed round-shaped morphologies and colloidal characteristics in good agreement with dynamic light scattering (DLS) data. Importantly, this approach allowed nanoparticles with very high drug contents to be produced, ranging from 10.5 wt.% (**4d**) to 31.2 wt.% (**4a**) (Table 1). This is a significant improvement on classic drug-loaded nanoparticles, which usually carry drug payloads of only a few percent.

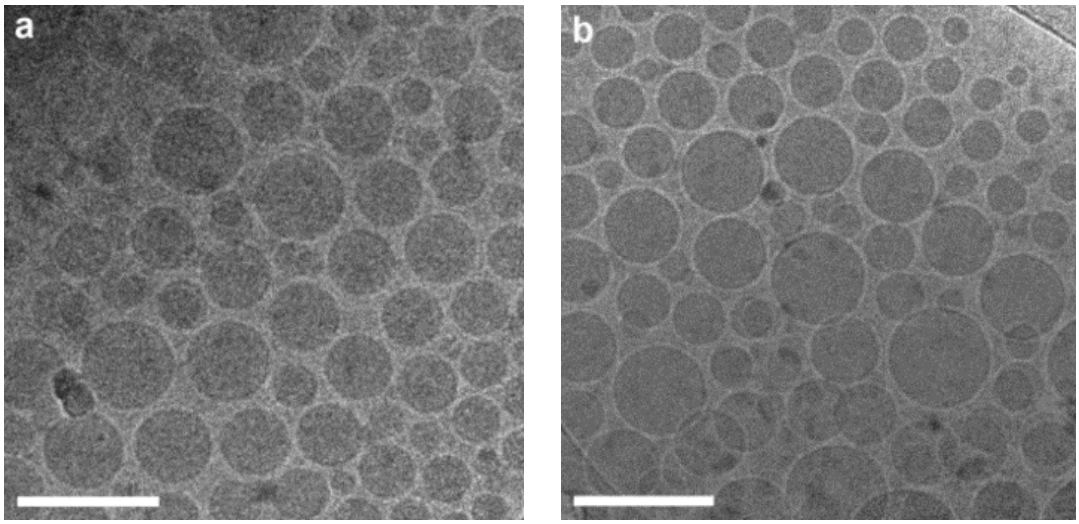

Figure 2. Cryogenic transmission electron microscopy of Gem-PI **4d** (a) and PI **5d** (b) nanoparticles. Scale bars = 200 nm.

The Gem-PI conjugate nanoparticles were then tested for their *in vitro* activity by measuring the half maximal inhibitory concentration (IC_{50}) of cell proliferation on four cancer cell lines: i) murine leukemia (L1210), ii) human leukemia (CCRF-CEM), iii) human pancreatic cancer (MiaPaCa-2) and iv) human lung carcinoma (A549). Gem-PI nanoparticles **4a-4d** showed significant anticancer activity on all tested cell lines (Table 2), while a control series of non-functionalized PI nanoparticles of similar molar masses were inactive (Table S7, Supporting Information). However, as expected owing to their prodrug nature, all nanoparticles showed lower cytotoxicity than free Gem while their IC_{50} values remained in the nanomolar range. Interestingly, as the controlled chain growth performed by the NMP process allowed for the fine tuning of the polymer chain length, a preliminary structure-activity relationship can be extracted from these results, which is of high importance in the rational design of a drug

delivery system. Indeed, for all tested cell lines, the higher the M_n of the Gem-PI conjugate, the greater the anticancer activity of the corresponding nanoparticles. This trend may be correlated with the surface hydrophobicity of the Gem-PI nanoparticles (which can be readily adjusted due to the employed LRP process), leading to a higher rate of endocytosis due to opsonin adsorption when the PI chain length is increased.[50]

Table 2. Anticancer Activity of Gemcitabine-Polyisoprene Conjugate Nanoparticles after 72 h of incubation (expressed as IC_{50} ± SD in nM)[a]

Cell line	**4a**	**4b**	**4c**	**4d**	**Gem**
MiaPaCa-2	810 ± 82	568 ± 53	169 ± 7	186 ± 11	36 ± 4
L1210	659 ± 5	358 ± 9	330 ± 18	252 ± 8	14 ± 1
CCRF-CEM	232 ± 20	144 ± 1	84 ± 2	91 ± 3	6 ± 1
A549	303 ± 8	216 ± 7	104 ± 5	87 ± 1	13 ± 1

[a] Determined by cell viability assay (MTT test).

The *in vivo* anticancer activity of these novel Gem-PI polymer prodrug nanoparticles was then investigated against human pancreatic (MiaPaCa-2) carcinoma xenograft model in mice following intravenous injections (on days 0, 4, 8, and 12) of Gem at 7 $mg.kg^{-1}$, Gem-PI nanoparticles (at 7 $mg.kg^{-1}$ Gem-equivalent dose) or non-functionalized PI nanoparticles of similar chain lengths (Figure 3a). Untreated mice (saline 0.9%) exhibited a rapid tumor growth which reached ~1350 mm^3 at day 34. Mice treated with Gem or non-functionalized PI nanoparticles (**5a**, **5e**) showed a similar pattern, with equivalent tumor volumes at the end of the treatment, demonstrating the absence of anticancer activity of Gem in this model. In contrast, treatment of mice with Gem-PI nanoparticles (**4b**) at the same Gem-equivalent dose led to a considerable decrease in the tumor progression. An even higher anticancer activity was obtained with Gem-PI nanoparticles (**4d**), leading to a tumor growth inhibition as high as 72% (compared to 46% for **4b**) and a tumor growth which plateaued after 23 days of treatment. As already observed in the cell culture experiments, nanoparticles obtained from the higher molar mass Gem-PI conjugate (**4d**) demonstrated greater *in vivo* anticancer activity than their lower molar mass counterparts (**4b**). This is of crucial importance as it shows that *in vitro* cytotoxicity trends for the polymer-drug conjugates can be extrapolated to *in vivo* experiments.

The relative body weight loss was also monitored throughout the treatment (Figure 3b). Importantly, Gem-treated mice exhibited significant weight loss (~-10%) compared to control injections, showing the toxicity arising from the free drug treatment. By contrast, the Gem-PI-treated mice maintained or slightly increased their body weight (~+3%), which supports both the efficient anticancer activity of Gem-PI polymer prodrug nanoparticles and the disappearance of Gem-related adverse effects.

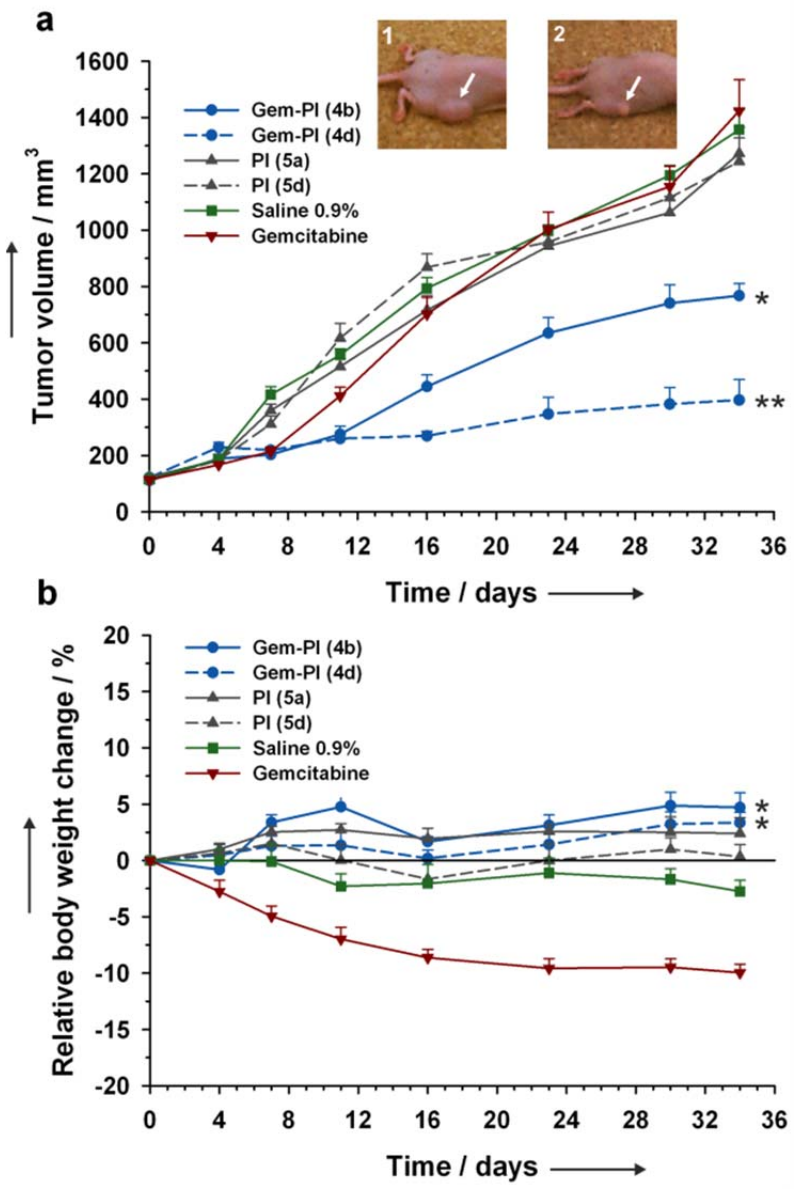

Figure 3. *In vivo* anticancer activity of gemcitabine (▼, 7 mg.kg^{-1}), polyisoprene-gemcitabine nanoparticles (●, **4b** and **4d**, 7 mg.kg^{-1} Gem-equivalent dose), control (■, saline 0.9%) and polyisoprene nanoparticles (**5a** and **5d**, ▲, same dose of polymer as **4d**) following intravenous treatment (on days 0, 4, 8 and 12) of mice bearing MiaPaCa-2 subcutaneous tumors: tumor progression as function of time (a) and relative body weight change as function of time (b). The values are the mean ± SD (n = 6). Statistical differences between Gem- and Gem-PI-treated groups (**4b** or **4d**) with confidence levels of > 95% (Student's t-test with Bonferroni correction for multiple comparisons) are marked by * ($p < 0.025$) or ** ($p < 0.005$). White arrows point to the position of the implanted tumor on representative mouse at end point for Gem-treated group (insert 1) and Gem-PI (**4d**)-treated group (insert 2).

3. Conclusions

In summary, the facile design of a new class of drug-polymer conjugate prodrug nanoparticles has been reported. The strategy relies on the controlled growth of PI by NMP from a gemcitabine-functionalized macroalkoxyamine initiator based on the SG1 control agent (a nitroxide which is non-cytotoxic even at very high doses),[51] allowing the resulting amphiphilic species to self-assemble into stable, narrowly dispersed nanoparticles of 130–160 nm in diameter. These nanoconstructs exhibit efficient anticancer activity both *in vitro* on various cancer cell lines as well as *in vivo* on human pancreatic carcinoma-bearing mice, while suppressing the inherent toxicity of the employed chemotherapeutics. The synthetic pathway, which can be virtually applied to any LRP techniques, is robust and very versatile as it solely requires: i) the use of hydrophilic/polar drugs; ii) a suitable drug functionalization and iii) the controlled growth of a hydrophobic polymer. As a consequence, this methodology is easy to carry out and can allow for the design of a broad range of drug-polymer conjugates with high drug payloads, leading to nanoparticles with more potent biological activities. Furthermore, the use of a controlled/living radical process allows for fine-tuning the polymer chain length. This is of crucial importance to determine structure-activity relationships in order to design optimized drug delivery systems.

References

1. Brambilla, D.; Le Droumaguet, B.; Nicolas, J.; Hashemi, S. H.; Wu, L.-P.; Moghimi, S. M.; Couvreur, P.; Andrieux, K. *Nanomedicine: NBM* **2011,** 7, 521.
2. Brigger, I.; Dubernet, C.; Couvreur, P. *Adv. Drug Delivery Rev.* **2002,** 54, 631.
3. Farokhzad, O. C.; Langer, R. *ACS Nano* **2009,** 3, 16.
4. Hans, M. L.; Lowman, A. M. *Curr. Opin. Solid State Mater. Sci.* **2002,** 6, 319.
5. Panyam, J.; Labhasetwar, V. *Adv. Drug Delivery Rev.* **2003,** 55, 329.
6. Elsabahy, M.; Wooley, K. L. *Chem. Soc. Rev.* **2012,** 41, 2545.
7. Kamaly, N.; Xiao, Z.; Valencia, P. M.; Radovic-Moreno, A. F.; Farokhzad, O. C. *Chem. Soc. Rev.* **2012,** 41, 2971.
8. Nicolas, J.; Mura, S.; Brambilla, D.; Mackiewicz, N.; Couvreur, P. *Chem. Soc. Rev.* **2013,** 42, 1147.
9. Albert, A. *Nature* **1958,** 182, 421.

10. Greenwald, R. B.; Choe, Y. H.; McGuire, J.; Conover, C. D. *Adv. Drug Delivery Rev.* **2003,** 55, 217.
11. Thomson, A. H.; Vasey, P. A.; Murray, L. S.; Cassidy, J.; Fraier, D.; Frigerio, E.; Twelves, C. *Br. J. Cancer* **1999,** 81, 99.
12. Seymour, L. W.; Ferry, D. R.; Kerr, D. J.; Rea, D.; Whitlock, M.; Poyner, R.; Boivin, C.; Hesslewood, S.; Twelves, C.; Blackie, R.; Schatzlein, A.; Jodrell, D.; Bissett, D.; Calvert, H.; Lind, M.; Robbins, A.; Burtles, S.; Duncan, R.; Cassidy, J. *Int. J. Oncol.* **2009,** 34, 1629.
13. Bissett, D.; Cassidy, J.; de Bono, J. S.; Muirhead, F.; Main, M.; Robson, L.; Fraier, D.; Magne, M. L.; Pellizzoni, C.; Porro, M. G.; Spinelli, R.; Speed, W.; Twelves, C. *Br. J. Cancer* **2004,** 91, 50.
14. Minko, T.; Kopečková, P.; Pozharov, V.; Kopeček, J. *J. Control. Rel.* **1998,** 54, 223.
15. Yang, D.; Liu, X.; Jiang, X.; Liu, Y.; Ying, W.; Wang, H.; Bai, H.; Taylor, W. D.; Wang, Y.; Clamme, J.-P.; Co, E.; Chivukula, P.; Tsang, K. Y.; Jin, Y.; Yu, L. *J. Control. Rel.* **2012,** 161, 124.
16. Soepenberg, O.; de Jonge, M. J. A.; Sparreboom, A.; de Bruin, P.; Eskens, F. A. L. M.; de Heus, G.; Wanders, J.; Cheverton, P.; Ducharme, M. P.; Verweij, J. *Clin. Cancer Res.* **2005,** 11, 703.
17. Schluep, T.; Hwang, J.; Cheng, J.; Heidel, J. D.; Bartlett, D. W.; Hollister, B.; Davis, M. E. *Clin. Cancer Res.* **2006,** 12, 1606.
18. Numbenjapon, T.; Wang, J.; Colcher, D.; Schluep, T.; Davis, M. E.; Duringer, J.; Kretzner, L.; Yen, Y.; Forman, S. J.; Raubitschek, A. *Clin. Cancer Res.* **2009,** 15, 4365.
19. Chen, X.; Parelkar, S. S.; Henchey, E.; Schneider, S.; Emrick, T. *Bioconjugate Chem.* **2012,** 23, 1753.
20. Vicent, M. J.; Duncan, R. *Trends Biotechnol.* **2006,** 24, 39.
21. Duncan, R. *Nat. Rev. Cancer* **2006,** 6, 688.
22. Putnam, D.; Kopeček, J., Polymer conjugates with anticancer activity Biopolymers II. In Peppas, N.; Langer, R., Eds. Springer Berlin / Heidelberg: 1995; Vol. 122, pp 55.
23. Wang, Z.; Chui, W.-K.; Ho, P. C. *Pharm. Res.* **2009,** 26, 1162.
24. Wang, J.; Liu, W.; Tu, Q.; Wang, J.; Song, N.; Zhang, Y.; Nie, N.; Wang, J. *Biomacromolecules* **2010,** 12, 228.
25. Bae, Y.; Fukushima, S.; Harada, A.; Kataoka, K. *Angew. Chem., Int. Ed.* **2003,** 42, 4640.
26. Bae, Y.; Jang, W.-D.; Nishiyama, N.; Fukushima, S.; Kataoka, K. *Mol. BioSyst.* **2005,** 1, 242.

27. Bae, Y.; Kataoka, K. *Adv. Drug Delivery Rev.* **2009,** 61, 768.
28. Nicolas, J.; Guillaneuf, Y.; Lefay, C.; Bertin, D.; Gigmes, D.; Charleux, B. *Prog. Polym. Sci.* **2013,** 38, 63.
29. Hawker, C. J.; Bosman, A. W.; Harth, E. *Chem. Rev.* **2001,** 101, 3661.
30. Grubbs, R. B. *Polymer Reviews* **2011,** 51, 104.
31. Matyjaszewski, K.; Xia, J. *Chem. Rev.* **2001,** 101, 2921.
32. Kamigaito, M.; Ando, T.; Sawamoto, M. *Chem. Rev.* **2001,** 101, 3689.
33. Perrier, S.; Takolpuckdee, P. *J. Polym. Sci., Part A: Polym. Chem.* **2005,** 43, 5347.
34. Boyer, C.; Bulmus, V.; Davis, T. P.; Ladmiral, V.; Liu, J.; Perrier, S. *Chem. Rev.* **2009,** 109, 5402.
35. Le Droumaguet, B.; Nicolas, J. *Polym. Chem.* **2010,** 1, 563.
36. Heredia, K. L.; Maynard, H. D. *Org. Biomol. Chem.* **2007,** 5, 45.
37. Sumerlin, B. S. *ACS Macro Letters* **2011,** 1, 141.
38. Nicolas, J.; Mantovani, G.; Haddleton, D. M. *Macromol. Rapid Commun.* **2007,** 28, 1083.
39. Chen, S. Y.; Huang, Y. M.; Tsiang, R. C. C. *J. Polym. Sci., Part A: Polym. Chem.* **2008,** 46, 1964.
40. Cheng, C.; Qi, K.; Khoshdel, E.; Wooley, K. L. *J. Am. Chem. Soc.* **2006,** 128, 6808.
41. Watanabe, T.; Sato, S.; Honda, Y.; Kuwahara, M. *Biomacromolecules* **2003,** 4, 321.
42. Yang, H.-C.; Silverman, J.; Wozniak, J. J. Low temperature heat shrinkable polymer material. US 4596728, 1986, US 4596728.
43. Hertel, L. W.; Boder, G. B.; Kroin, J. S.; Rinzel, S. M.; Poore, G. A.; Todd, G. C.; Grindey, G. B. *Cancer Res.* **1990,** 50, 4417.
44. Galmarini, C. M.; Mackey, J. R.; Dumontet, C. *Leukemia* **2001,** 15, 875.
45. Heinemann, V.; Xu, Y.-Z.; Chubb, S.; Sen, A.; Hertel, L. W.; Grindey, G. B.; Plunkett, W. *Cancer Res.* **1992,** 52, 533.
46. Harrisson, S.; Couvreur, P.; Nicolas, J. *Macromolecules* **2011,** 44, 9230.
47. Chenal, M.; Boursier, C.; Guillaneuf, Y.; Taverna, M.; Couvreur, P.; Nicolas, J. *Polym. Chem.* **2011,** 2, 1523.
48. Harrisson, S.; Couvreur, P.; Nicolas, J. *Polym. Chem.* **2011,** 2, 1859.
49. Harrisson, S.; Couvreur, P.; Nicolas, J. *Macromol. Rapid Commun.* **2012,** 33, 805.
50. Owens Iii, D. E.; Peppas, N. A. *Int. J. Pharm.* **2006,** 307, 93.
51. Chenal, M.; Mura, S.; Marchal, C.; Gigmes, D.; Charleux, B.; Fattal, E.; Couvreur, P.; Nicolas, J. *Macromolecules* **2010,** 43, 9291.

Supporting Information

1. Materials

Gemcitabine hydrochloride was purchased from Sequoia Research Products Limited (UK). *N*-*tert*-butyl-*N*-[1-diethylphosphono-(2,2-dimethylpropyl)] nitroxide (SG1, 85%) was obtained from Arkema (France). 2-[*N*-*tert*-butyl-*N*-(1-diethoxyphosphoryl-2,2-di-methylpropyl)aminoxy] propionic acid (AMA-SG1) and ethyl 2-methyl-2-[*N*-*tert*-butyl-*N*-(1-diethoxyphosphoryl-2,2-di-methylpropyl)aminoxy] propionate (EiB-SG1) were prepared according to a published method.[1] All other materials were purchased from Aldrich at the highest available purity and used as received.

2. Analytical methods

2.1 Nuclear Magnetic Resonance Spectroscopy (NMR).

NMR spectroscopy was performed in 5 mm diameter tubes in $CDCl_3$, DMSO-d_6 or acetone-d_6 at 25 °C. ^{1}H and ^{13}C NMR spectroscopy was performed on a Bruker Avance 300 spectrometer at 300 MHz (^{1}H) or 75 MHz (^{13}C). The chemical shift scale was calibrated on the basis of the solvent peak. ^{31}P and ^{19}F NMR spectroscopy was performed on a Bruker 200 spectrometer at 81 MHz (^{31}P) or 188 MHz (^{19}F). The chemical shift scale was calibrated relative to an external standard (85% H_3PO_4 or $CFCl_3$).

2.2 Size Exclusion Chromatography (SEC).

SEC was performed at 30 °C with two columns from Polymer Laboratories (PL-gel MIXED-D; 300 × 7.5 mm; bead diameter 5 mm; linear part 400 to 4×10^5 g.mol^{-1}) and a differential refractive index detector (SpectraSystem RI-150 from Thermo Electron Corp.). The eluent was chloroform at a flow rate of 1 mL.min^{-1} and toluene was used as a flow-rate marker. The calibration curve was based on polystyrene (PS) standards (peak molar masses, M_p = 162–523 000 g.mol^{-1}) from Polymer Laboratories. A polyisoprene (PI) calibration curve was constructed by converting the PS standard peak molecular weights, MPS, to PI molecular weights, MPI, using Mark-Houwink-Sakurada (MHS) constants determined for both polymers in CCl_4 at 25 °C. For PI, the MHS constants used were $K_{PI} = 2.44 \times 10^4$ and $\alpha_{PI} = 0.712$. For PS, $K_{PS} = 7.1 \times 10^4$ and $\alpha_{PS} = 0.54$ (MW < 16700 g.mol^{-1}) or $K_{PS} = 1.44 \times 10^4$ and $\alpha_{PS} = 0.713$ (MW > 16 700 g.mol^{-1}).[2] This technique allowed M_n (the number-average molar mass), M_w (the weight-average molar mass), and M_w/M_n (the dispersity, $Đ$) to be determined.

2.3 Transmission electron microscopy (TEM).

The morphology of the different nanoassemblies was examined by cryogenic transmission electron microscopy (cryo-TEM). Briefly, 5 µL of the nanoparticle suspension (5 $mg.mL^{-1}$) was deposited on a Lacey Formvar/carbon 300 mesh copper microscopy grid (Ted Pella). Most of the drop was removed with a blotting filter paper and the residual thin film remaining within the holes was vitrified by plunging into liquid ethane. Samples were then observed using a JEOL 2100HC microscope.

2.4 Dynamic Light Scattering (DLS) and Zeta Potential.

Nanoparticle diameters (D_z) and zeta potentials (ζ) were measured by dynamic light scattering (DLS) with a Nano ZS from Malvern (173° scattering angle) at a temperature of 25 °C. The surface charge of the nanoparticles was investigated by ζ-potential (mV) measurement at 25 °C after dilution with 1 mM NaCl, using the Smoluchowski equation.

3. Synthesis methods

3.1 Synthesis of gemcitabine-AMA-SG1 conjugate (3).

Gemcitabine HCl (200 mg, 0.66 mmol) and diisopropyl ethyl amine (116 µL, 0.66 mmol) were dissolved in 5 mL of dry DMF. Benzotriazol-1-yl-oxytripyrrolidinophosphonium hexafluorophosphate (PyBOP, 344 mg, 0.66 mmol) and AMA-SG1 (242 mg, 0.66 mmol) were dissolved in 5 mL dry DMF and added by syringe. Diisopropyl ethyl amine (275 µL, 1.6 mmol) was added dropwise. The solution was stirred under N_2 for 24 h, then diluted with 100 mL EtOAc, washed with 10% HCl, sat. $NaHCO_3$ and brine, and dried over $MgSO_4$. The solvent was removed under vacuum and the product was separated by chromatography on silica using 0-5% MeOH in EtOAc as eluent. Yield: 241 mg white solid (0.39 mmol, 59.6%).

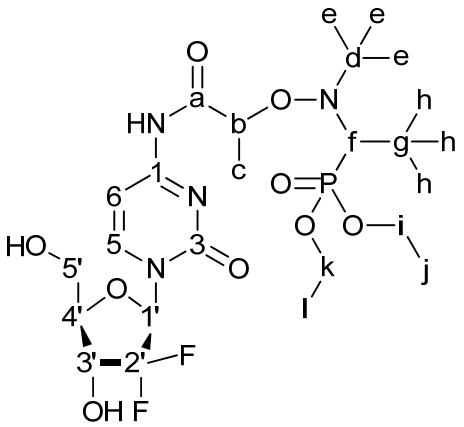

^{1}H NMR (DMSO-d_6, 300 MHz) : *Major diastereomer*: δ 11.0 (1H, *s*, CONH), 8.30 (1H, *d*, *J* = 7.4 Hz, H^6), 7.28 (1H, *d*, *J* = 7.3 Hz, H^5), 6.36 (1H, *d*, *J* = 6.4 Hz, 3'-OH), 6.20 (1H, *t*, *J* =

7.2 Hz, $H^{1'}$), 5.34 (1H, *t*, J = 4.8 Hz, 5'-OH), 4.69 (1H, *q*, *J* = 6.3 Hz, H^{b}), 3.5-4.5 (5H, *m*, H^{i}, H^{k}, $H^{3'-5'}$), 3.44 (1H, *d*, $^{2}J_{H-P}$ = 27.3 Hz, H^{f}), 1.42 (3H, *t*, *J* = 6.4 Hz, H^{c}), 1.00-1.35 (6H, *m*, H^{i} and H^{k}), 1.14 (9H, *s*, H^{e} or H^{h}), 1.13 (9H, *s*, H^{e} or H^{h}) ppm. *Minor diastereomer*: δ 11.2 (1H, *s*, CONH), 8.29 (1H, *d*, *J* = 7.6 Hz, H^{5}), 7.31 (1H, *d*, J = 7.6 Hz, H^{6}), 6.36 (1H, *d*, J = 6.4 Hz, 3'-OH), 6.19 (1H, *t*, *J* = 7.3 Hz, $H^{1'}$), 5.35 (1H, *t*, *J* = 5.1 Hz, 5'-OH), 4.88 (1H, *q*, 6.8 Hz, H^{b}), 3.5-4.5 (5H, *m*, H^{i}, H^{k}, $H^{3'-5'}$), 3.21 (1H, *d*, $^{2}J_{H-P}$ = 24.6 Hz, H^{f}), 1.38 (3H, *t*, *J* = 6.9 Hz, H^{c}), 1.15-1.28 (6H, *m*, H^{i} and H^{k}), 1.09 (9H, *s*, H^{e} or H^{h}), 1.03 (9H, *s*, H^{e} or H^{h}) ppm.

^{13}C NMR: (acetone-d_6, 75 MHz): *Major diastereomer*: δ 174.2 (C^{a}), 163.0 (C^{1}), 155.6 (C^{3}), 145.5 (C^{6}), 123.1 (*t*, $C^{2'}$, $^{1}J_{C-F}$ = 259 Hz), 96.6 (C^{5}), 85.1 (*t*, $C^{1'}$, $^{2}J_{C-F}$ = 32 Hz), 83.9 (C^{b}), 81.8 ($C^{4'}$), 68.6 (*t*, $C^{3'}$, $^{2}J_{C-F}$ = 23 Hz), 62.2 (C^{d}), 61.9 (C^{i}, *d*, $^{2}J_{C-P}$ = 5.4 Hz), 60.3 (C^{k}, *d*, $^{2}J_{C-P}$ = 7.7 Hz), 58.8 ($C^{5'}$), 35.5 (C^{g}, *d*, $^{2}J_{C-P}$ = 4.3 Hz), 27.9 (C^{e}), 19.0 (C^{c}), 15.9 (C^{l}, *d*, $^{3}J_{C-P}$ = 6.2 Hz), 15.7 (C^{j}, *d*, $^{3}J_{C-P}$ = 6.1 Hz) ppm. *Minor diastereomer*: δ 174.4 (C^{a}), 163.4 (C^{1}), 156.0 (C^{3}), 145.4 (C^{6}), 123.1 (*t*, $C^{2'}$, $^{1}J_{C-F}$ = 259 Hz), 96.8 (C^{5}), 85.1 (*t*, $C^{1'}$, $^{2}J_{C-F}$ = 32 Hz), 83.9 (C^{b}), 81.8 ($C^{4'}$), 68.6 (*t*, $C^{3'}$, $^{2}J_{C-F}$ = 23 Hz), 62.3 (C^{d}), 62.0 (C^{i}, *d*, $^{2}J_{C-P}$ = 5.6 Hz), 60.6 (C^{k}, *d*, $^{2}J_{C-P}$ = 7.5 Hz), 58.8 ($C^{5'}$), 35.5 (C^{g}, *d*, $^{2}J_{C-P}$ = 4.3 Hz), 27.8 (C^{e}), 19.1 (C^{c}), 15.9 (C^{j}, *d*, $^{3}J_{C-P}$ = 6.2 Hz), 15.7 (C^{l}, *d*, $^{3}J_{C-P}$ = 6.4 Hz) ppm.

^{31}P NMR (DMSO-d_6, 81 MHz): δ 36.85 (*major*), 37.06 (*minor*) ppm.

^{19}F NMR (DMSO-d_6, 188 MHz): δ -115.1 ppm.

MS (ESI): 613 $(M+H)^{+}$. Calc. for $C_{25}H_{44}F_2N_4O_9P^{+}$: 613.3

3.2 Polymerization of isoprene from 3 (4a-d).

A stock solution was prepared comprising 180 mg gemcitabine-AMA-SG1 (**3**, 0.031 mmol), 3.1 mL isoprene (3.1 mmol, 100 eq) and pyridine (3.1 mL). This was divided between 4 pressure tubes and freeze-thaw degassed. The tubes were placed in an oil bath at 115 °C and removed after 2 h, 4 h, 8 h and 16 h respectively. Unreacted isoprene and pyridine were removed under vacuum. Samples were characterized by SEC and NMR (Table S1, Figures S1-S4).

Table S1. Characterization data for gemcitabine-polyisoprene conjugates **4a-d**.

Sample	Time (h)	Conv. (%)	M_n[a] (g.mol^{-1})	M_w[a] (g.mol^{-1})	$Đ$[a]	DP_n (SEC)[b]	DP_n (NMR)[c]	Gem/chain[d]	DP_n (theo)	%Gem (wt.%)[e]
4a[f]	2	7.6	840	1130	1.35	3.4	10	0.67	8	31.2
4b	4	11.7	1190	1540	1.29	9	28	0.75	12	22.1
4c	8	18.9	1560	1990	1.28	14	33	1.0	19	16.9
4d	16	30.7	2510	3520	1.40	28	47	1.1	31	10.5

[a]SEC ($CHCl_3$, PI universal calibration using PS standards). [b]$DP_n = (M_n - MW_3)/MW_{isoprene} = (M_n - 613)/68.11$. [c]Calculated from ratio of areas under the peak at 3.1-3.3 ppm (H α to P in SG1 moiety) and 5.0-5.5 ppm (vinylic H in isoprene repeat unit (1,4-addition), corresponding to 81.2% of total isoprene units).[2] [d]ratio of integrals of peaks corresponding to the anomeric proton of the gemcitabine moiety and the proton α to phosphorus of the SG1 moiety. [e] $\%Gem = MW_{Gem}/M_{n,PI} = 263.2/M_{n,PI}$. [f] ESI MS (m/z): i) 635.4 + n × 68.06 $(Gem\text{-}(I)_n\text{-}SG1+Na)^+$, calc. m/z 771.5 (n = 2), found m/z 771.5; ii) 659.5 $(Gem\text{-}(I)_n\text{-}Gem+Na)^+$ calc. m/z = 795.2, found m/z = 794.6 (n = 2). Other peaks derived from fragmentation.

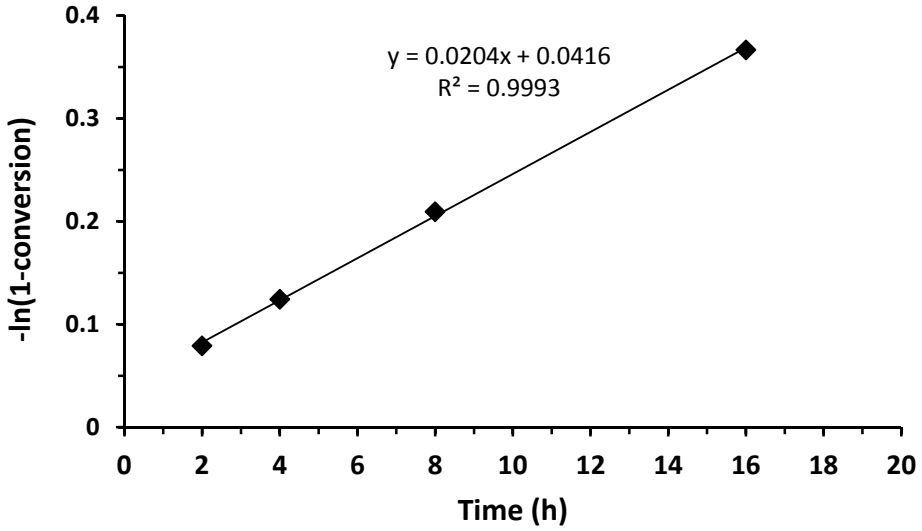

Figure S1. Linear evolution of -*ln*(1-conversion) with time for polymerization of isoprene initiated by **3**.

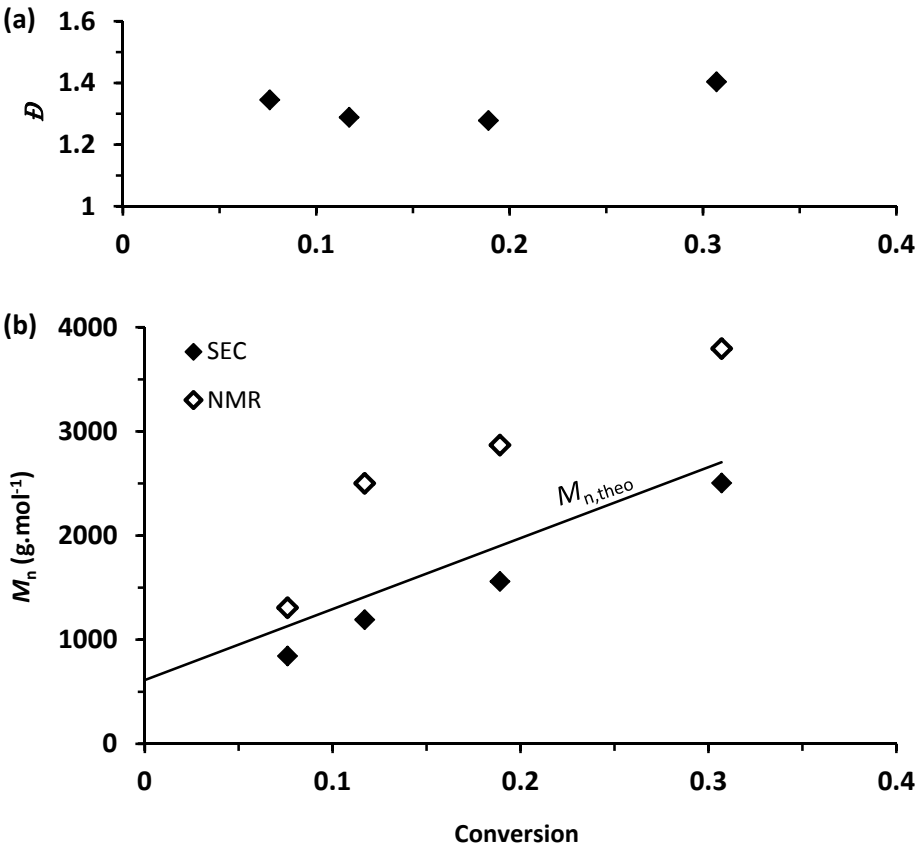

Figure S2. Dispersity, *Đ* (a) and number-average molar mass, M_n, (b) as a function of conversion. *Đ* was determined by SEC, and M_n by SEC and ^{1}H NMR. The line in Figure S2b represents the theoretical M_n.

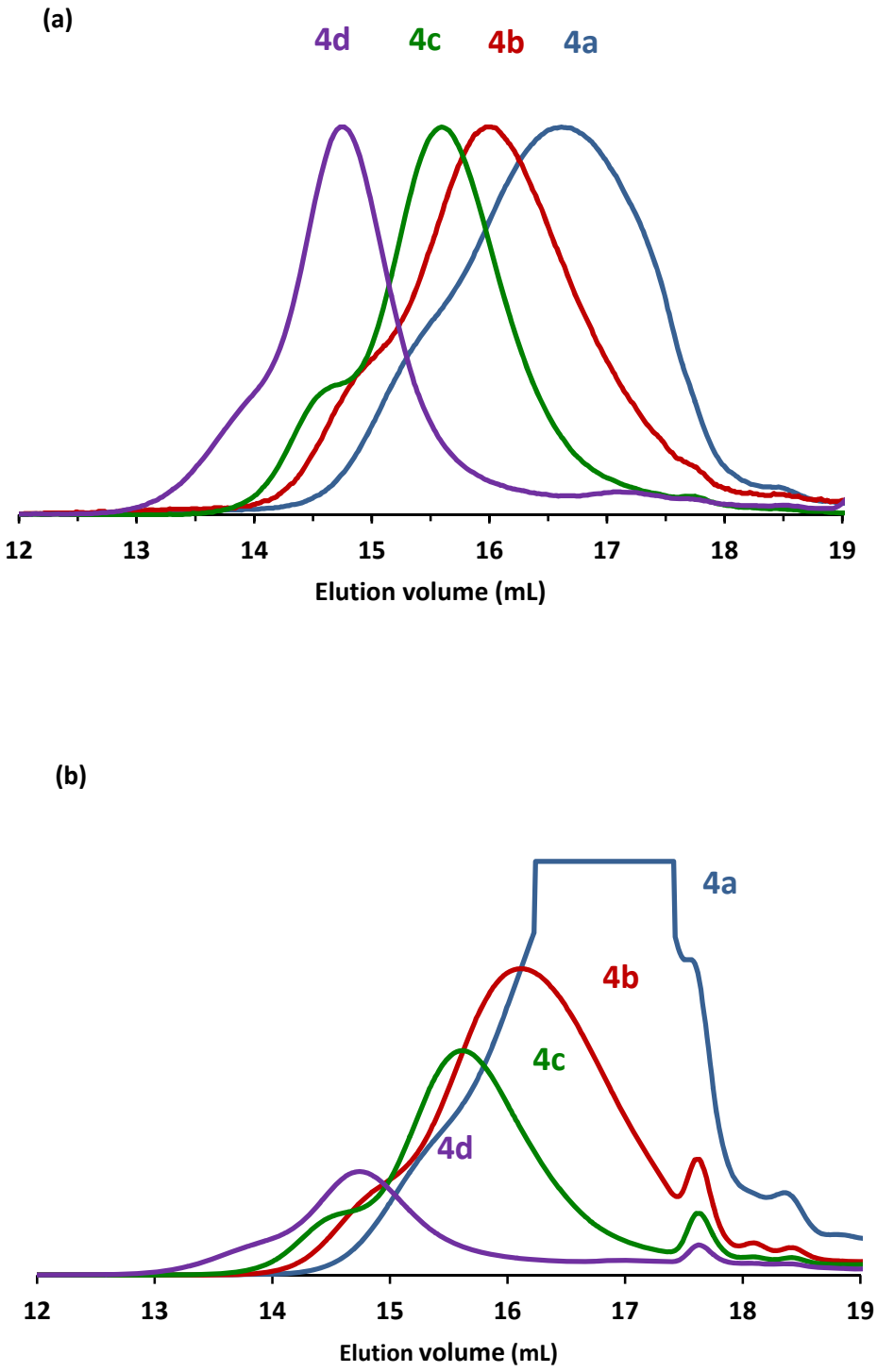

Figure S3. Size exclusion chromatograms ($CHCl_3$ eluent, 1 $mL.min^{-1}$) for polyisoprene-gemcitabine conjugates, using DRI (a) and UV (268 nm) (b) detection.

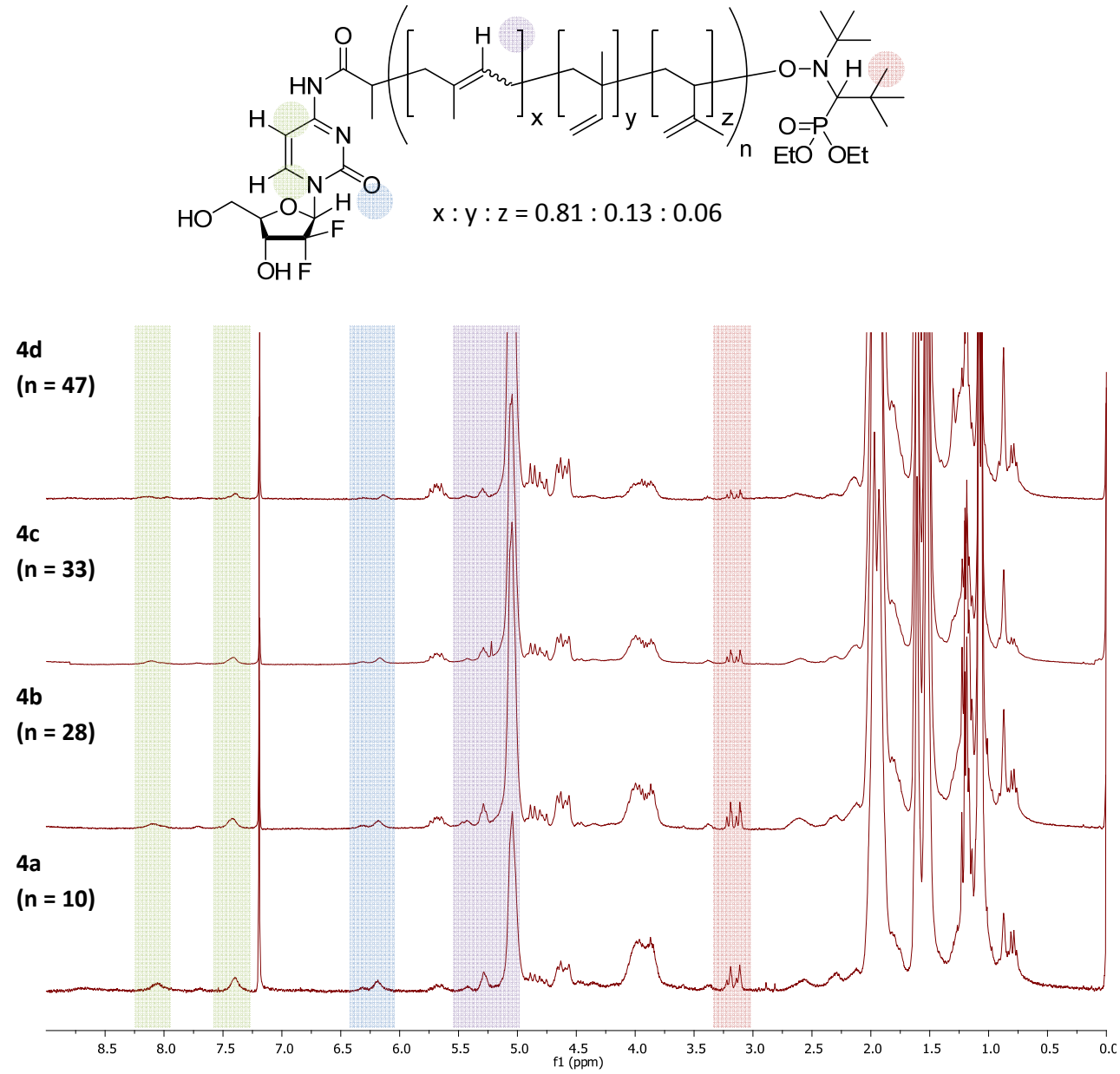

Figure S4. Proton NMR ($CDCl_3$, 300 MHz) spectra of gemcitabine-polyisoprene conjugates **4a-d**, with characteristic proton resonances highlighted. A single broad resonance centered on -116 ppm was observed in the ^{19}F NMR spectra ($CDCl_3$, 188 MHz), while the ^{31}P spectra ($CDCl_3$, 81 MHz) displayed resonances at 23.2 and 23.0 ppm.

3.3 Polymerization of isoprene from AMA-SG1 (5a-e).

AMA-SG1 (6 × 50 mg, 0.14 mmol) was placed in 6 × 15 mL capacity pressure tubes (Ace Glass 8648-164) fitted with plunger valves and thermowells. Isoprene (6 × 1.4 mL, 0.92 g, 14 mmol) and solvent (1.4 mL dioxane (**a**, **d**) or 1.4 mL pyridine (**b**, **e**)) was added and the tubes

were subjected to three cycles of freeze-thaw degassing, then backfilled with argon. The tubes were placed in an oil bath at 115 °C for 4-16 h and then cooled to room temperature by placing in a bath of cold water. The resulting polyisoprenes were analyzed by SEC (Table S2 and Figure S5). Kinetic data for these polymerizations are available in the following references.[2,3]

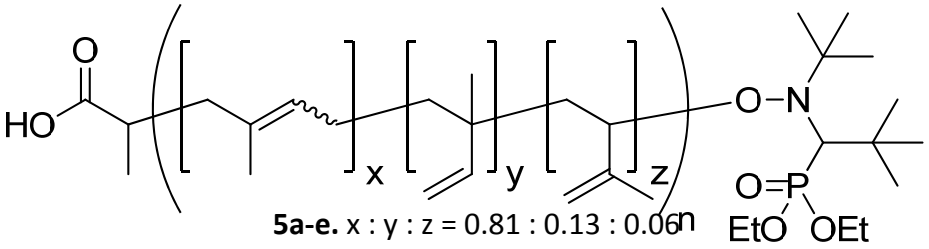

5a-e. x : y : z = 0.81 : 0.13 : 0.06

Table S2. Characterization data for polyisoprene control samples **5a-e**.

Sample	Solvent	Time (h)	Conv. (%)	M_n[a] (g.mol^{-1})	M_w[a] (g.mol^{-1})	$Đ$[a]	DP_n (SEC)[b]	DP_n (theo)
5a	dioxane	4	16.1	1080	1340	1.23	10	16
5b	pyridine	8	30.8	2230	2500	1.12	27	31
5c	bulk	16	35.8	2330	2720	1.17	29	36
5d	dioxane	16	45.8	2580	3020	1.17	32	46
5e	pyridine	16	54.3	3340	3860	1.16	44	54

[a]SEC ($CHCl_3$, PI universal calibration using PS standards). [b]$DP_n = (M_n - MW_{\mathbf{AMA\text{-}SG1}})/MW_{isoprene} = (M_n - 367)/68.11$.

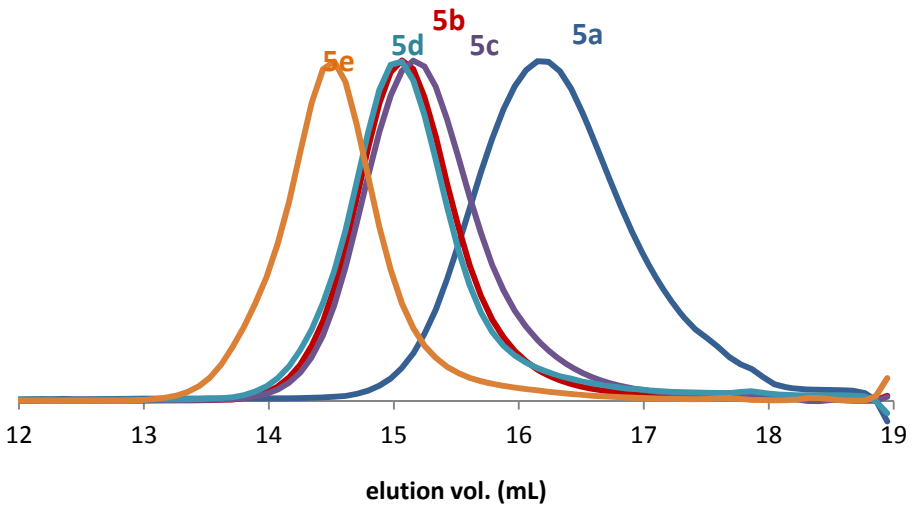

Figure S5: Size exclusion chromatograms ($CHCl_3$, 1 $mL.min^{-1}$) for polyisoprene control samples (**5a-e**).

3.4 Preparation of *O,O'*-(TBDMS)$_2$-gemcitabine.

To a mixture of gemcitabine (2 g, 6.7 mmol), *tert*-butyldimethylsilyl chloride (2.54 g, 16.8 mmol) and imidazole (1.37 g, 20.2 mmol) in 40 mL of distilled DMF, were added dropwise triethyl amine (Et_3N, 1.5 mL, 7.4 mmol). The mixture was stirred at 25°C for 24 h. DMF was removed under reduced pressure and the residue was taken up in saturated $NaHCO_3$ aqueous solution before being extracted with ethyl acetate. The organic phase was washed with brine before being dried over $MgSO_4$. The residue was concentrated under reduced pressure and purified by flash chromatography (SiO_2, AcOEt 100%) to give 3.15 g (6.38 mmol, 95%) of a white solid. $[\alpha]_D^{26.6}$ + 2.19 (c = 1, MeOH).

^{1}H NMR (400 MHz, $CDCl_3$): 8.25 (1H, *s*, C-NH), 7.61 (1H, *d*, J 7.56, C=CH-C), 6.32 (1H, *dd*, *J* 4.48, 10.76, O=CH-N), 5.80 (1H, *d*, J 7.56, C=CH-N), 4.29 (1H, *dt*, J 3.6, 8.28, O-CH-CF), 3.97 (1H, *d*, *J* 11.7, O-CHA-CH), 3.86 (1H, *d*, *J* 7.88, O-CHB-CH), 3.78 (1H, *dd*, *J* 2.0, 11.76 , OC-CH-CO), 0.92 (9H, *s* , CH-CSi), 0.89 (9H, *s* , CH-CSi), 0.12 (3H, *s*, CH-Si-O-CCF), 0.1 (9H, *s*, CH-Si-O) ppm.

^{13}C NMR (100 MHz, $CDCl_3$): 166.11(N=C-N), 155.78(O=C-N), 140.57 (N-C=C), 122.21 (F-C-N, JC-F 260.7), 95.46 (C=C-C),84.34 (F-C-C-N, JC-F 23.3, 23.5), 81.01 (F-C-C-C-O, JC-F 9.0), 69.98 (F-C-C-O-Si, JC-F 18.1,18.3), 60,27 (C-C-O-Si), 25.97 (3C, Si-C-CH3), 25.67 (3C, Si-C-CH3), 18.43 (Si-C-CH3), 18.13 (Si-C-CH3), 5.38 (H3C-Si-O), 5.34 (H3C-Si-O), 5.16 (H3C-Si-O), 4.63 (H3C-Si-O) ppm.

^{19}F NMR: 114.81 (2F, *dd*, *J* 128.3, 198.05) ppm.

IR (neat) : 2956 (m), 2929 (m), 2857 (m), 1636 (s), 1472 (m),1403 (s), 1362 (s), 1254 (s), 1206 (s), 1148 (s), 1088 (m), 955 (s), 833 (m), 780 (m), 731 (m), 676 (m).
MS (ESI) : 490 [M+, 100%]. mp.: 119.3°C [AcOEt]. Elemental Analysis: $C_{21}H_{39}F_2N_3O_4Si_2$, Theory: C 51.29, H 7.99, N 8.55, Exp.: C 51.15, H 8.11, N 8.48.

3.5 Preparation of *O,O'*-(TBDMS)$_2$-gemcitabine-AMA-SG1 conjugate.

O,O'-(TBDMS)$_2$-gemcitabine (200 mg, 0.44 mmol, benzotriazol-1-yl-oxytripyrrolidinophosphonium hexafluorophosphate (PyBOP, 210 mg, 0.44 mmol) and AMA-SG1 (148 mg, 0.44 mmol) were dissolved in 10 mL dry DMF. Diisoproyl ethyl amine (200 µL, 1.1 mmol) was added dropwise. The solution was stirred at room temperature under N_2 for 72 h, then diluted with 100 mL EtOAc, washed with 10% HCl, sat. $NaHCO_3$ and brine, and dried over $MgSO_4$. The solvent was removed under vacuum and the product was separated by chromatography on silica using 10% acetone in $CHCl_3$ as eluent. Yield: 184 mg colorless oil (major diastereomer), 129 mg colorless crystals (minor diastereomer). Total yield: 313 mg, (0.37 mmol, 85 %).

^{1}H NMR ($CDCl_3$, 300 MHz) : *Major diastereomer*: δ 10.65, 10.54 (1H, CONH)*, 8.01 (1H, *d*, *J* = 6.7 Hz, H^6), 7.41 (1H, *d*, *J* = 7.6 Hz, H^5), 6.34 (1H, *dd*, $^3J_{H\text{-}F}$ = 10.0, 4.3 Hz, $H^{1'}$), 4.72 (1H, *q*, *J* = 6.5 Hz, H^b), 3.7-4.4 (5H, *m*, H^i, H^k, $H^{3'\text{-}5'}$), 3.47 (1H, *d*, $^2J_{H\text{-}P}$ = 27.8 Hz, H^f), 1.50 (3H, *t*, *J* = 6.7 Hz, H^c), 1.2-1.4 (6H, *m*, H^i and H^k), 1.16 (9H, *s*, H^e or H^h), 1.15 (9H, *s*, H^e or H^h) 0.94 (9H, *s*, $(CH_3)_3CSi$), 0.90 (9H, *s*, $(CH_3)_3CSi$), 0.12 (12H, *m*, $(CH_3)_2Si$) ppm. *Minor diastereomer*: δ 9.7 (1H, *s*, CONH), 8.01 (1H, *d*, *J* = 7.5 Hz, H^5), 7.34 (1H, *d*, J = 7.6 Hz, H^6), 6.22 (1H, *dd*, $^3J_{H\text{-}F}$ = 14.2, 6.9 Hz, $H^{1'}$), 4.56 (1H, *q*, 6.7 Hz, H^b), 3.7-4.5 (5H, *m*, H^i, H^k, $H^{3'\text{-}5'}$), 3.30 (1H, *d*, $^2J_{H\text{-}P}$ = 26.2 Hz, H^f), 1.58 (3H, *t*, *J* = 6.8 Hz, H^c), 1.2-1.4 (6H, *m*, H^i and H^k), 1.14 (18H, *s*, H^e and H^h), 0.92 (9H, *s*, $(CH_3)_3CSi$), 0.87 (9H, *s*, $(CH_3)_3CSi$), 0.09 (12H, *m*, $(CH_3)_2Si$) ppm.

*Two broad singlets were observed, each with an area corresponding to *c.* 0.5H. This may indicate tautomerism between forms A and B below:

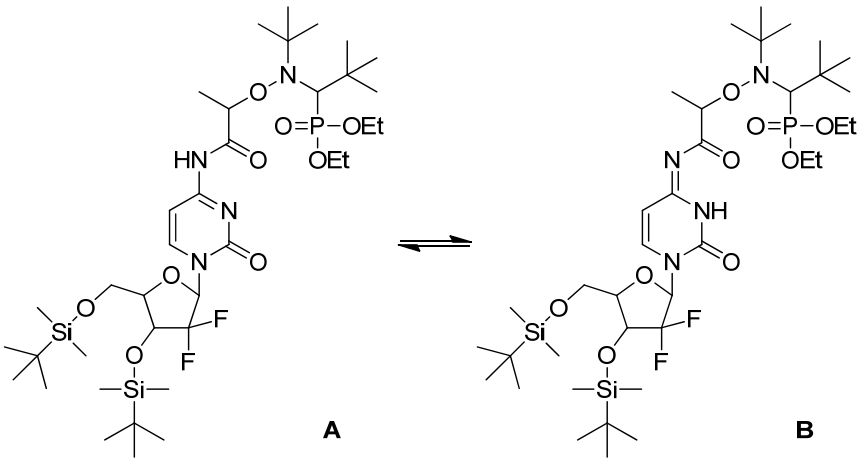

^{13}C NMR: ($CDCl_3$, 75 MHz): *Major diastereomer*: δ 171.8, 171.7 (C^a)*, 162.7 (C^1), 155.0 (C^3), 143.5 (C^6), 121.9 (*t*, $C^{2'}$, $^1J_{C\text{-}F}$ = 260 Hz), 96.9 (C^5), 84.6 (*dd*, $C^{1'}$, $^2J_{C\text{-}F}$ = 40, 25 Hz), 81.2 ($C^{4'}$, *d*, $^3J_{C\text{-}F}$ = 7.2 Hz), 78.0, 77.9 (C^b)*, 69.4 (*dd*, $C^{3'}$, $^2J_{C\text{-}F}$ = 25, 17 Hz), 68.7 (*d*, C^f, $^1J_{C\text{-}P}$ = 140 Hz), 61.6 (C^d), 61.8 (C^i, *d*, $^2J_{C\text{-}P}$ = 7.2 Hz), 61.3 (C^k, *d*, $^2J_{C\text{-}P}$ = 7.3 Hz), 59.9 ($C^{5'}$), 35.2 (C^g, *d*, $^2J_{C\text{-}P}$ = 4.4 Hz), 30.6 (*d*, C^h, $^3J_{C\text{-}P}$ = 5.6 Hz), 28.1 (C^e), 25.8, 25.4 (($\underline{C}H_3)_3CSi$), 18.2, 17.9 $(CH_3)_3\underline{C}Si$), 16.2 (C^l, *dd*, $^3J_{C\text{-}P}$ = 6.3, 2.8 Hz), 15.9 (C^j, *d*, $^3J_{C\text{-}P}$ = 6.2 Hz), -4.9, -5.4, -5.5 (2C), ($Si(CH_3)_2$) ppm. *Minor diastereomer*: δ 174.0 (C^a), 162.6 (C^1), 155.4 (C^3), 144.1 (C^6), 122.0 (*t*, $C^{2'}$, $^1J_{C\text{-}F}$ = 260 Hz), 96.8 (C^5), 84.6 (*m*, $C^{1'}$), 81.5 ($C^{4'}$, *d*, $^3J_{C\text{-}F}$ = 8.1 Hz), 78.4 (C^b), 69.5-70.5 (*m*, $C^{3'}$), 69.3 (*d*, C^f, $^1J_{C\text{-}P}$ = 140 Hz), 62.6 (C^d), 62.0 (C^i), 60.3 (C^k, *d*, $^2J_{C\text{-}P}$ = 7.4 Hz), 60.0 ($C^{5'}$), 35.8 (C^g, *d*, $^2J_{C\text{-}P}$ = 4.2 Hz), 30.0 (C^h), 28.3 (C^e), 25.9, 25.6 (($\underline{C}H_3)_3CSi$), 18.1, 17.9 $(CH_3)_3\underline{C}Si$), 16.3 ($C^{i,j}$, *d*, $^3J_{C\text{-}P}$ = 6.6 Hz), -5.2, -5.4, ($Si(CH_3)_2$) ppm.

*Double peaks were observed for these carbons, possibly due to tautomerism between forms A and B.

^{31}P NMR ($CDCl_3$, 81 MHz): δ 23.4 (*major*), 22.6 (*minor*) ppm.

^{19}F NMR ($CDCl_3$, 188 MHz): *Major diastereomer* : δ -115.7, -113.8 (AB' system, $^2J_{F\text{-}F}$ = 240 Hz) ppm. *Minor diastereomer*: δ -115.6, -113.7 (AB' system, $^2J_{F\text{-}F}$ = 239 Hz) ppm.

3.6 Polymerization of isoprene from *O,O'*-(TBDMS)$_2$-gemcitabine-AMASG1 conjugate (6a-c).

O,O'-(TBDMS)$_2$-gemcitabine-AMA-SG1 conjugate (4 × 50 mg, 0.06 mmol) was placed in 4 × 15 mL capacity pressure tubes (Ace Glass 8648-164) fitted with plunger valves and thermowells. Isoprene (6 × 1.2 mL, 0.82 g, 12 mmol) and dioxane (6 × 1.2 mL) were added and the tubes were subjected to three cycles of freeze-thaw degassing, then backfilled with argon. The tubes were placed in an oil bath at 115 °C for 2, 2.5, 3, 4, 5 or 6 h and then cooled

to room temperature by placing in a bath of cold water. The resulting polyisoprenes, **6a-c**, were analyzed by SEC and NMR (Table S3).

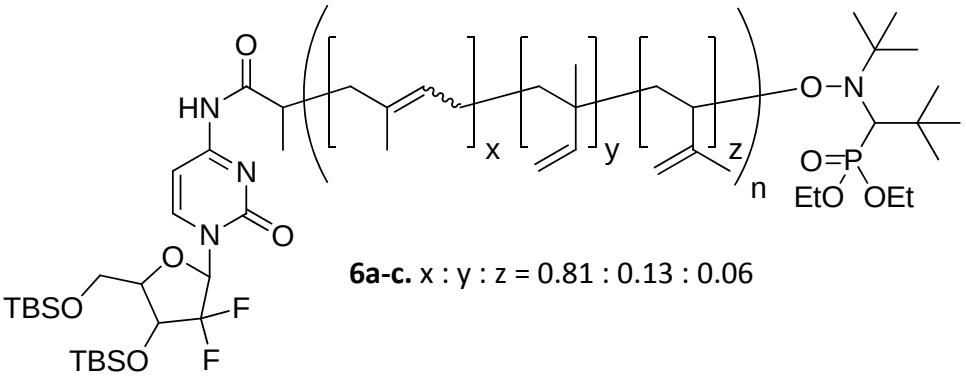

6a-c. x : y : z = 0.81 : 0.13 : 0.06

Table S3. Characterization data for TBDMS-protected polyisoprene samples **6a-c**.

Sample	Time (h)	Conv. (%)	M_n[a] (g.mol^{-1})	M_w[a] (g.mol^{-1})	$Đ$[a]	DP_n (SEC)[b]	DP_n (NMR)	DP_n (theo)	Gem/chain (NMR)
6a	2.5	21.3%	2600	3030	1.17	26	57	43	1.1
6b	4	19.4%	2940	3430	1.17	31	60	39	0.97
6c	6	23.0%	3230	3800	1.18	35	58	46	0.73

[a]SEC ($CHCl_3$, PI universal calibration using PS standards). [b]$DP_n = (M_n - MW_{\mathbf{EiB\text{-}SG1}})/MW_{isoprene} = (M_n - 841)/68.11$.

3.7 Deprotection of *O,O'*-(TBDMS)$_2$-gemcitabine-polyisoprene (7a-c).

TBDMS-protected polyisoprene **6** (30 mg) was dissolved in 0.5 mL THF and cooled to 0 °C. Tetrabutylammonium fluoride (1M in THF, 50 µL) was added and the solution was allowed to stand for 15 min before pouring into 10 mL of MeOH. The polyisoprene was allowed to settle out over 36 h. Polymers were analyzed by NMR and SEC (RI and UV detection) (Table S4 and Figures S6-S8). NMR analysis showed complete disappearance of TBDMS protecting groups. Partial loss of gemcitabine was also observed, both by NMR and SEC (UV detection).

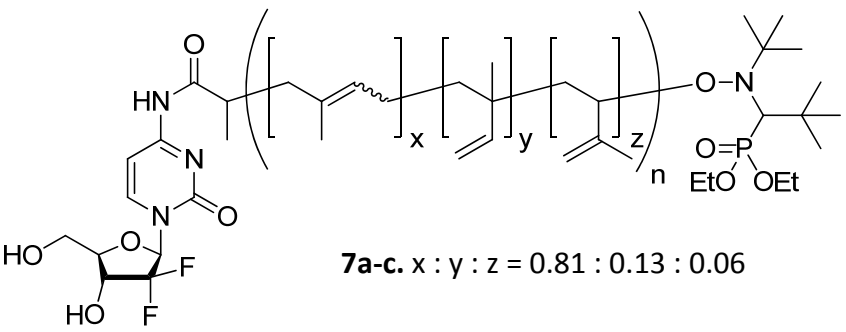

7a-c. x : y : z = 0.81 : 0.13 : 0.06

Table S4. Characterization data for deprotected gemcitabine-polyisoprene samples **7a-c**.

Sample	M_n (g.mol^{-1})[a]	M_w (g.mol^{-1})[a]	$Đ$[a]	DP_n (SEC)[b]	DP_n (NMR)[c]	Gem retained (%)[d]	Gem/chain (NMR)[e]
7a	2350	2780	1.19	28	35	70	0.50
7b	2420	2820	1.17	26	33	69	0.34
7c	3140	3610	1.15	31	60	79	0.50

[a]SEC ($CHCl_3$, PI universal calibration using PS standards). [b]$DP_n = (M_n - MW_{\mathbf{EiB\text{-}SG1}})/MW_{isoprene} = (M_n - 841)/68.11$. [c]Calculated from ratio of areas under the peak at 3.1-3.3 ppm (H α to P in SG1 moiety) and 5.0-5.5 ppm (vinylic H in isoprene repeat unit (1,4-addition), corresponding to 81.2% of total isoprene units). [d]Change in peak UV absorption/peak RI absorption after deprotection (Gem retained = $(UV_{peak,protected}\ RI_{peak,deprotected})/(UV_{peak,deprotected}\ RI_{peak,protected})$, see Figure S6). [e]ratio of integrals of peaks corresponding to the anomeric proton of the gemcitabine moiety and the proton α to phosphorus of the SG1 moiety.

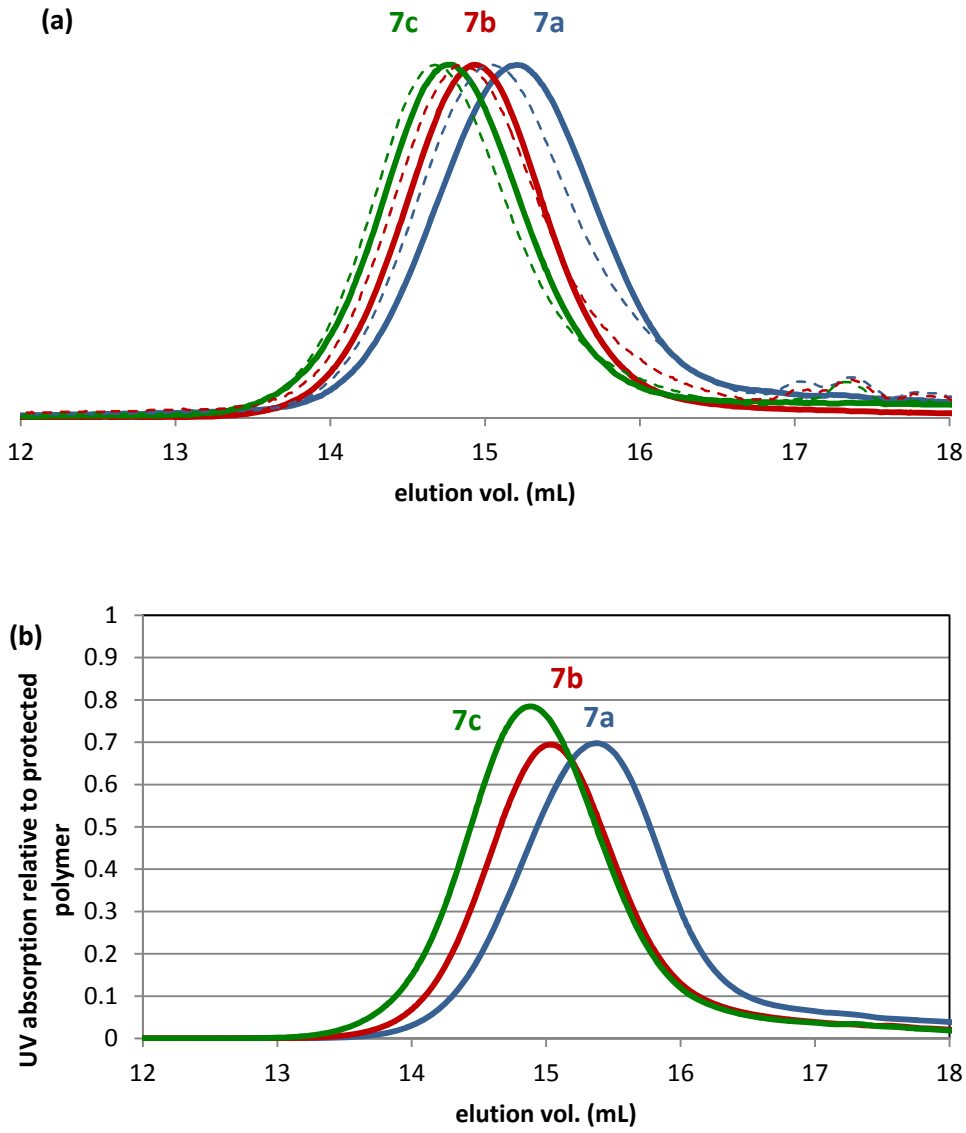

Figure S6. Size exclusion chromatograms for **7a-c**. (a) RI detection. Narrow (dashed) lines are chromatograms of TBDMS-protected polymers **6a-c**. (b) UV detection (268 nm), normalized to maximum UV absorption for corresponding polymer before deprotection.

(a)

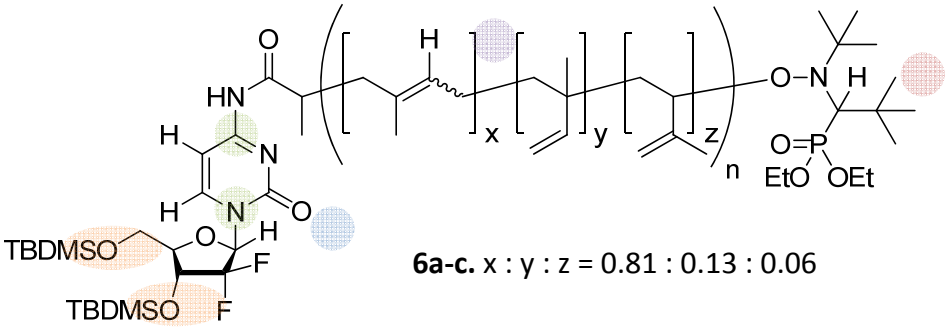

6a-c. x : y : z = 0.81 : 0.13 : 0.06

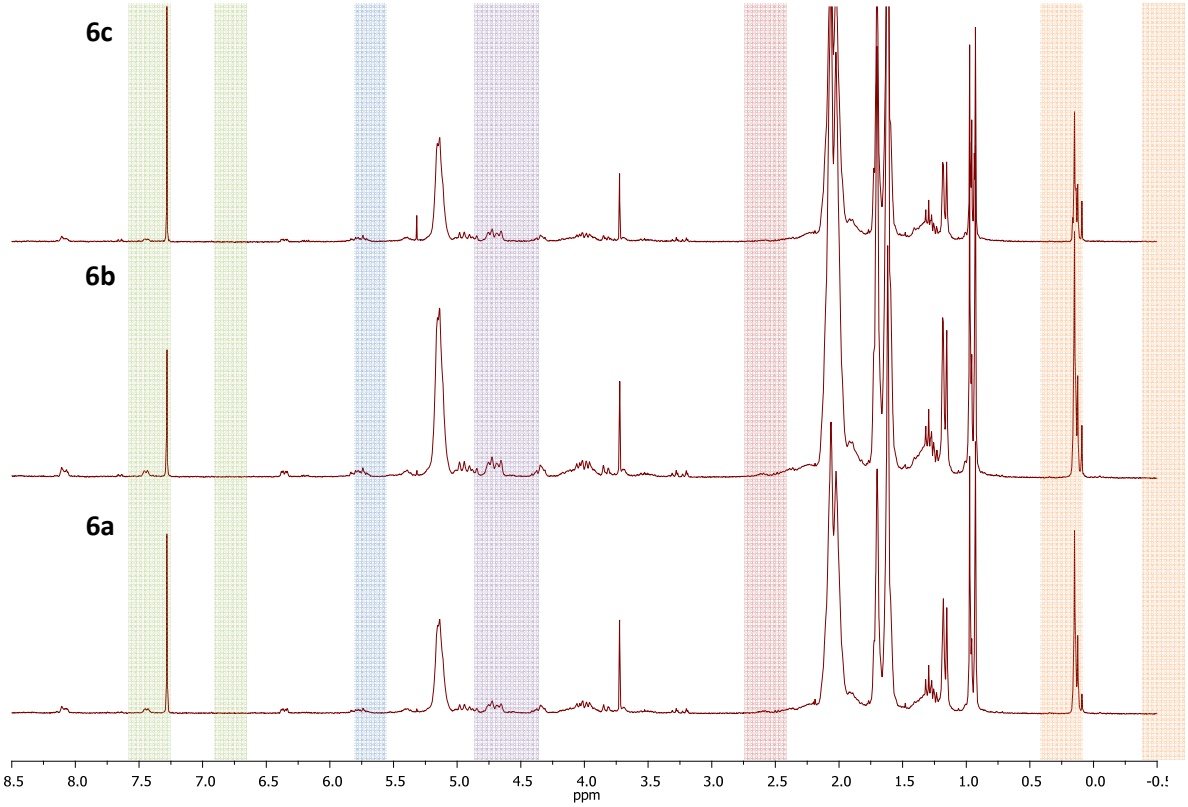

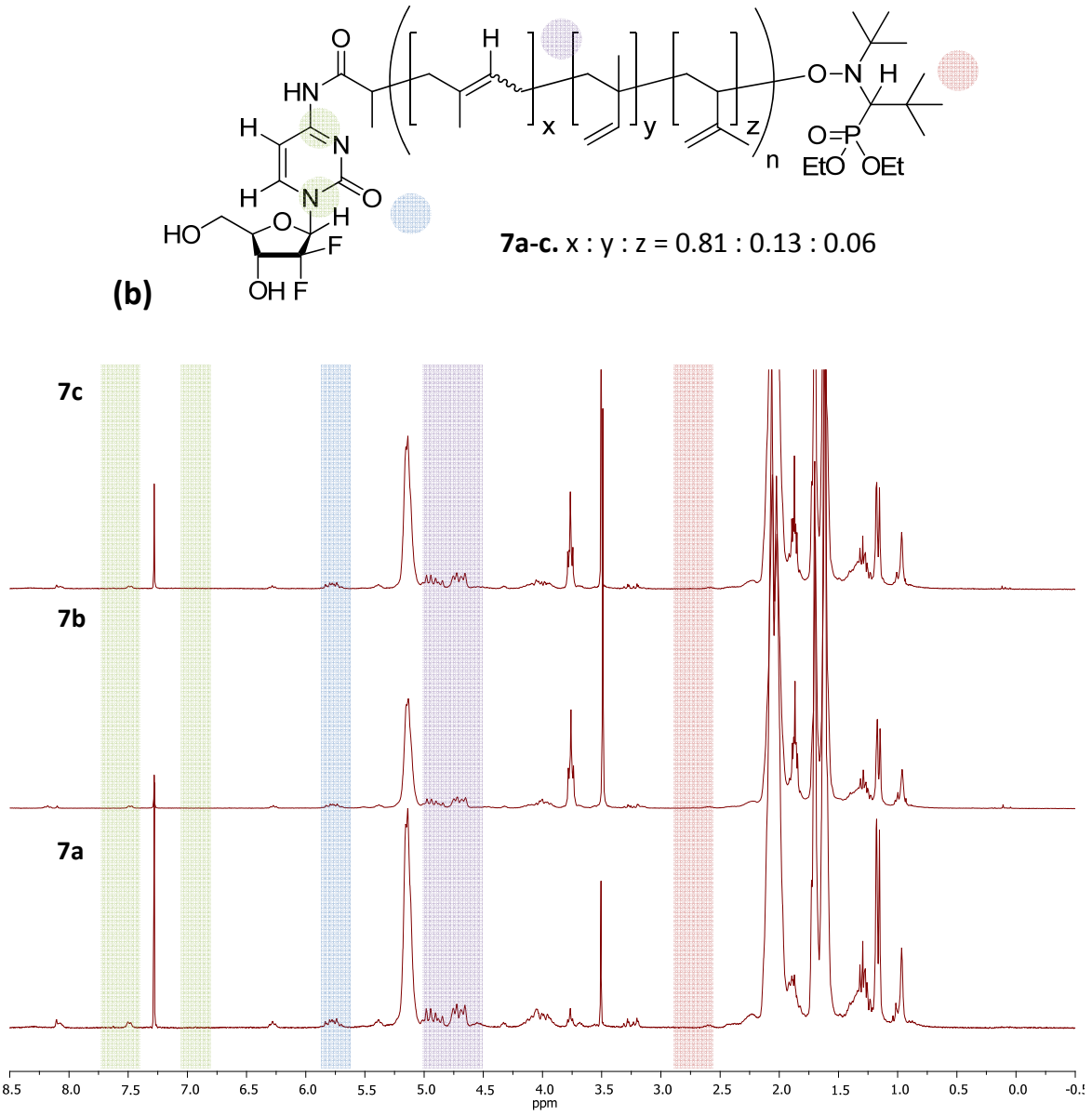

Figure S7. Polyisoprene-gemcitabine conjugates **6**/**7a-c** before (a) and after (b) removal of TBDMS protecting groups.

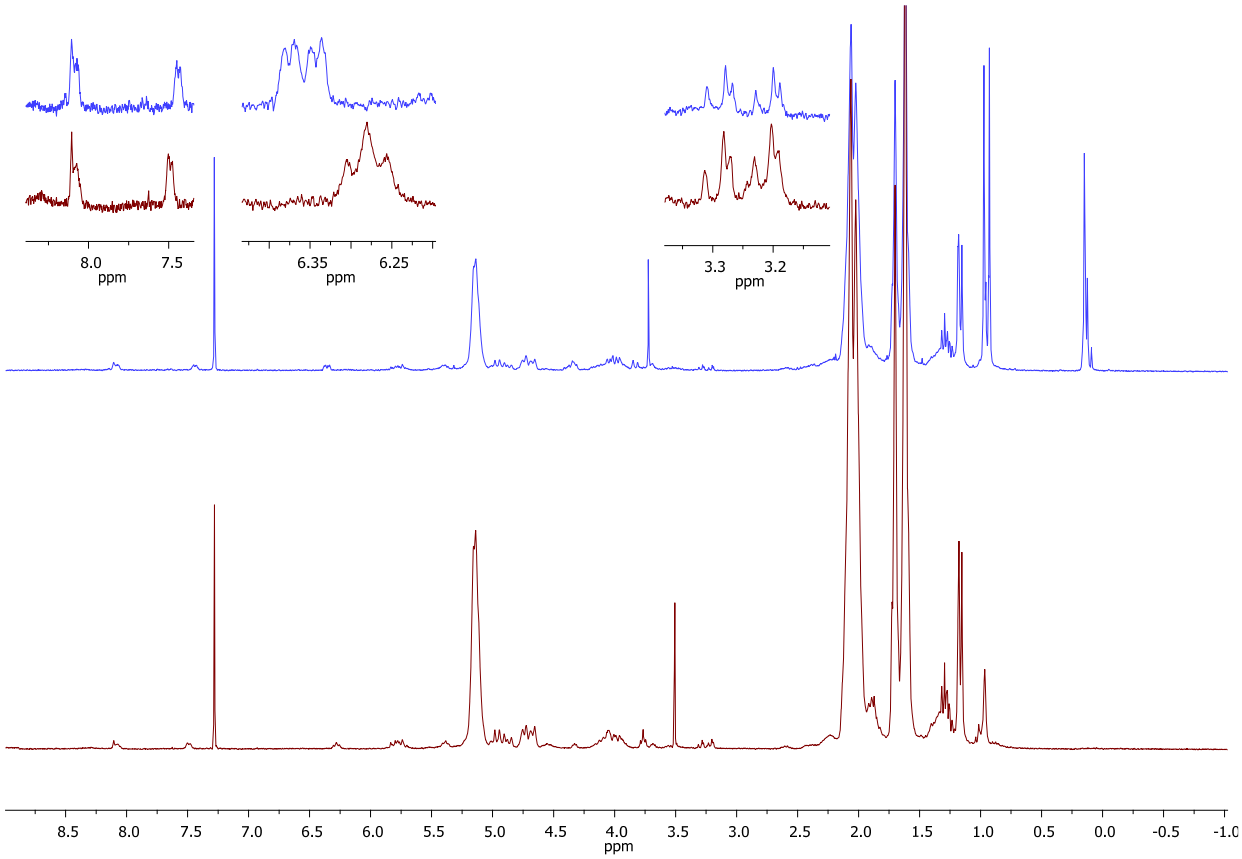

Figure S8. Comparison of ^{1}H NMR spectra of **6a** (blue, before deprotection) and **7a** (red, after deprotection). Expansions show aromatic (7.5-8.0 ppm) and anomeric (6.2-6.4 ppm) protons of gemcitabine, and proton α to phosphorus of SG1 moiety. Note disappearance of MeSi signals near 0 ppm and change in shape and position of anomeric proton signal (from *dd* to *t*) due to change in H-F coupling constants and chemical environment.

3.8 Nanoparticle preparation from 4a-d and 5a-e

Nanoparticles were prepared by the nanoprecipitation technique. Briefly, 15 mg of conjugates **4a-d** (Table S1) or control PI **5a-e** (Table S2) were dissolved in 3 mL of THF, and added dropwise to 6 mL MilliQ water under stirring. THF was removed *in vacuo*. Average diameter (D_z) and zeta potential measurements were carried out in triplicate. Results are gathered in Tables S5-S6 and in Figure S9.

Table S5. Size, PSD and zeta potential data for nanoparticles of gemcitabine-polyisoprene conjugates (Gem-PI) **4a-d**.

Sample	M_n (g.mol^{-1})	D_z (nm)	s.d. (nm)	PSD[a]	s.d.	ζ (mV)	s.d. (mV)
4a	840	159	4	0.10	0.01	-77	3
4b	1200	137	3	0.10	0.02	-70	5
4c	1560	133	4	0.11	0.02	-66	5
4d	2510	138	1	0.11	0.01	-68	4

[a]Particle size distribution (DLS apparatus).

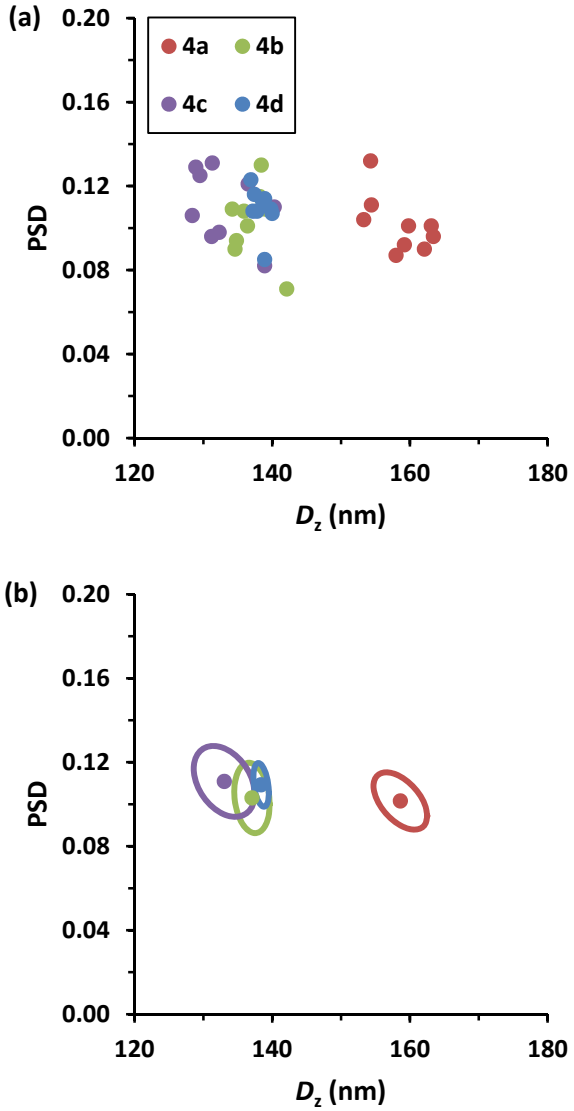

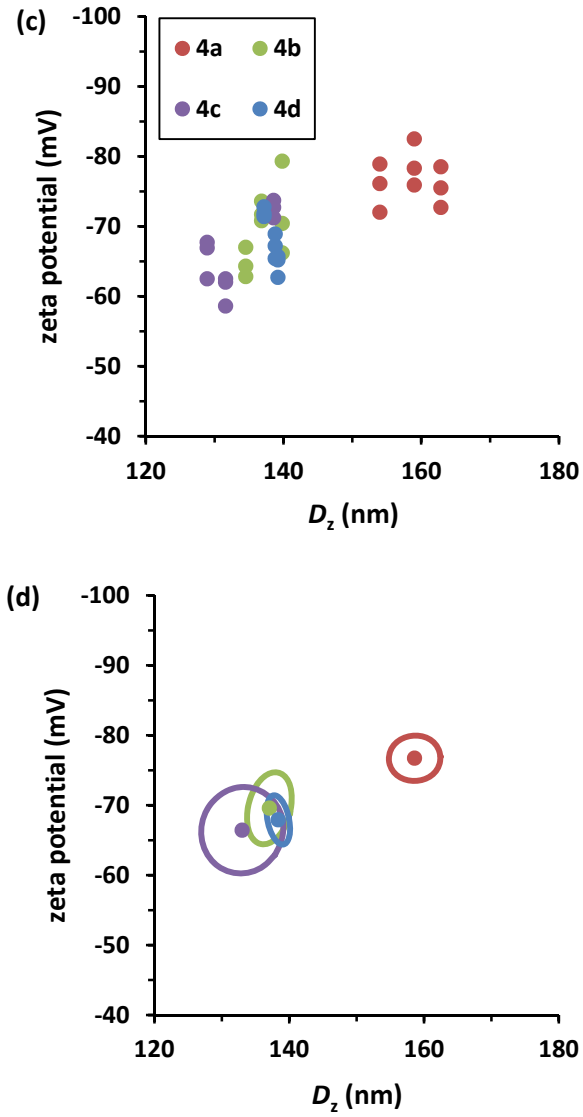

Figure S9. Average diameter (D_z), particle size distribution (PSD) and zeta potential measurements for nanoparticles of gemcitabine-polyisoprene (Gem-PI) conjugates **4a-d**. Graphs at left (a, c) show results of individual measurements; graphs at right show means and standard error ellipses (b, d). Three independent nanoparticle solutions were prepared for each conjugate, and measured in triplicate.

Table S6. Size, PSD and zeta potential data for control polyisoprene (PI) nanoparticle suspensions **5a-e**.

Sample	M_n (g.mol^{-1})	D_z (nm)	s.d. (nm)	PSD[a]	s.d.	ζ (mV)	s.d. (mV)
5a	1080	191	1.3	0.09	0.027	-66.5	11.3
5b	2230	229	2.9	0.20	0.020	-64.8	7.04
5c	2330	129	0.9	0.09	0.001	-65.6	16.7
5d	2580	122	1.0	0.11	0.021	-64.5	15.1
5e	3340	195	0.7	0.15	0.003	-62.0	16.1

[a]Particle size distribution (DLS apparatus).

4. Anticancer activity experiments

4.1 Cell lines and cell culture

Human leukemia cell line (CCRF-CEM), human pancreatic cancer cell line (MiaPaCa-2) and human lung carcinoma cell line (A549) were obtained from the American Type Culture Collection. Murine leukemia cell line (L1210) was kindly provided by Dr. Lars Petter Jordheim (Université Claude Bernard Lyon I, Lyon, France). All cell lines were maintained as recommended. Briefly, A549 cells were maintained in F12-K medium. CCRF-CEM and L1210 were cultured in RPMI 1640 medium. MiaPaCa-2 cells were grown in Dulbecco's minimal essential medium (DMEM). All media were supplemented with 10% heat-inactivated fetal bovine serum (FBS) (56 °C, 30 min), penicillin (100 U/mL) and streptomycin (100 μg.mL^{-1}). Medium for MiaPaCa-2 cell line was supplemented additionally with 2.5% heat-inactivated horse serum (Gibco) (56 °C, 30 min). Cells were maintained in a humid atmosphere at 37 °C with 5% CO_2.

4.2 *In vitro* anticancer activity of on various cancer cell lines

MTT [3-(4,5-dimethylthiazol-2-yl)-2,5-diphenyl tetrazolium bromide] was used to test cytotoxicity of polyisoprene-gemcitabine prodrug nanoparticles and cell viability. Briefly, cells (5×10^3/well) were seeded in 96-well plates. After overnight incubation, the cells were then exposed to a series of concentrations of polyisoprene-gemcitabine prodrug nanoparticles (**4a-d**), control polyisoprene nanoparticles (**5a-e**) or free gemcitabine (**1**) for 72 h. After drug

exposition, the medium was removed and 100 µL of MTT solution (0.5 $mg.mL^{-1}$ in DMEM containing 10% FBS) was added to each well. The plates were incubated for 2 h at 37 °C and 100 µL of 20% SDS solution were then added to each well for 24 h at 37 °C. Absorbance was measured at 570 nm using a plate reader (Metertech Σ 960, Fisher Bioblock, Illkirch, France). The percentage of surviving cells was calculated as the absorbance ratio of treated to untreated cells. The inhibitory concentration 50% (IC_{50}) of the treatments was determined from the dose-response curve. All experiments were set up in quadruplicate to determine means and SDs. No significant cytotoxicity was observed for control polyisoprene (**5a-e**) nanoparticles (Table S7).

Table S7. IC_{50} for Control Polyisoprene (PI) Nanoassemblies (**5a-e**).

Cell line	5a	5b	5c	5d	5e
Miapaca2	> 100 µM	> 100 µM	> 100 µM	91 µM	74 µM
L1210	> 100 µM	> 100 µM	> 100 µM	> 100 µM	96 µM
CCRF-CEM	44 µM	60 µM	63 µM	20 µM	12 µM
A549	> 100 µM	> 100 µM	> 100 µM	88 µM	94 µM

4.3 *In vivo* anticancer activity on solid tumour-bearing mice

Six-eight week old female athymic nude mice were purchased from Harlan Laboratory. All animals were housed in appropriate animal care facilities during the experimental period, and were handled according to the principles of laboratory animal care and legislation in force in France. The antitumor efficacy of polyisoprene-gemcitabine prodrug nanoassemblies has been investigated on the human pancreatic carcinoma xenograft model MiaPaCa-2 at equimolar doses comparatively to free gemcitabine. 200 µL of the MiaPaCa-2 cell suspension, equivalent to 1×10^7 cells, were injected subcutaneously into nude mice toward the upper portion of the right flank, to develop a solid tumor model. Tumors were allowed to grow to a volume of ~100 mm^3 before initiating the treatment. Tumor length and width were measured with calipers, and the tumor volume was calculated using the following equation: V_{tumor} = length × $width^2/2$. Tumor-bearing nude mice were randomly divided into 6 groups of 6 each and all groups received four intravenous injections on days 0, 4, 8 and 12 in the lateral tail vein with either (i) gemcitabine 7 $mg.kg^{-1}$, (ii) Gem-PI nanoparticles (**4b**) at a Gem-equivalent dose of 7 $mg.kg^{-1}$ (3.2 $mg_{Gem\text{-}PI}.mL^{-1}$), (iii) Gem-PI nanoparticles (**4d**) at a Gem-equivalent dose of 7 $mg.kg^{-1}$ (6.7 $mg_{Gem\text{-}PI}.mL^{-1}$), (iv) PI nanoparticles (**5a, 5e**) at an equivalent PI

concentration to **4b** and **4d** (2.9 and 6.8 $mg_{PI}.mL^{-1}$, respectively), (v) saline 0.9%. The injected volume was 10 $\mu L.g^{-1}$ of body weight. The mice were monitored regularly for changes in tumor size and weight.

5. References

1. Harrisson, S.; Couvreur, P.; Nicolas, J. *Polym. Chem.* 2011, 2, 1859.
2. Harrisson, S.; Couvreur, P.; Nicolas, J. *Macromolecules* 2011, 44, 9230.
3. Harrisson, S.; Couvreur, P.; Nicolas, J. *Macromol. Rapid Commun.* 2012, 33, 805.

Discussion générale

La technique de « squalénisation » a été développée par l'équipe de Patrick Couvreur en 2006.[1] Dès lors, elle fût appliquée à de nombreux principes actifs et principalement aux analogues nucléosidiques (gem, ddI, ddC, etc).[1-7] Malgré des résultats *in vitro* et surtout *in vivo* particulièrement prometteurs, aucune stratégie mettant en œuvre un ciblage actif, qui est généralement considéré comme plus efficace, n'avait été développée. De plus, la PEGylation de tels assemblages supramoléculaires (notamment *via* la co-nanoprécipitation de Sq couplé au PEG (Sq-PEG) et de Sq-Gem), s'est révélée infructueuse et a conduit à une déstructuration colloïdale.[8] Enfin, la synthèse de l'acide squalénique, le précurseur de tous les conjugués de type Sq-principe actif, s'obtient à partir d'une synthèse en cinq étapes avec 10-15% de rendement global.[1] Il semblait donc opportun de mettre au point un autre chemin de synthèse qui conduirait à des conjugués de type Gem-isoprénoide donnant des nanoparticules avec des activités anticancéreuses in vivo au moins aussi bonnes que celles obtenues à partir du conjugué Sq-Gem.

La discussion générale qui va suivre a pour but de reprendre les principaux résultats obtenus au cours de ma thèse et de présenter des perspectives qui en découlent.

1. Nanoparticules multifonctionnelles de prodrogues à base de squalène pour le ciblage des cellules cancéreuses

La première tâche à laquelle je me suis attelée est la synthèse et la formulation de nanoparticules de Sq-Gem fonctionnalisées. La méthode très simple que nous avons développée consiste à effectuer le co-auto-assemblage en solution aqueuse de trois conjugués : (i) **Gem-Sq** (la prodrogue de référence) pour l'effet thérapeutique ; (ii) la **biotine-Sq**, pour effectuer le ciblage des récepteurs à la biotine surexprimés à la surface de nombreuses cellules cancéreuses et (iii) la **rhodamine-Sq (Rho-Sq)**, pour marquer les nanoparticules et permettre ainsi leur suivi lors des diverses expériences (Figure 1).

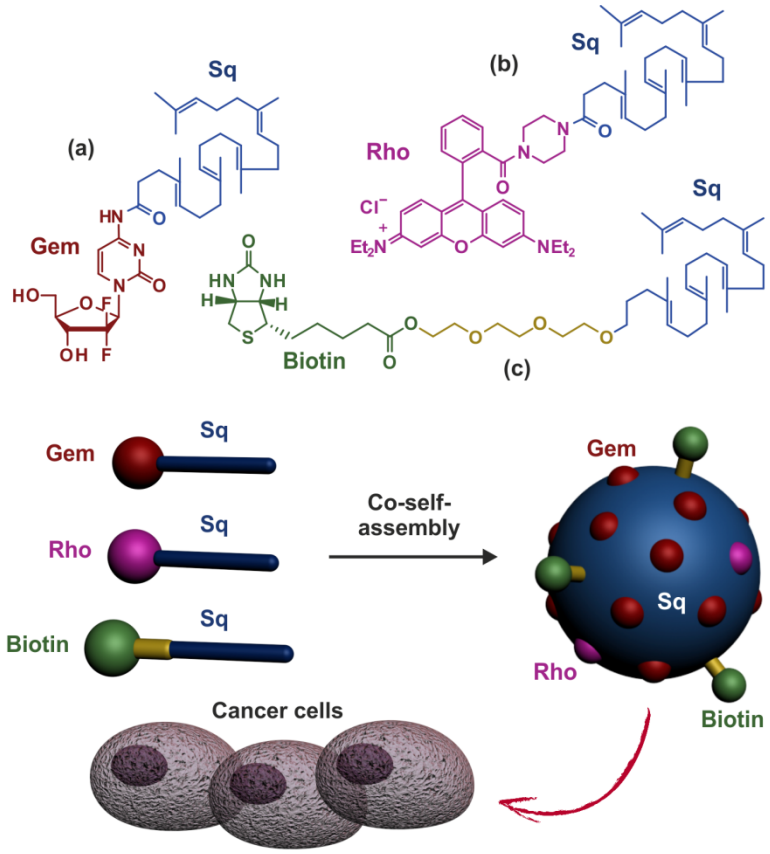

Figure 1. Co-auto-assemblage de Gem-Sq (a), Rho-Sq (b) et Biotin-Sq (c) pour préparer des nanoparticules multifonctionnelles permettant de cibler les cellules cancéreuses.[9]

La Gem-Sq et la Rho-Sq ont été obtenues à partir de l'acide squalénique tandis que la biotine-Sq a été synthétisée à partir du trisnorsqualenol via un espaceur de tri(éthylène glycol), destiné à promouvoir la disponibilité de la biotine à la surface des nanoparticules résultantes. Les nanoparticules multifonctionnelles ont été préparées par co-auto-assemblage d'un mélange de Gem-Sq/Biotin-Sq/Rho-Sq (86:9:5 % en masse) par nanoprécipitation. Les nanoparticules obtenues sont stables sur une durée d'au moins sept jours avec des tailles de l'ordre de 150 nm, une distribution étroite des tailles de particules et un potentiel zêta de -25 ± 3 mV.

Nous avons démontré le ciblage actif de ces nanoparticules multifonctionnelles par des expériences d'internalisation et de cytotoxicité sur trois lignées cellulaires cancéreuses : Hela (cancer du col de l'utérus), MCF-7 (cancer du sein humain) et M109 (cancer du poumon murin), qui surexpriment toutes le récepteur de la biotine. Il a été montré que les nanoparticules biotinylées étaient internalisées en plus grande quantité par ces cellules cancéreuses et qu'elles induisaient une cytotoxicité plus forte. Par ailleurs, il semblerait que

ces nanoparticules restent intactes durant l'internalisation (24 h) grâce à un double marquage réalisé avec deux conjugués fluorescents : la Rhod-Sq et le Chol-BODIPY. Il a même été remarqué que, quel que soit le signal de fluorescence choisi lors du suivi en cytométrie de flux, la meilleure internalisation est toujours observée avec les nanoparticules biotinylées.

En outre, en utilisant des inhibiteurs spécifiques de l'endocytose, nous avons constaté que les nanoparticules biotinylées ont été internalisées par endocytose, et ce principalement par la voie des clathrines et des caveolae alors que les nanoparticules non fonctionnalisées n'ont pas été affectées par la présence de ces bloqueurs.

L'ensemble de ces résultats est très satisfaisant et prometteur dans la mesure où il est désormais possible d'imaginer des systèmes nanoparticulaires à base de Sq modulables, à la façon d'un Lego®, où il serait possible de changer à loisir : le principe actif, le ligand de reconnaissance pour le ciblage actif et la molécule fluorescente. En effet, on peut imaginer tour à tour : (i) vouloir effectuer de l'imagerie directement in vivo en utilisant des fluorophores émettant dans le proche infra-rouge tels que les hemicyanines de type FP682 ou DY-700; (ii) utiliser l'acide folique ou bien l'anisamide pour cibler les récepteurs surexprimés à la surface des cellules cancéreuses ; ou encore (iii) coupler d'autres principes actifs tels que le paclitaxel, le cisplatin ou bien la doxorubicine par exemple.

2. Nanoparticules furtives à base de squalène

Dans cette partie, nous avons apporté une réponse au problème de la PEGylation des nanoparticules de Sq-Gem. L'idée a été d'augmenter l'hydrophobie du « segment squalène » en construisant, par polymérisation radicalaire contrôlée de type RAFT, un polymère de type polyméthacryate avec des chaines pendantes de Sq. L'hypothèse que nous avons formulée était que l'enchevêtrement des chaines de poly(squalene méthacrylate) (PSqMA) induirait une bien meilleure rigidité lors de la PEGylation, en évitant ainsi une déstabilisation colloïdale (Figure 2). En pratique, la Gem a été couplée à un agent RAFT de type trithiocarbonate et le conjugué ainsi synthétisé a été utilisé comme agent RAFT lors de la polymérisation du SqMA, afin d'obtenir une petite librairie de conjugués de masses molaires variables et bien contrôlées. Pour conférer des propriétés de « furtivité » à ces nanoparticules, leur PEGylation a été entreprise et nous avons comparé ces nanoparticules aux nanoparticules non-PEGylées.

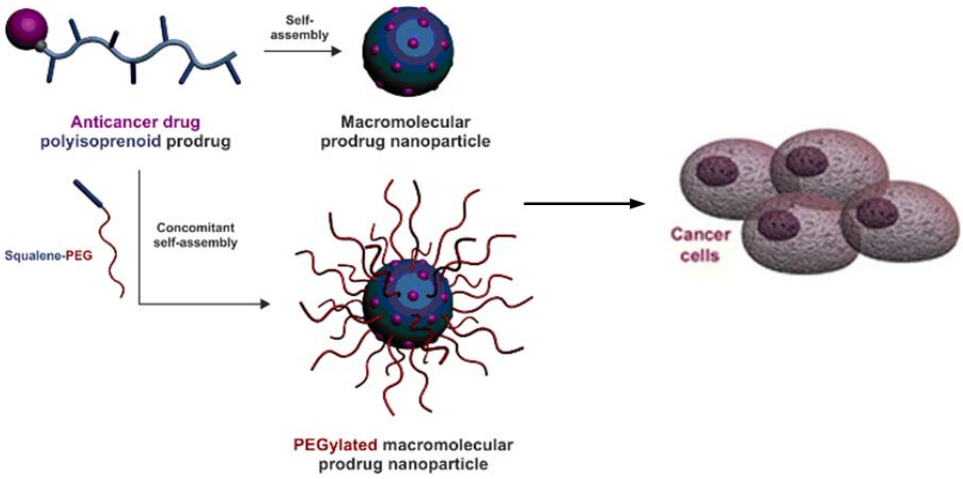

Figure 2. Synthèse de nanoparticules de Gem-poly(squalene methacrylate) (Gem-PSqMA) et leur PEGylation par co-auto-assemblage avec le Sq-PEG.[10]

Les polymères de Gem-PSqMA synthétisés ont des M_n variant de 4400 à 11300 g/mol, avec les dispersités faibles allant de 1.18 et 1.28 (DP_n variant de ~8 à ~28). Après nanoprécipitation de ces conjugués, des nanoparticules de diamètres variant entre 120 à 160 nm et de distribution étroite (0.17) ont été obtenues avec une très bonne stabilité colloïdale allant jusqu'à environ 4 semaines. Ceci nous a donc montré que des polymères fonctionnalisés en fin de chaine par la Gem pouvaient donner des nanoparticules stables.

Dans une seconde étape, nous avons donc entrepris de PEGyler ces nanoparticules. La méthode la plus simple a consisté en la co-nanoprécipitation des conjugués Gem-PSqMA avec le Sq-PEG, comme cela était fait au préalable avec la Gem-Sq. Nous avons démontré la présence du PEG à la surface de ces nanoparticules non seulement par XPS mais également par des expériences d'activation du complément. Néanmoins, le résultat le plus important a été le suivant : quelle que soit la concentration de Sq-PEG utilisée lors de la PEGylation, le diamètre des nanoparticules résultantes reste constant. Ceci montre donc que ces nouvelles nanoparticules de prodogues macromoléculaires peuvent résister à la PEGylation, contrairement à leurs homologues de Sq-Gem.[8]

Les nanoparticules de Gem-PSqMA ont ensuite montré une activité anticancéreuse importante *in vitro* sur différentes lignées cellulaires (MiaPaCa-2, A549, CCRF-CEM, L1210 WT et P388S). Mais le résultat le plus important, que nous avons obtenu très récemment, est sans conteste le fait que ces nanoparticules possèdent ne activité anticancéreuse *in vivo* sur des souris porteuses de tumeurs MiaPaCa-2 (Figure 3).[11]

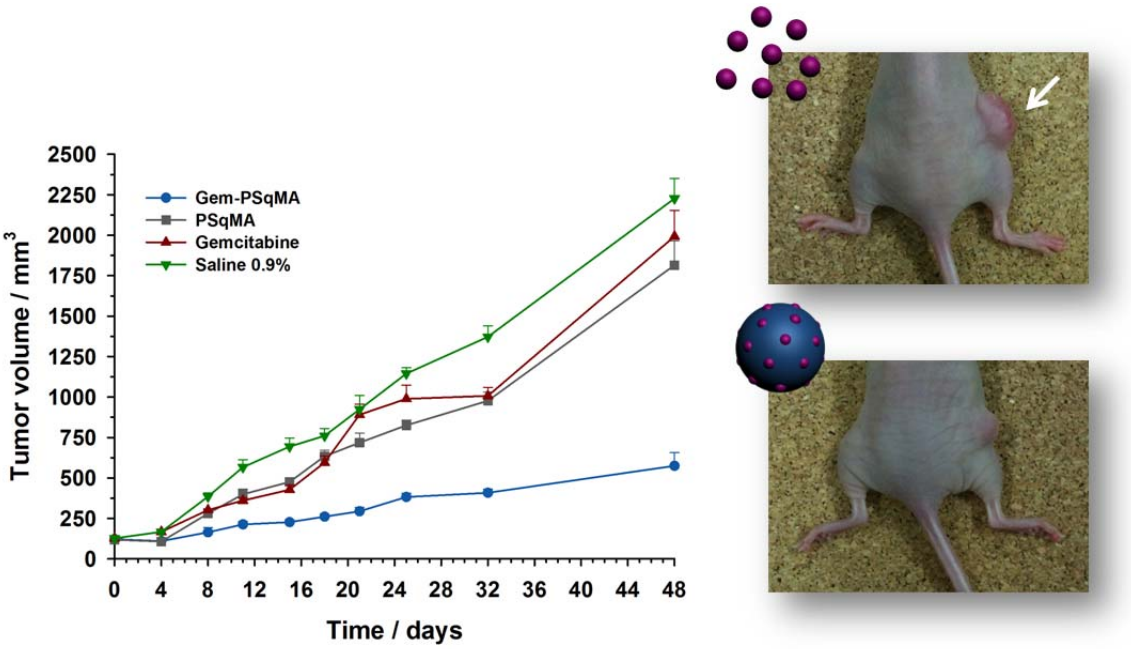

Figure 3. Gauche : Evolution de la croissance tumorale pour des souris porteuses de tumeurs MiaPaCa-2 en fonction du traitement : NaCl 0.9%, Gem (4 mg/kg), Gem-PSqMA (4 mg/kg Gem) et PSqMA. Droit : photo de souris à j32 montrant la tumeur pour une souris traité par la Gem libre et par les nanoparticules de Gem-SqMA.[11]

Il est donc possible de synthétiser des nanoparticules de prodrogues macromoléculaires à base de Sq qui, non seulement peuvent être PEGylées, mais qui possèdent toujours une activité anticancéreuse *in vitro* et surtout *in vivo*. Ces résultats ouvrent ainsi des perspectives très intéressantes. La gamme de M_n utilisée dans nos études n'ayant pas permis d'extraire des relations de type structure (M_n)/activité, il serait alors intéressant d'élargir la fenêtre de M_ns pour espérer observer un effet de la longueur de chaine de PSqMA sur l'activité anticancéreuse. De même, grâce à la flexibilité de la polymérisation de type RAFT, il est possible d'imaginer d'autres combinaisons principes actifs/polymères et ainsi développer toute une gamme de nanoparticules de prodrogues macromoléculaires à visée anticancéreuse. Enfin, en changeant la nature du principe actif, il est envisageable de traiter d'autres pathologies ; nous pensons notamment aux maladies infectieuses ou parasitaires avec l'utilisation de principes actifs adéquats.

3. Nanoparticules de polyisoprène avec activité anticancéreuse *in vivo*

Cette partie, à laquelle je n'ai que partiellement participée (sujet du stage post-doctoral du Dr. Simon Harrisson et avec la participation du Dr. Andrey Maksimenko), a consisté en une simplification du système classique Gem-Sq sur le plan de la synthèse chimique. En effet, l'acide squalénique, qui est le précurseur de tous les conjugués de type Sq-principe actif, est obtenu à l'issue d'une synthèse en 5 étapes avec seulement 10-15% de rendement total.[1] De plus, la dernière étape d'oxydation met en œuvre le réactif de Jones, particulièrement toxique et rédhibitoire pour un éventuel développement pharmaceutique. C'est pourquoi, plutôt que de trouver une voie de synthèse alternative de l'acide squalénique (toujours non établie à ce jour), l'idée a été de concevoir d'autres prodrogues composées de dérivés isopréniques. Nous nous sommes alors tournés vers l'isoprène, qui est le motif structurel de base de nombreux dérivés lipidiques naturels et biocompatibles (Sq, rétinol, vitamine E etc). De plus, le polyisoprène (PI) est biocompatible,[12] dégradable chimiquement[13] et sa polymérisation est parfaitement bien contrôlée, notamment par les techniques RAFT[14] et NMP.[15-16] Fort de notre expérience dans la synthèse de prodrogues macromoléculaires de Gem-PSqMA par polymérisation radicalaire contrôlée,[10] nous avons alors entrepris la synthèse de composés de type Gem-PI par NMP. La Gem a tout d'abord été fonctionnalisée par une alcoxyamine basée sur le nitroxyde SG1, l'un des nitroxydes les plus performants ayant été développés à ce jour.[17] Il est à noter que, contrairement au composé Gem-agent RAFT synthétisé précédemment,[10] il n'est ici pas nécessaire de protéger les groupements hydroxyles de la Gem, ce qui simplifie encore plus la synthèse. La NMP de l'isoprène a ensuite été amorcé par l'alcoxyamine fonctionnelle Gem-SG1 et nous avons synthétisé une petite librairie de conjugués de M_n variables, tout en gardant un contrôle correct. Dans la mesure où les chaines de PI sont courtes, les taux de chargement en Gem sont ici élevés, variant de 10 à 31%.

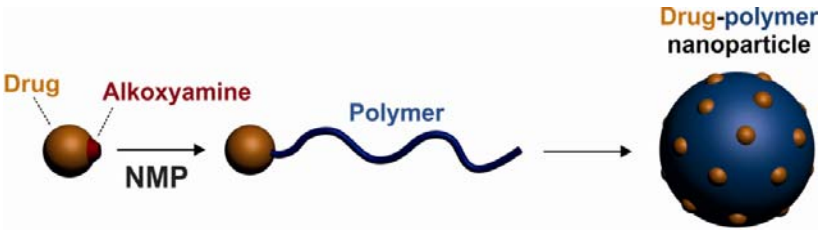

Figure 4. Stratégie pour obtenir les nanoparticules drogue-polymère conjugué par polymérisation des nitroxydes (NMP).[18]

Des nanoparticules stables ont été préparées par nanoprécipitation et ont montré une importante activité anticancéreuse *in vitro* sur plusieurs lignées cellulaires cancéreuses telles que MiaPaCa-2, L1210, CCRF-CEM et A549. De manière très intéressante, nous avons noté une influence de la longueur de la chaine de PI sur la cytotoxicité ; plus le DP_n est élevé, plus l'activité anticancéreuse des nanoparticules est importante. Le résultat le plus important est sans aucun doute le fait que ces nanoparticules ont également une activité anticancéreuse in vivo sur la souris porteuse de tumeurs de type MiaPaCa-2. Afin de vérifier que la tendance structure/activité observée *in vitro* était valable *in vivo*, nous avons injecté par voie intraveineuse des nanoparticules Gem-PI possédant des longueurs de chaine de PI différentes (1.2 et 2.5 kDa) ; les nanoparticules ayant les chaines de PI les plus grandes se sont avérées avoir la meilleure activité anticancéreuse. Il semblerait donc que les tendances observées in vitro soit transposables in vivo, ce qui aurait pour avantage d'économiser des animaux et du temps. La sélection des meilleures nanoparticules pourraient alors se faire in vitro avant un passage sur le petit animal.

Ces derniers résultats sont très importants dans la mesure où, en seulement trois étapes (deux réactifs sur trois étant commerciaux) avec un rendement cumulé de l'ordre de 60% (*i.e.*, synthèse de l'alcoxyamine-Gem), il est possible de préparer des nanoparticules de Gem-PI avec une forte activité anticancéreuse *in vitro* et surtout *in vivo*. Ceci simplifie énormément la synthèse chimique de prodrogues isoprénoides et laisse entrevoir de formidables ouvertures dans le domaine de la libération de principes actifs. En effet, en se basant sur cette stratégie, appelée « *drug-initiated method* », une multitude de combinaisons PI-principes actif peuvent alors être envisagées, et pas seulement restreintes au domaine du cancer. Par ailleurs, la flexibilité de la polymérisation radicalaire contrôlée permettrait l'insertion à façon de groupes fonctionnels dans la chaine de PI pour effectuer soit du ciblage actif (en utilisant des ligands de reconnaissance tels que la biotine, l'anisamide, l'acide folique, etc.), soit du marquage (molécules fluorescente), ou soit les deux. En perspective, il sera intéressant de tester des effets additifs, voire synergétiques en co-nanoprécipitant en même temps plusieurs composés de type PI-principes actifs, de sorte à concevoir des nanoparticules pouvant libérer plusieurs principes actifs à la fois.

Références

1. Couvreur, P.; Stella, B.; Reddy, L. H.; Hillaireau, H.; Dubernet, C.; Desmaële, D.; Lepêtre-Mouelhi, S.; Rocco, F.; Dereuddre-Bosquet, N.; Clayette, P.; Rosilio, V.; Marsaud, V.; Renoir, J.-M.; Cattel, L. *Nano Lett.* **2006,** *6*, 2544.
2. Couvreur, P.; Reddy, L. H.; Mangenot, S.; Poupaert, J. H.; Desmaele, D.; Lepetre-Mouelhi, S.; Pili, B.; Bourgaux, C.; Amenitsch, H.; Ollivon, M. *Small* **2008,** *4*, 247.
3. Reddy, L. H.; Couvreur, P. *Curr. Pharm. Des.* **2008,** *14*, 1124.
4. Reddy, L. H.; Dubernet, C.; Mouelhi, S. L.; Marque, P. E.; Desmaele, D.; Couvreur, P. *J. Control. Rel.* **2007,** *124*, 20.
5. Reddy, L. H.; Ferreira, H.; Dubernet, C.; Mouelhi, S. L.; Desmaele, D.; Rousseau, B.; Couvreur, P. *Anti-Cancer Drugs* **2008,** *19*, 999.
6. Reddy, L. H.; Ferreira, H.; Dubernet, C.; Mouelhi, S. L.; Desmaele, D.; Rousseau, B.; Couvreur, P. *J. Nanopart. Res.* **2008,** *10*, 887.
7. Reddy, L. H.; Khoury, H.; Paci, A.; Deroussent, A.; Ferreira, H.; Dubernet, C.; Decleves, X.; Besnard, M.; Chacun, H.; Lepetre-Mouelhi, S.; Desmaele, D.; Rousseau, B.; Laugier, C.; Cintrat, J.-C.; Vassal, G.; Couvreur, P. *Drug Metab. Dispos.* **2008,** *36*, 1570.
8. Bekkara-Aounallah, F.; Gref, R.; Othman, M.; Reddy, L. H.; Pili, B.; Allain, V.; Bourgaux, C.; Hillaireau, H.; Lepetre-Mouelhi, S.; Desmaele, D.; Nicolas, J.; Chafi, N.; Couvreur, P. *Adv. Funct. Mater.* **2008,** *18*, 3715.
9. Bui, D. T.; Nicolas, J.; Maksimenko, A.; Desmaele, D.; Couvreur, P. *Chem. Commun.* **2014**, DOI: 10.1039/c3cc47427e.
10. Bui, D. T.; Maksimenko, A.; Desmaele, D.; Harrisson, S.; Vauthier, C.; Couvreur, P.; Nicolas, J. *Biomacromolecules* **2013,** *14*, 2837.
11. Manuscrit en préparation
12. Yang, H.-C.; Silverman, J.; Wozniak, J. J. Low temperature heat shrinkable polymer material. US 4596728, 1986, US 4596728.
13. Cheng, C.; Qi, K.; Khoshdel, E.; Wooley, K. L. *J. Am. Chem. Soc.* **2006,** *128*, 6808.
14. Jitchum, V.; Perrier, S. *Macromolecules* **2007,** *40*, 1408.
15. Harrisson, S.; Couvreur, P.; Nicolas, J. *Macromolecules* **2011,** *44*, 9230.
16. Harrisson, S.; Couvreur, P.; Nicolas, J. *Macromol. Rapid Commun.* **2012,** *33*, 805.
17. Nicolas, J.; Guillaneuf, Y.; Lefay, C.; Bertin, D.; Gigmes, D.; Charleux, B. *Prog. Polym. Sci.* **2013,** *38*, 63.

18. Harrisson, S.; Nicolas, J.; Maksimenko, A.; Bui, D. T.; Mougin, J.; Couvreur, P. *Angew. Chem., Int. Ed.* **2013,** *52*, 1678.

Conclusion générale

Au cours de cette thèse, nous avons cherché à améliorer la technique de squalénisation d'analogues nucléosidiques, et en particulier de la gemcitabine, afin de lever trois verrous importants : (i) la synthèse de nanoparticules de squalène fonctionnalisés pour cibler activement les cellules cancéreuses, ce qui n'avait jamais été fait, (ii) la PEGylation de nanoparticules à base de squalène, qui est jusqu'alors impossible et (iii) la simplification du schéma de synthèse pour obtenir des nanoparticules polyisopréniques avec une activité anticancéreuse *in vivo*, ce qui n'avait jamais été tenté auparavant.

Le travail de ma thèse s'est inscrit dans le cadre d'un ERC Advanced Grant "TERNANOMED", obtenu par Patrick Couvreur en 2010, et dont l'objectif global reposait sur la conception et l'évaluation biologique de nouvelles nanoparticules d'isoprenoides (moléculaires et macromoléculaires).

A l'issue de ces trois années de travail de thèse, j'ai proposé une approche simple et efficace pour fonctionnaliser les nanoparticules de Sq-Gem afin de les rendre fluorescentes et ciblantes. J'ai également proposé une solution au problème de la PEGylation de ces nanoparticules en utilisant la méthode '*drug-initiated*' afin d'augmenter l'hydrophobie du segment squalène. Du fait de l'utilisation d'un procédé de polymérisation radicalaire contrôlée, la structure de ces nouveaux conjugués, et plus précisément la longueur de la chaine de polymère, peut être variée à façon et de manière contrôlée. Enfin, j'ai participé à l'élaboration d'une nouvelle approche afin de concevoir, de manière très simple et avec un rendement élevé, des nanoparticules de Gem-isoprénoide en faisant pousser de manière contrôlée de courtes chaines de polyisoprène à partir de le Gem.

Ces avancées permettent d'envisager de nouvelles pistes de recherche et ainsi accroitre l'arsenal de systèmes nanoparticulaires efficace contre le cancer.

Résumé de la thèse :

De nouvelles nanoparticules de prodrogues à base de polyisoprénoïdes (e.g., squalène, poly(squalenyl méthacrylate) ou polyisoprène), et en utilisant la gemcitabine comme agent anti-cancéreux, ont été synthétisées et ont démontré une activité anticancéreuse importante in vitro et in vivo.

Mots clés :

gemcitabine, squalène, squalénisation, nanoparticules, ciblage, PEGylation, polyisoprène, cancer.

Laboratoire de rattachement :

Institut Galien Paris-Sud, UMR CNRS 8612

Tour D5, 2eme étage

UFR «Faculté de Pharmacie de Chatenay-Malabry»

Université Paris-Sud 11

5, rue Jean-Baptiste Clément

92296 Châtenay-Malabry

France